Heavy quark systems at finite temperature from lattice QCD

PhD Thesis

Attila Pásztor

Institute of Theoretical Physics
Eötvös Loránd University
Budapest, 2015

Advisor: Prof. Sándor Katz, DSc., head of department

Physics Doctoral School, Particle and Astrophysics Program

Head of doctoral school: Prof. László Palla, DSc.

Program leader: Prof. László Palla, DSc.

Contents

1 Introduction **7**

1.1 Lattice QCD . . . 13

1.1.1 Correlation functions . . . 14

1.1.2 Lattice action . . . 15

1.1.3 Continuum limit . . . 22

1.1.4 Quenched approximation vs dynamical quarks . . . 24

1.1.5 The Hybrid Monte Carlo algorithm . . . 25

1.1.6 Gauge field smearing . . . 29

1.2 The naive potential picture of quarkonia at $T > 0$ . . . 31

1.3 The spectral function . . . 32

1.3.1 Kubo formulas and heavy quark diffusion . . . 38

2 Charmonium spectral functions **43**

2.1 The Maximum Entropy Method(MEM) . . . 45

2.1.1 Inverse problems and the use of prior information . . . 46

2.1.2 Outline of the MEM procedure . . . 47

2.1.3 Heuristic argument for the form of prior probability . . . 49

2.1.4 Bayesian averaging over the regularization . . . 50

2.1.5 The method of maximizing Q . . . 52

2.1.6 Implementation . . . 53

2.1.7 A comment on alternative methods . . . 55

2.2 Mock data analysis . . . 55

2.2.1 A comment on anisotropic lattices . . . 58

2.3 Error analysis . . . 59

2.4 Simulation details . . . 61
2.4.1 Charm mass tuning . . . 62
2.4.2 Approximation of the pseudo-critical temperature . . . 62
2.5 Maximum Entropy Analysis . . . 63
2.5.1 Zero temperature analysis . . . 64
2.5.2 Finite temperature analysis . . . 65
2.6 The ratio G/G_{rec} . . . 71
2.7 What do we expect in the case of melting? . . . 75

3 The static $Q\bar{Q}$ free energy and screening masses 79
3.1 An introduction to static potentials . . . 79
3.1.1 Static potential in non-relativistic QM . . . 79
3.1.2 Static potential in gauge theory at $T = 0$ . . . 81
3.1.3 Real-time static potential at $T > 0$ . . . 83
3.2 Static quark free energy . . . 86
3.2.1 Simulation details . . . 89
3.2.2 Renormalization procedure and continuum extrapolation . . . 89
3.3 Screening masses . . . 98
3.3.1 Non-perturbative definition . . . 98
3.3.2 Lattice determination . . . 102
3.3.3 Correlated fitting and continuum extrapolation . . . 104
3.3.4 Comparisons with other approximations . . . 111

4 Summary 113

5 Appendix 115
5.1 Some properties of covariance matrices of data . . . 115
5.1.1 Eigenvalue smoothing . . . 117

Acknowledgement

I would like to thank all the members of the Budapest-Wuppertal collaboration, especially my advisor Sándor Katz, for his continuous help.

I thank Szabolcs Borsányi and Norbert Trombitás, for generating the gauge field configurations necessary for the analysis presented here. I also thank Simon Mages and Csaba Török, for helping me cross-check some parts of my work.

I would also like to thank Antal Jakovác and Péter Petreczky, for insightful comments.

Computations were carried out on GPU clusters at the Universities of Wuppertal and Budapest as well as on supercomputers in Forschungszentrum Juelich.

This work was supported by the DFG Grant SFB/TRR 55, ERC no. 208740. and the Lendület program of HAS (LP2012-44/2012).

Finally, I would like to thank my family, my parents, and Mónika, for always supporting me.

Chapter 1

Introduction

QCD is the theory describing the Strong interactions. The elementary particles of QCD - quarks and gluons - are not observable in nature. What we see as final and initial states in scattering experiments are bound states called hadrons (p, n, π, K, ...). The most important property of QCD is probably asymptotic freedom. This means that as the momentum transfer in QCD processes becomes higher, the effective coupling decreases, asymptotically approaching zero. This makes perturbative predictions possible [1]. At high energies, perturbative QCD can be used and gives consistent explanation of a variety of experimental data, like scaling variations in deep inelastic lepton-nucleon scattering, jet production in e^+e^- scattering, τ-decay etc. At low energies, the opposite of asymptotic freedom kicks in, the coupling constant becomes larger, and perturbation theory breaks down.

At low energies, we need non-perturbative calculation methods, to get the predictions of QCD. The most well-developed method today is lattice gauge theory [2]. Here we define a theory on a finite space-time lattice, and with gradual decrease in the lattice spacing, and continuum extrapolation, we can get a prediction of continuum QCD. Lattice QCD has achieved considerable success in calculating the experimentally known properties of the strong interactions, like the hadron spectrum. For a review, see [3].

Another consequence of asymptotic freedom is the fact that at high temperatures, the coupling becomes smaller. We expect the bound states to dissolve, and a new kind of matter, the so called quark-gluon plasma, to manifest. From this, we expect a transition to occur, somewhere close to the QCD scale ($\Lambda_{QCD} \approx 200$MeV). Asymptotic freedom

then allows for a perturbative study of the quark-gluon plasma: at high temperature T, the only energy scale available is T itself, and the coupling constant itself is small at large T: $g(T) \sim 1/\ln(T/\Lambda)$. However, this situation is spoiled by the existence of infrared divergences, which lead to a hierarchy of energy, or length, scales. In addition to the perturbative scale $1/T$, there is an electric scale $1/(gT)$, and a magnetic scale $1/(g^2T)$, and perhaps other length scales, depending on the problem, that limit the applicability of naive perturbation theory. Nevertheless, some progress can be made with perturbative methods. The standard textbooks on perturbative finite temperature field theory are [4] and [5].

In addition to the $T = 0$ properties, like the hadron spectrum, lattice QCD is also well suited to calculating equilibrium properties at a fixed temperature. Two important examples of importance here are the order of the QCD transition, which was found to be an analytic cross-over [6] with a pseudo-critical temperature[1] of $T_c \approx 150MeV$ (see Ref. [7]) and the equation of state at zero baryon chemical potential [8, 9]. The $\mu_B \neq 0$ case is considerably more difficult, because of the sign problem. For a review on the equation of state, see [10].

The main motivation for investigating the thermodynamic properties of QCD comes from cosmology and astrophysics. As the early universe expanded after the Big Bang, a deconfinement transition occurred at $T \approx 150$ MeV, from the so called quark-gluon plasma to a confined phase with hadrons. The nature of this transition affects our understanding of the history of the universe. For a review, see [11]. The case of low temperature, but non-zero baryon chemical potential $\mu_B > 0$ is relevant for neutron stars (and some hypothetical exotic objects, like quark stars). The existence of a critical point is also hypothesized, ending a line of first-order transitions in the $\mu_B - T$ plane. This is expected because at $T = 0$ and high μ_B, most calculations predict a first-order transition [12]. The "popular" version of the QCD phase diagram can be seen in Figure 1.1. A particularly interesting phenomena is emerging at large chemical potentials. Due to asymptotic freedom at large chemical potentials we obtain a system with weakly interacting fermions. Since these attract each other they can form Cooper pairs and lead to a color superconducting

[1] Since the transition is a cross-over, we have no clear definition of a transition temperature, one can use different definitions, like the position of the peak in the chiral susceptibility, or the inflection point of the Polyakov-loop, or many others. These temperatures are close to each other, but not identical.

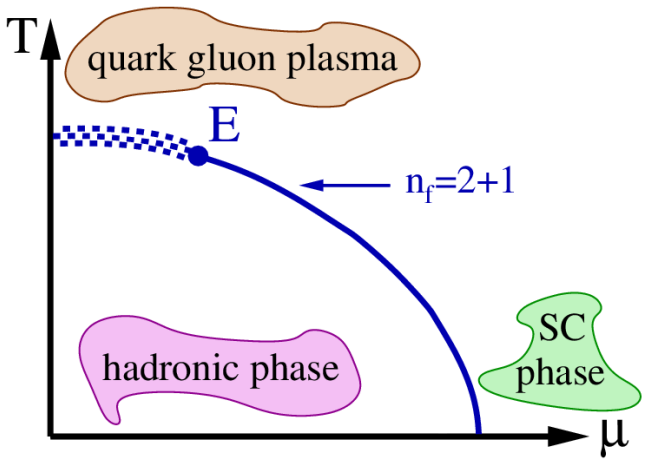

Figure 1.1: A sketch of the most popular hypothesized scenario for the QCD phase diagram in the baryon chemical potential - temperature plane. At $T = 0$ and $\mu > 0$ chemical potential most calculations predict a first order transition. At $\mu = 0$ and $T > 0$ lattice calculations predict a crossover. The crossover (dotted line) and the first order transition (solid line) are separated by a critical point E. At large chemical potentials, a color superconducting phase is expected.

phase.

There is also considerable experimental work being done on the nature of hot QCD. Experiments at the CERN SPS, at RHIC and at the LHC have all given considerable contributions to the field. The main motivation for the theoretical work presented here comes from the direction of these experiments.

We investigate bound states of heavy quark-antiquark pairs (heavy quarkonia) in a finite temperature medium. These have been under heavy investigation since the eighties, when a famous paper [13] suggested J/Ψ suppression as a possible signature for QGP formation in heavy ion experiments. The basic idea was simple. At high temperature, because of the QCD analog of Debye screening the potential between a $\bar{Q}Q$ pair becomes of the Yukawa-form, and for sufficiently high temperature the binding becomes sufficiently weak that the $\bar{Q}Q$ meson does not form. The J/Ψ shows a prominent peak in the dilepton channel of collider experiments. Also, within this potential model, the dissociation temperature of J/Ψ was estimated to be close to T_c, meaning that the disappearance of this peak could be a good indicator of deconfinement. Furthermore, it was argued that

the different quarkonia states would dissociate at different temperatures, meaning they could be used as a thermometer for the plasma. There is an analogy here to the spectral analysis of stellar media, where the presence and absence of different spectral lines can be used to determine the temperature.

A suppression of the J/Ψ peak was indeed found in the fixed target 158A GeV Pb-Pb collisions in the NA50 experiment in CERN. The collaboration published this result in a paper [14] entitled: *"Evidence for deconfinement of quarks and gluons from the J/Ψ suppression pattern measured in Pb + Pb collisions at the CERN SPS"* . Similar suppression is also present in the collision experiments at 200 A GeV Au-Au collisions at RHIC, and at 2.76 A GeV collisions at the LHC.

A more careful theoretical analysis of quarkonia shows however, that the situation is quite a bit more complicated than it was originally thought. Even in the case of a static equilibrium plasma, which is theoretically the easiest case to handle correctly[2], the behavior of heavy quarkonia at the interesting temperature regime of approximately $1...3T_c$ is very hard to predict, and, as I will argue, is poorly understood. This behavior in the static plasma is exactly what we will focus on in this work.

The text has two distinct parts. The first one considers an attempt at the brute-force determination of charmonium spectral functions. We show that up to $1.4T_c$ the most prominent temperature dependence in the lattice data for J/Ψ comes from the appearance of a diffusion peak in the spectral function, and not from a change in the bound state peak. The second section is concerned with systems of static $\bar{Q}Q$ pairs in the plasma. This corresponds to the infinite quark mass limit of charmonium systems. In this limiting case, we calculate some interesting physical quantities, namely: the excess free energy of the plasma from putting in the two static charges, and the longest correlation lengths (or equivalently, the screening masses) of correlators of operators with certain symmetry properties, one corresponding to electric and the other to magnetic gluons. For this second calculation, we can use physical quark masses and carry out a continuum extrapolation as well.

[2]To what extent static equilibrium properties can be applied to the interpretation of heavy ion experiments is a whole new question entirely, which the author does not want to go into in this work.

My PhD thesis was carried out in the Budapest-Wuppertal collaboration, which already has state-of-the-art lattice QCD codes, and actually, all of the gauge field configurations that I used were already used in other publications. My contributions were[3]:

1. Writing a C++ code for the Maximum Entropy analysis of correlators in Euclidean field theories. The features of the code include:

   - Usage of arbitrary precision arithmetic.
   - The optimization can be done in both the full N_ω dimensional space, or the N_{data} dimensional subspace, with the possibility of changing the subspace with a projection, and several minimization routines available in both subspaces.
   - Bayesian averaging over the regularization parameter.
   - Because of the large number of iterations needed for the optimization, and the large number of runs needed for the systematic and statistical error estimation, the analysis itself was computationally costly, therefore a queuing script for the parallelization of the runs on the cluster in Budapest was also needed.

2. Testing the code and the reliability of the Maximum Entropy method in general, using mock data analysis. In particular I argued, that a relatively stable quantity of the reconstruction is the position of the ground state peak.

3. Determining the charmonium correlators at finite temperature using the lattice QCD code of the Budapest-Wuppertal collaboration on already existing configurations with 2+1 dynamical Wilson fermions, and performing the Maximum Entropy analysis of these correlators, with particular emphasis on systematic and statistical error estimation. At temperatures up to $1.3T_c$ the position of the ground state peak is consistent with a constant in both the pseudoscalar and vector channels, corresponding to the η_c and J/Ψ mesons respectively.

4. Using the ratio G/G_{rec}, I showed that the temperature dependence of the pseudoscalar correlator is consistent with a temperature independent spectral function, while the correlator in the vector channel is consistent with a temperature dependent transport peak at $\omega \approx 0$ and a temperature independent part at $\omega > 0$.

5. I introduced a new (numerical) renormalization procedure for the Polyakov loop, using only finite temperature data. The renormalization prescription was of the

[3]These are the thesis points.

same kind as in Ref. [15], but the procedure to carry out the renormalization was much simpler in that case, because of differences between Wilson and staggered fermions. I modified the renormalization procedure, to be applicable to staggered fermions as well.

6. Using already existing measurements of the Polyakov-loop on lattices with 2+1 flavours of dynamical staggered quarks at the physical point, I calculated the continuum limit extrapolation of the single static quark free energy, in the temperature range of $T = 130...390$MeV.

7. Using already existing measurements of the Polyakov-loop correlators on lattices with 2+1 flavours of dynamical staggered quarks at the physical point, I calculated the continuum limit extrapolations of the static $\bar{Q}Q$ pair free energies in the temperature range of $T = 150...350$MeV

8. I performed the correlated fitting of and the continuum limit extrapolation of the electric and magnetic screening masses in the quark gluon plasma, in the temperature range 160...450MeV.

The work leading to this thesis was published in two refereed papers:

- Sz. Borsányi, S. Dürr, Z. Fodor, C. Hoelbling, S. D. Katz, S. Krieg, S. Mages, D. Nógrádi, **A. Pásztor**, A. Schäfer, K. K. Szabó, B. C. Tóth, N. Trombitás
  "Charmonium spectral functions from 2+1 flavour lattice QCD"
  arXiv:1401.5940
  JHEP 1404 (2014) 132

- Sz. Borsányi, Z. Fodor, S. D. Katz, **A. Pásztor**, K. K. Szabó, Csaba Török :
  "Static $\bar{Q}Q$ pair free energy and screening masses from correlators of Polyakov loops: continuum extrapolated lattice results at the QCD physical point"
  arXiv:1501.02173 [hep-lat]
  Accepted to JHEP

And also in the conference proceedings:

- Sz. Borsányi, S. Dürr, Z. Fodor, C. Hoelbling, S. D. Katz, S. Krieg, S. Mages, D. Nográdi, **A. Pásztor**, A. Schäfer, K. K. Szabó, B. C. Tóth, N. Trombitás:
  "Spectral functions of charmonium with 2+1 flavours of dynamical quarks "

arXiv:1410.7443 [hep-lat]

The 32nd International Symposium on Lattice Field Theory

The structure of this text is the following:

- In the remaining part of this chapter, we give a brief introduction to lattice QCD, to J/Ψ suppression and also to finite temperature spectral functions.
- In Chapter 2 we introduce the maximum entropy method, and discuss the lattice determination of charmonium spectral functions.
- In Chapter 3 we give an introduction to the proposed static $\bar{Q}Q$ potentials in the literature, and discuss our lattice determination of the static $\bar{Q}Q$ free energy, and the electric and magnetic screening masses.
- A short Appendix discusses some properties of the covariance matrices of our lattice data.

1.1 Lattice QCD

In this section we will briefly go through the basic concepts of lattice gauge theory. A good, detailed textbook on lattice gauge theory is Ref. [2].

Thermodynamical quantities can be determined from the grand canonical partition function. The partition function in Euclidean field theory is:

$$Z = \int \mathcal{D}U\mathcal{D}\bar{\Psi}\mathcal{D}\Psi \exp\left(-S_{\mathrm{E}}(U,\Psi,\bar{\Psi})\right), \tag{1.1}$$

where U is the gauge field (gluons), Ψ represents the fermion fields (quarks), and S_{E} is the Euclidean action. QCD is an $SU(3)$ gauge theory, with fermions in the fundamental representation, so the gauge field U, is an $SU(3)$ matrix in every point and direction. The fermions are represented by Grassmann numbers. The Euclidean action depends on some parameters: the β gauge coupling (connected to the continuum gauge coupling by $\beta = \frac{6}{g^2}$), the quark masses m_i and chemical potentials μ_i. In this text we will always work with zero chemical potentials. If we want to describe several quark species, we have to introduce quark fields for all of them, eq. (1.1) only has one for simplicity. There are six quarks in nature, 3 of them (c,b,t) however, are much heavier than the others, and are usually not treated as dynamic degrees of freedom in lattice simulations. At low

energies these quarks are not present in the final or initial states of the processes and they can not be produced during them. For the other 3 quarks, the usual approximation is $m_{ud} = m_u = m_d < m_s$, i.e. one usually assumes an exact SU(2) isospin symmetry[4].

To define the integral measure, one has to use some kind of regularization. The lattice regularization assumes a discrete hypercubic lattice Λ instead of a continuum space-time. The fields are then defined on the points and links of the lattice. To preserve the continuum gauge symmetry the gauge fields have to live on the bonds between the lattice sites, and fermions have to live on the lattice sites themselves. The integral measure is then:

$$\prod_{x\in\Lambda,\mu=1,2,3,4} dU_{x,\mu} \prod_{x\in\Lambda} d\Psi_x \prod_{x\in\Lambda} d\bar{\Psi}_x, \tag{1.2}$$

meaning one has to evaluate the sum of the expression $e^{-S_{\mathrm{E}}}$ over all possible configurations of the gauge and fermion fields. This is analogous to a 4 dimensional system in statistical mechanics, where one has to sum e^{-E/k_BT} over all possible configurations. The important difference is that, in statistical mechanics, the temperature is in the Boltzmann factor, in lattice gauge theory one can prove that if gauge fields have periodic and the fermions have anti-periodic boundary conditions in time, one gets a finite temperature system, where the temperature is given by:

$$T = \frac{1}{N_t a_t}, \tag{1.3}$$

where N_t is the number of points in the time direction and a_t is the lattice spacing in the time direction. The boundary conditions implement the trace operation in (1.1). Practically, lattices with $N_t \geq N_s$, are called zero temperature ones, where N_s is the number of points in the spacial direction, and $N_t \ll N_s$ are called finite temperature ones[5].

1.1.1 Correlation functions

A physical quantity O, depending on the gauge and fermion fields has an expectation value:

$$\langle O \rangle = \frac{1}{Z} \int \mathcal{D}U\mathcal{D}\Psi\mathcal{D}\bar{\Psi} O\left[U,\Psi,\bar{\Psi}\right] \exp\left(-S_{\mathrm{E}}(U,\Psi,\bar{\Psi})\right). \tag{1.4}$$

[4]If one wants to include isospin breaking in a calculation, one also has to include QED, since the effect of these two things are of the same magnitude. This was done recently in Ref. [16]

[5]Assuming that the system size in the spatial direction satisfies $L \gg \frac{1}{m_\pi}$ and that the lattice is isotropic ($a_t = a_s$) for $N_t \geq N_s$ we have $T = \frac{1}{N_t a} \leq \frac{1}{N_s a} = \frac{1}{L} \ll m_\pi$.

If O is an operator constructed from the field operators, then $\langle\hat{O}\rangle = \langle O\rangle$. An important quantity is the two point correlation function of some operators, defined as the vacuum expectation value (VEV):

$$\langle 0|\hat{O}(t)\hat{O}^\dagger(0)|0\rangle = \lim_{T\to 0} \langle \hat{O}(t)\hat{O}^\dagger(0)\rangle \,. \tag{1.5}$$

The large distance behavior of the correlators can be understood in the following way. The Euclidean time evolution of an operator is described by the Hamiltonian $\hat{O}(t) = e^{t\hat{H}}\hat{O}(0)e^{-t\hat{H}}$. Inserting a complete set of states $|n\rangle$, the two point function (or correlator) becomes:

$$\langle 0|\, \hat{O}(t)\hat{O}^\dagger(0)\, |0\rangle = \sum_n \left|\langle 0|\, \hat{O}(0)\, |n\rangle\right|^2 e^{-(E_n - E_0)t}. \tag{1.6}$$

Where we have written in the vacuum state $|0\rangle$ explicitly. If the vacuum expectation value of O is zero[6] the dominant contribution as $t \to \infty$ comes from the lowest energy state where the matrix element $\left|\left\langle 0|\hat{O}(0)|n\right\rangle\right|$ is nonzero, meaning that in a given quantum number channel the exponential decay of the correlator will give the energy (mass) of the lowest energy state. The correlation length

$$\xi = \frac{1}{ma}, \tag{1.7}$$

where m is the mass of the lowest state and a is the lattice spacing. This is the basis of lattice spectroscopy at zero temperature[7].

At nonzero temperature the situation is more complicated, because of the heat bath, every possible energy can be excited, and the contributions are very hard to differentiate. Here the important quantity will be the spectral function, which we will define later in this text.

1.1.2 Lattice action

To carry out the lattice regularization, one has to discretize the S_E Euclidean action as well. This step is not unique, there are different lattice actions with the same continuum limit. We will restrict ourselves to isotropic lattices, where the lattice spacings in all

[6] If the vacuum expectation value of O is not zero, we have to consider the connected correlator $\langle O(t)O^\dagger(0)\rangle - \langle O\rangle\langle O^\dagger\rangle$

[7] Because of the finite time extent, the exponential is not actually the correct ansatz when fitting the hadron masses. For example, for mesons, it is $C\cosh(ma - N_t/2)$.

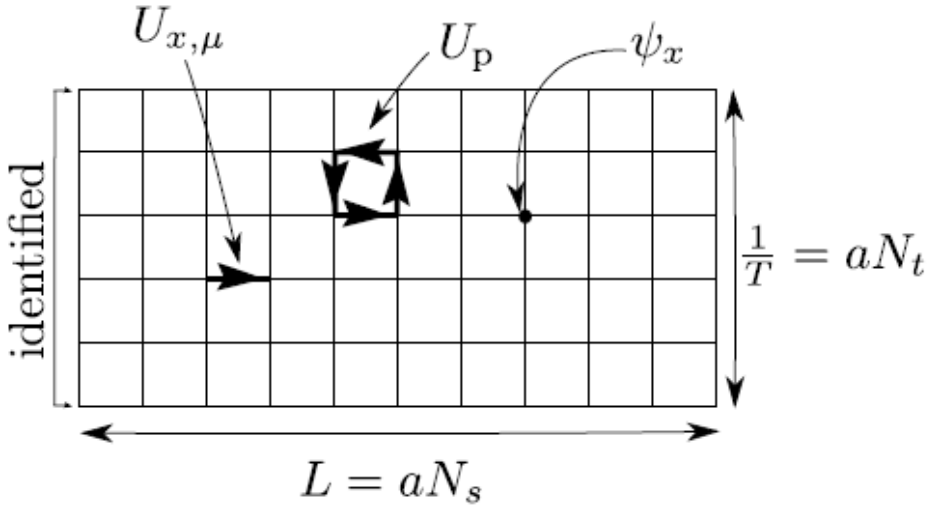

Figure 1.2: A sketch of a 1+1 dimensional isotropic spacetime lattice. The fermionic variables live on the lattice sites, the gauge fields live on the links. The plaquette is a closed loop of size 1×1 (in higher dimensions the plaquette does not have to go in the time-like and a space-like dimension, both directions can be space-like). The temperature is determined by the time extent of the lattice.

directions are the same. At a finite lattice spacing, the expectation value of a quantity A scales as[8]:

$$\langle A \rangle_a = \langle A \rangle + \mathcal{O}(a^n), \tag{1.8}$$

where $\langle A \rangle$ is the continuum expectation value, $\langle A \rangle_a$ is the expectation value at finite lattice spacing. The bigger n is, the "better" the action is, since one has results closer to the continuum theory at bigger lattice spacings. Here we briefly review the different lattice actions we use.

The lattice action can usually be decomposed into a gluonic and a fermionic part: $S = S_G + S_F$. Let us start with the gluonic action. In lattice gauge theory, unlike in the continuum formulation, the gauge fields are elements of the Lie group and not the Lie algebra, they are parallel transporters along the lattice links, related to the Lie algebra valued fields A_μ by:

$$U_{x,\mu} = e^{igA_\mu(x)^a T^a a_\mu}, \tag{1.9}$$

where μ is some direction on the lattice, a_μ is the lattice spacing in that direction, the T^a are the hermitian generators of the $su(N)$ Lie-algebra, and g is the (bare) gauge coupling.

[8]Here, we assume that the quantity A is renormalized, and therefore has a finite continuum limit.

Using these small parallel transporters, the parallel transporter for any curve between two points, say x and y can be constructed by multiplying the parallel transporters along the lattice sites. The general rule is that if we have a curve $\mathcal{C}_2 \circ \mathcal{C}_1$ composed by taking the curve $\mathcal{C}_1$ following it by $\mathcal{C}_2$, then we have:

$$U(\mathcal{C}_2 \circ \mathcal{C}_1) = U(\mathcal{C}_2)U(\mathcal{C}_1), \tag{1.10}$$

reversing the direction of the path amounts to taking the inverse of the transporter, and under gauge transformations a parallel transporter $U(\mathcal{C}_{yx})$ connecting the points x and y transforms as:

$$U(\mathcal{C}_{yx}) \xrightarrow{\Lambda} \Lambda^{-1}(y)U(\mathcal{C}_{yx})\Lambda(x), \tag{1.11}$$

from which (using the cyclicity of the trace) it immediately follows that the trace of any parallel transporter along a closed loop is gauge invariant. The simplest gauge invariant action is the plaquette or Wilson action. The plaquette is the product (see Fig. 1.2):

$$U_P(x;\mu\nu) = U_{x,\mu}U_{x+a\mu,\nu}U^\dagger_{x+a\nu,\mu}U^\dagger_{x,\nu}, \tag{1.12}$$

and the action constructed from plaquettes is:

$$S_G^{\text{Wilson}} = -\beta\frac{1}{N_c}\sum_{x,\mu<\nu}\text{Re}\,\text{Tr}\left(U_P(x;\mu\nu) - 1\right). \tag{1.13}$$

This is the simplest gauge invariant action constructed from the gauge fields. Expanding in powers of the lattice spacing one finds that:

$$S_G^{\text{Wilson}} = -\frac{\beta}{4N_c}\sum_x a^4\,\text{Tr}\left(F_{\mu\nu}(x)F^{\mu\nu}(x)\right) + \mathcal{O}(a^5), \tag{1.14}$$

meaning that if we make the identification $\beta = 2N_c/g^2$ we get the continuum Yang-Mills action. In the following we restrict ourselves to $SU(3)$ and set $N_c = 3$.

To improve on the action, one can add more gauge invariant terms to the Wilson action. The next simplest term is the ordered product of links along a 2×1 rectangle, giving the following action:

$$S_G^{\text{Sym}} = \beta\left[\frac{c_0}{3}\sum_{\text{plaq}}\text{Re}\,\text{Tr}\left(1 - U_{\text{plaq}}\right) + \frac{c_1}{3}\sum_{\text{rect}}\text{Re}\,\text{Tr}\left(1 - U_{\text{rect}}\right)\right]. \tag{1.15}$$

It can be shown that at tree level this improves the scaling if $c_0 + 8c_1 = 1$ and $c_1 = -1/12$. This action is called the Symanzik tree level improved gauge action [17].

The discretization of fermion fields is much more difficult than the case of the gauge fields. The naive discretization, obtained by substituting the derivatives of the continuum Dirac operator with finite differences is:

$$S_F^{\text{naive}} = \sum_x \left[am\bar{\Psi}_x\Psi_x + \frac{1}{2}\sum_\mu \left(\bar{\Psi}_x U_{x;\mu}\gamma_\mu \Psi_{x+a\hat{\mu}} - \bar{\Psi}_x U_{x-a\hat{\mu};\mu}\gamma_\mu \Psi_{x-a\hat{\mu}}\right)\right]. \tag{1.16}$$

This suffers from the well-known doubling problem, meaning that in the first Brillouin zone it has $16 = 2^4$ poles, not one. There are various methods for the solution of this problem, but they are restricted by a no-go theorem. To state it, consider a general bilinear massless fermion lattice action, written as:

$$\sum_{xy}\sum_{ij} \bar{\Psi}_x D_{x;y}\Psi_y, \tag{1.17}$$

where we have suppressed flavour, color, and Dirac indices. The Nielsen-Ninomiya theorem states that there is no lattice Dirac operator D satisfying all of the following properties:

1. Correct continuum limit
2. No fermion doublers
3. Chiral symmetry, i.e. $\{D, \gamma_5\} = 0$
4. Locality, i.e. $\exists c, \lambda > 0$ such that $||D_{xy}|| \leq ce^{-\lambda|x-y|}$

This means that fermion discretizations have to break one of these desirable properties. Clearly we can not break property number 1.

The main idea behind the Wilson discretization is to introduce a term with a second derivative, that vanishes in the continuum limit, but makes the doubler masses larger, proportional to $1/a$ (which makes them infinite in the continuum limit):

$$S_F^{\text{Wilson}} = \sum_x \left(\Psi_x\bar{\Psi}_x - \kappa \sum_{\mu=\pm1}^{\pm4} \bar{\Psi}_x U_{x;\mu}(r+\gamma_\mu)\Psi_{x+a\hat{\mu}} \right), \tag{1.18}$$

with $\kappa = 1/(2am + 8r)$. The Wilson parameter is usually chosen to be[9] $r = 1$. The problem with this action is that it breaks chiral symmetry even in the zero quark mass limit, meaning that the quark masses have an additive renormalization, in addition to the

[9]The main motivation for this choice is that link- and site-reflection positivity can both be proved, see [2].

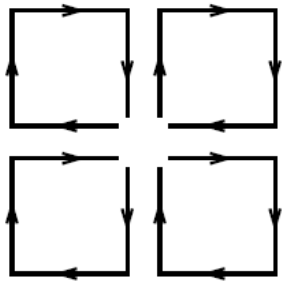

Figure 1.3: Product of link variables contributing to the lattice gauge field strength tensor $F_{\mu\nu}(x)$, called a clover. The point x is in the middle of the diagram.

multiplicative one. This means that for every value of β, the bare quark masses have to be retuned in the action, and they can even become negative. The other problem is that n in (1.8) is only 1. These two things together mean that one needs very large and very fine lattices to study chiral symmetry restoration.

The improved version of the Wilson action we will use is called the clover improved Wilson action [18]:

$$S_F^{\mathrm{SW}} = S_F^{\mathrm{W}} - \frac{c_{\mathrm{SW}}}{4} \sum_x \sum_{\mu,\nu} \bar{\psi}_x \, \sigma_{\mu\nu} F_{\mu\nu,x} \, \psi_x \,, \tag{1.19}$$

where S_F^{W} is the Wilson fermion action, and $\sigma_{\mu\nu} = [\gamma_\mu, \gamma_\nu]$. The reason this action is called clover improved is because the product of link variables contributing to the gauge field strength tensor $F_{\mu\nu}$ looks like a clover. See Figure 1.3.

The staggered, or Kogut-Susskind discretization decomposes the spinor components of the fermions to the points of a hypercube, and after a diagonalization in spin space, we only keep one component, reducing the number of species by a factor 4. To see how this happens, we start with the naive action, i.e. equation (1.16), and diagonalize in spin space, by the transformations:

$$\Psi_{x\alpha} \equiv \Psi(x)_\alpha = T_{\alpha\beta}\,(x)\,\chi\,(x)_\beta \equiv T_{\alpha\beta}\,(x)\,\chi_{x\beta} \tag{1.20}$$

$$\bar{\Psi}_{x\alpha} \equiv \bar{\Psi}(x)_\alpha = \bar{\chi}\,(x)_\beta\,\bar{T}_{\beta\alpha}\,(x) \equiv \bar{\chi}_{x\beta}\bar{T}_{\beta\alpha}\,(x)\,, \tag{1.21}$$

such that $\bar{T}(x)\gamma_\mu T(x + a\hat{\mu}) = \eta_\mu(x)\mathbb{1}$, which implies $\bar{T}(x)\gamma_\mu T(x - a\hat{\mu}) = \eta_\mu(x - a\hat{\mu})\mathbb{1}$, we

then have:

$$S_F = \frac{1}{2}\sum_{x,\alpha}\Bigg[\sum_{\mu}\Big(\eta_\mu(x)\,\bar{\chi}_\alpha(x)\,U_{x,\mu}\chi_\alpha(x+a\hat{\mu}) - \\ - \eta^*_\mu(x-a\hat{\mu})\,\bar{\chi}_\alpha(x)\,U_{x-a\hat{\mu},\mu}\chi_\alpha(x-a\hat{\mu})\Big) + \\ + am\bar{\chi}_\alpha(x)\,\chi_\alpha(x)\Bigg]. \quad (1.22)$$

Here, there is a 4 times degeneracy in α, dropping the sum in α, the action will describe 4 fermion species with the same mass. A choice of $T(x)$ that implements this diagonalization is: $T(x) = \gamma_1^{n_1}\gamma_2^{n_2}\gamma_3^{n_3}\gamma_4^{n_4}$, where $an_i = x_i$. With this choice the staggered action becomes:

$$S_F^{\text{staggered}} = \sum_x\left[am\bar{\chi}\chi + \frac{1}{2}\sum_\mu \eta_\mu(x)\left(\bar{\chi}_x U_{x;\mu}\chi_{x+a\hat{\mu}} - \bar{\chi}_x U_{x-a\hat{\mu};\mu}\chi_{x-a\hat{\mu}}\right)\right], \quad (1.23)$$

where $\eta_\mu(x) = (-1)^{x_1+x_2+\ldots x_{\mu-1}}$ and the χ fields have only 1 spin component. The advantages of this formalism are that from chiral symmetry we will have an unbroken part of $U(1)_L \times U(1)_R$, meaning there will be no additive mass renormalization, and the differences from continuum results are $\mathcal{O}(a^2)$. Also, it is computationally less costly than Wilson fermions. The disadvantage is that the different elements of a Dirac spinor see different gauge fields, leading to taste symmetry breaking. The coarser the lattices, the worse it is. Also, in the continuum limit, there remain 4 degenerate species of fermions. Simulation of 2+1 flavours of fermions with staggered discretization involves the not proven fourth root trick[10], discussed shortly.

Chiral fermions satisfy the Ginsparg-Wilson relation:

$$\{\gamma_5, D\} = aD\gamma_5 D, \quad (1.24)$$

providing a lattice version of chiral symmetry that does not break, but satisfying the Nielsen-Ninomiya theorem. A construction that satisfies this relation is the Neuberger construction. We define:

$$A = 1 - aD_W, \quad (1.25)$$

where D_W is the massless Wilson type Dirac-operator, and the Neuberger (or overlap) type Dirac-operator to be:

$$D = \frac{1}{a}\left(1 - \frac{A}{\sqrt{A^\dagger A}}\right). \quad (1.26)$$

[10]The resulting action is not local but every numerical evidence suggest that it is in the correct universality class.

This discretization combines the advantages of the Wilson and overlap discretizations, since it has a lattice version of chiral symmetry, but is still conceptually clear, as it does not need the fourth root trick (discussed below). The disadvantage is that it is computationally much more costly, since the fermion matrix is dense in this case, not sparse.

In general the fermion action is bilinear in the fermion fields:

$$S_F = \sum_{x,y} \bar{\Psi}_x Q_{xy}(U) \Psi_y, \tag{1.27}$$

where color, flavour and spin indices have been suppressed. Fermions are represented by Grassmann variables, leading to[11]:

$$\int \mathcal{D}\bar{\Psi}\mathcal{D}\Psi e^{-S_F} = \det Q(U). \tag{1.28}$$

The analytical evaluation of the fermionic part of the functional integral is necessary, since the calculations are done with Monte Carlo algorithms and importance sampling, and we cannot do that for Grassmann variables. The partition function then can be rewritten as:

$$Z = \int \mathcal{D}U \det Q(U) e^{-S_g(U)} = \int \mathcal{D}U e^{-(S_g(U) - \ln \det Q)}, \tag{1.29}$$

meaning that the theory including both fermions and gluons leads to an effective theory with only gluonic degrees of freedom and $S_{\text{eff}} = S_g - \ln \det Q(U)$. This action is non-local, the fermionic determinant $\det Q$ can contain interactions between points arbitrarily far away on the lattice. This is the main reason why the numerical simulation of full QCD is much more difficult than the simulation of pure gauge theories.

If we want to describe more fermion species, we get:

$$Z(m_1, m_2, ..., m_{N_f}) = \int \mathcal{D}U \det Q(m_1; U) ... \det Q(m_{N_f}; U) e^{-S_g(U)}. \tag{1.30}$$

In the case of Wilson and overlap fermions this can be used to describe 2+1 fermion flavours. For staggered fermions one needs to use and extra trick. Since one Ψ field describes 4 fermions with the staggered action, the simulation of N_f fermion flavour goes with:

$$Z(N_f) = \int \mathcal{D}U \left[\det Q(U)\right]^{N_f/4} e^{-S_g(U)}. \tag{1.31}$$

[11] If we consider a functional integral that gives the expectation value of some function of the fermionic fields, we can also evaluate the fermionic part of the functional integral analytically (for a fixed gauge background), and it is given by the usual Wick contractions.

We expect this expression to describe N_f flavours in the continuum limit. With equation (1.29) we have seen that it can be derived from a local continuum theory, but it is not so clear in this case. Every numerical result so far seems to indicate that this so called fourth root trick works.

1.1.3 Continuum limit

The ultimate goal of lattice gauge theory is to give results in the $a \to 0$ limit, corresponding to the continuum theory, not at a finite lattice spacing, so it is desirable to make a continuum extrapolation, whenever feasible. The extrapolation goes as follows. We saw that the correlation length of some operator, in lattice units is:

$$\xi = \frac{1}{ma}, \tag{1.32}$$

with m being a mass in the theory. To make the zero lattice spacing limit with fixed masses, the correlation length ξ has to diverge. This is analogous to statistical physical systems at the critical point.

In pure gauge theory at $T = 0$, there is only one free parameter in the theory, the pure gauge coupling:

$$\beta = \frac{6}{g^2}, \tag{1.33}$$

and this is the parameter that controls the continuum limit. The continuum limit is controlled by a renormalization group equation, mathematically similar to the Callan-Symanzik equations in the usual field theoretical renormalization group, but in spirit closer to the Wilsonian renormalization (since we keep the renormalized couplings fixed). Asymptotic freedom means, that if we approach the continuum limit with fixed renormalized couplings, the bare coupling g will go to zero. This is controlled by the lattice β function[12], that can be expressed in perturbation theory as:

$$\beta_{\mathrm{LAT}} = -\left(a\frac{\partial g}{\partial a}\right)_{g_R=\mathrm{fix}} = -\beta_0 g^3 - \beta_1 g^5 + ..., \tag{1.34}$$

with $\beta_0 > 0$. Solving for the lattice spacing, an integration constant with dimensions of mass appears (this is called dimensional transmutation), and we get:

$$a = \Lambda_{\mathrm{LAT}}^{-1} \exp\left(-\frac{1}{2\beta_0 g^2}\right) (\beta_0 g^2)^{-\frac{\beta_1}{2\beta_0^2}} \left(1 + \mathcal{O}(g^2)\right). \tag{1.35}$$

[12]Not to be confused with the bare parameter β.

Solving equation (1.35) for g shows that we will have $g \to 0$ as $a \to 0$, this a manifestation of asymptotic freedom: the existence of a Gaussian UV fixed point of the theory. Now, the lattice spacing itself does not appear in the lattice action, or even if it does, it can be absorbed into the fields. So, we have to fix the scale by some arbitrary prescription. For example, with the plaquette action at $\beta = 6.0$, the string tension from the static potential is $a\sqrt{\sigma} = 0.22$. This means that if we fix the scale with $\sigma = 460\text{MeV}$, we get $a\,(\beta = 6.0) = 0.095\text{fm}$. Equation (1.35) then gives $a(\beta)$ everywhere else (at least close to the continuum limit, where perturbation theory applies).

In pure gauge theory every quantity with dimensions of a mass, like a glueball mass, is proportional to Λ_{LAT}, and therefore will scale as[13]:

$$ma = C \exp\left(-\frac{1}{2\beta_0 g^2}\right) \left(\beta_0 g^2\right)^{-\frac{\beta_1}{2\beta_0^2}} \left(1 + \mathcal{O}(g^2)\right). \tag{1.36}$$

Now, if we consider say the ratio of two glueball masses, say m_1 and m_2, the exponential factor will drop out, and we will be left with:

$$\frac{m_1}{m_2} = \frac{C_1}{C_2}\left(1 + \mathcal{O}(a^2)\right). \tag{1.37}$$

This behavior is called scaling, and is the basis for determining the continuum limits of masses in the theory. The same reasoning applies to the ratio of any 2 quantities with dimensions of mass, say a glueball mass and the string tension (which we used in the previous paragraph as an example for scale fixing).

Now let us consider QCD at $T = 0$. From the point of view of asymptotic freedom the continuum limit is similar to that of pure gauge theory. The continuum limit still means the $g \to 0$ limit[14]. The additional complication here is that other than the gauge coupling, the bare quark masses also appear as parameters of the theory. For instance, if we have one additional mass parameter in the theory, we do not know a priori, how the new free parameter, the quark mass, has to be adjusted as we take the continuum limit. To fix this, an additional condition is needed. This is usually chosen in a way that the ratio of some masses in the theory (say the pion mass and the proton mass), stay constant. The line in the g, m_q plane, where this ratio stays constant is known as a line of constant

[13]This equation also suggests the non-perturbative origin of the mass m.

[14]Fermions give a contribution of opposite sign as the gauge bosons to the coefficient β_0, but the property of asymptotic freedom persists for $N_f < 17$.

physics (LCP). Of course if we have more parameters, we need more conditions to fix this line. LCPs defined from keeping different quantities fixed are of course different, but if the fixed quantities correspond to the same continuum theory, they will converge to each other in the continuum limit. The LCPs are usually determined non-perturbatively, with zero temperature simulations at different values of the bare parameters.

Finally, we consider continuum extrapolation at finite temperature. The LCP - determined from $T = 0$ simulations - gives us the way in which we need to change the parameters of the action to make the mass ratios, like m_π/m_K fixed as we do the continuum limit. If we then fix the scale by choosing a physical hadron mass, the LCP will give us a function: the lattice spacing (say in Fermis) given by the gauge coupling constant β:

$$\text{LCP} \quad \longrightarrow \quad \text{a}(\beta). \tag{1.38}$$

The temperature is given by $T = 1/(N_t a)$. This means we have two ways of controlling the temperature. We either change the lattice spacing a, or we change the number of lattice sites in the temporal direction N_t. Both have their merits. If we control the temperature by changing a (or β) we can have a good systematic scan of temperature dependent variables (say a susceptibility) and will be able to know the temperature dependence in many points. But, this presumes that we know the LCP in many points. Then if we want to do a continuum limit at a fixed temperature we can do in by changing N_t, since at a fixed temperature $1/N_t^2 \propto a^2$. This is the procedure usually followed in calculations with staggered fermions. For Wilson fermions determining the LCP at many points is difficult (due to the fact that Wilson fermions explicitly break chiral symmetry, and therefore introduce an additive renormalization for the quark masses). Here, the opposite choice is made. The temperature is controlled by N_t while the continuum limit, done at a fixed temperature, is controlled by β.

1.1.4 Quenched approximation vs dynamical quarks

There are some phenomenological facts in low energy hadron physics, like the OZI rule, that suggest that closed quark loops give small contributions to the path integral. This is the basis of the so called quenched approximation, which amounts to replacing the quark determinant in equation (1.31) with a gauge field independent constant. This is an enormous simplification for Monte Carlo simulations, since in the quenched approximation, the updating can be done with the pure gauge action S_G. Then some observable

containing fermions will be:

$$\left\langle \psi_{y_1}\bar{\psi}_{x_1}...\psi_{y_n}\bar{\psi}_{x_n}\right\rangle = \frac{1}{Z}\int D[U]e^{-S_G}\sum_{z_1,...,z_n}\epsilon^{z_1...z_n}_{y_1...y_n}Q[U]^{-1}_{z_1x_1}...Q[U]^{-1}_{z_nx_n}, \tag{1.39}$$

where $Q[U]^{-1}$ is the inverse quark matrix, i.e. the quark propagator. Early calculations with the quenched approximation showed great promise. For example, the quenched approximation reproduces the measured light hadron spectrum reasonably well. See e.g. [19]. We have to stress however, that this is an uncontrolled approximation.

For example, at finite temperature the quenched approximation proved to be wrong. Quenched simulations at $\mu_B = 0$ show a first order phase transition, while simulations with dynamical quarks at the physical quark masses show an analytic cross-over [6]. The transition temperature is also significantly lower with dynamical quarks. These results suggest that the quenched approximation is not appropriate at finite temperature, and therefore it is important to include dynamical quarks when studying the deconfinement aspects of the transition, like we do in this work.

1.1.5 The Hybrid Monte Carlo algorithm

Here we briefly review the Hybrid Monte Carlo algorithm. For a more complete, pedagogical treatment see [2] or [20]. Lattice QCD simulations are based on Monte Carlo integration with importance sampling. The partition function for $N_f = 2$ flavours of quarks is:

$$Z = \int \mathcal{D}U(\det Q(m;U))^2 e^{-S_G(U)}. \tag{1.40}$$

at zero chemical potential the quark determinant is real and therefore the product

$$p(U) = \frac{1}{Z}(\det Q(m;U))^2 e^{-S_G(U)} = \frac{1}{Z}e^{-S_{\text{eff}}(U)} \tag{1.41}$$

is a normalized probability density on the space of all link variables U. The physics described by the theory are extracted from expectation values of the form:

$$\langle O\rangle = \int \mathcal{D}U p(U)O(U). \tag{1.42}$$

To calculate these we need a representative ensemble $\{U_1, ..., U_N\}$ of gauge fields that are obtained by choosing the fields randomly with probability $p(U)\mathcal{D}U$. If we have such an ensemble, then the expectation values in the lattice theory are given by:

$$\langle O\rangle = \lim_{N\to\infty}\sum_{i=1}^{N} O(U_i). \tag{1.43}$$

Of course, in numerical computations we can not take the $N \to \infty$ limit, we always have a finite sample size. To estimate the statistical errors we use the jackknife method [2].

Some distributions, e.g. multi-dimensional Gaussian distributions[15] can be generated directly. In general, however, representative ensembles are generated through some recursive procedure (a Markov process) which obtains the field configurations one after another according to some stochastic algorithm. Markov processes are characterized by a transition probability density $T(U \to U')$ that specifies the probability $T(U \to U')\mathcal{D}U'$ for the next configuration to be in the volume element $\mathcal{D}U'$ surrounding U' when the current configuration is U. When trying to construct such transition probabilities, one is guided by the following plausible requirements:

1. $T(U \to U') \geq 0$ for all U, U'. $\int \mathcal{D}U' T(U \to U') = 1$ for all U.
2. $\int \mathcal{D}U T(U \to U') p(U) = p(U')$ for all U'
3. Every gauge field configuration U has an open neighborhood N such that $T(U \to U') \geq \epsilon$ for some positive ϵ and all $U, U' \in N$.

Property 3 ensures that, in every step, the Markov process spreads out in an open neighborhood of the current field configuration. Moreover, using the compactness of the field manifold, it is possible to show that the process will reach any region in field space in a finite number of steps. For the simulations of pure gauge fields, one-link update algorithms (like the Metropolis or the heat-bath algorithm) are often used. The difficulty with the inclusion of dynamical quarks in the simulations is that the determinants of the fermion matrix depend non-locally on the gauge field. In particular, one-link update algorithms would require a computational effort proportional to the square of the lattice volume and are therefore not practical. The Hybrid Monte Carlo (HMC) [21] algorithm updates all link variables at once and has a much better scaling behavior with respect to the lattice volume.

First, since the calculation of the determinant is costly, we introduce pseudofermion fields. These are complex scalar fields $\Phi(x)$. Using the rules of Gaussian integration, the determinant of an invertible, hermitian, and positive definite matrix H can be written as:

$$\det H \sim \int \mathcal{D}\Phi^\dagger \mathcal{D}\Phi \exp\left(-\Phi^\dagger(x) H^{-1}_{x,y} \Phi(y)\right), \tag{1.44}$$

[15] Simulation of free scalar fields would be an example of this.

now since the fermion matrix Q is generally not hermitian, we can't use this formula. But only a slight modification is needed. If $\det Q$ is real and positive, then $\det Q = \sqrt{\det\left(Q^\dagger Q\right)}$. Using this we have:

$$\left(\det Q\left(U\right)\right)^2 \sim \int \mathcal{D}\Phi^\dagger \mathcal{D}\Phi \exp\left(-\Phi^\dagger(x)\left[Q^\dagger(U)Q(U)\right]^{-1}_{x,y}\Phi(y)\right), \tag{1.45}$$

meaning that the fermionic part of the functional integral is reduced to a bosonic one, with a new part in the action:

$$S_{\mathrm{PF}} = \sum_{x,y} \Phi^\dagger \left[Q^\dagger(U)Q(U)\right]^{-1}\Phi, \tag{1.46}$$

with this, the action to simulate reads:

$$S(U,\Phi) = S_G(U) + \sum_{x,y}\Phi^\dagger(x)\left[M^\dagger(U)M(U)\right]^{-1}_{x,y}\Phi(y), \tag{1.47}$$

where we have suppressed flavour, spinor, and color indices. Writing these explicitly, we would have $U_{x,\mu,cd}$, where c, d are color indices, and $\Phi_{x,q,\alpha,c}$, where q is a flavour, α is a spinor, and c is a color index.

In the HMC algorithm, we think about this modified action as a potential in a Hamiltonian. To do this, we have to introduce the conjugate momenta for the link variables. These are elements of the $su(3)$ Lie algebra, that we can write as $P_{x,\mu} = \sum_{a=1}^{8} i\lambda_a P_{x,\mu,a}$, where the λ_a are the Gell-Mann matrices. Let us define $P^2/2 = \sum_{x,\mu}\left|P_{x,\mu}\right|^2/2$. With these notations the Hamiltonian can be defined as:

$$H(P,U) = \frac{P^2}{2} + S(U) + \sum_{x,y}\Phi^\dagger(x)\left[M^\dagger(U)M(U)\right]^{-1}_{x,y}\Phi(y). \tag{1.48}$$

By performing the Gaussian integral in π it is easy to see that:

$$\int \mathcal{D}U O(U) e^{-S(U)} = \text{const.} \times \int \mathcal{D}\mathrm{U}\mathcal{D}\pi\mathrm{O(U)e^{-H}}, \tag{1.49}$$

meaning that the addition of the field π does not affect the physics content of the theory. In this form the theory looks like a classical statistical mechanical system that describes gas molecules. We can therefore solve the corresponding Hamiltonian equations in a t fictitious time, unrelated to the Euclidean time in the original formulation. The solutions of these equations may be visualized as trajectories $U(t)$ and $P(t)$ in field space (more correctly, phase space) in the variable t. The pseudofermion fields $\Phi^\dagger$ and Φ are generated directly, with a global heatbath algorithm. Using HMC, the steps leading from the current gauge field $U(x,\mu)$ to the next field $U'(x,\mu)$ are the following:

1. For a fixed field U, the field P is generated randomly with probability density proportional to $e^{-\frac{1}{2}P^2}$, and similarly for the pseudofermion fields Φ and $\Phi^\dagger$. This is done via a global heatbath algorithm.

2. The molecular-dynamics equations are integrated from $t = 0$ to $t = \tau$, taking P and U as the initial values of the fields.

3. The new gauge field U' is set to the field $U(t = \tau)$ obtained from the molecular-dynamics evolution with probability $\min(1, e^{-\Delta H})$, with $\Delta H = H(t = \tau) - H(t = 0)$

Notice, that if the Hamiltonian equations can be solved exactly, then $\Delta H = 0$, meaning U' is set to the field $U(t = \tau)$ with probability 1. This would already lead to a consistent algorithm satisfying the three conditions required from a Markov process. Numerical algorithms however violate the conservation of the Hamiltonian. In this case, this acceptance probability is needed.

There might be some additional difficulties with $N_f = 2 + 1$ flavours with respect to $N_f = 2$, since the determinant of the strange quark operator is not guaranteed to have the same sign at all gauge configurations. The presence of positive and negative contributions to the partition function could potentially ruin the probabilistic foundations on which numerical simulations are based. In practice however, this is not a problem anymore. The reason is simple. In the continuum, we know that $\det M > 0$ for any positive quark mass. If the quarks have only multiplicative renormalization, like with staggered fermions, then this problem does not appear at all, even at finite lattice spacing. With Wilson quarks, the problem can potentially appear, because of additive mass renormalization. However, close enough to the continuum, it should already be true that the regions in field space, where the strange-quark determinant is negative, have a totally negligible weight in the functional integral. Historically this was not always true, but today, when we can use large lattice volumes, small lattice spacings, and improved actions, there is no such problem anymore. For this reason instead of M_s we consider the operator $|M_s| = \sqrt{M_s^2}$. This is guaranteed to have a positive determinant. Although well defined, the operator $|M_s|$ is not directly accessible and one is forced to use approximations of it. The approximation we will use in this work is a rational function approximation. This is where the name of the algorithm RHMC [22] comes from. An other approximation considered in the literature is a polynomial approximation, giving rise to the PHMC [23] algorithm.

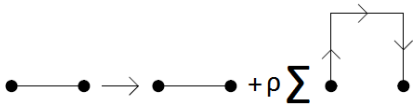

Figure 1.4: Illustration of APE smearing. Every spatial link is replaced by itself plus a real weight times to sum of its four spatial neighboring staples, projected back into $SU(3)$. This projection is not unique and needs to be carefully defined to preserve the symmetries of the original link variables.

1.1.6 Gauge field smearing

A customary procedure to improve the scaling of lattice calculations is gauge field smearing. This means an averaging of the the links in a local and gauge covariant way. Of course, such an averaging washes out fluctuations on small scales, leading to a modified ultraviolet behavior of the gauge fields. One might ask: Is this correct? If the smearing radius is fixed in lattice units, then, as long as a continuum limit is taken, the smearing radius will also go to zero, leading to physical behavior of the n-point functions. The reason this is often done, is that it improves the signal-to-noise ratio of many observables. In the case of staggered fermions it also reduces taste breaking. In the case of Wilson fermions, it improves the chiral behavior. Because of these beneficial properties, we use smearing in the fermionic part of the action. If we call the original link variables U, and the smeared variables V, then the action looks like:

$$S = S_G[U] + S_F[V]. \tag{1.50}$$

The smearing method applied in both the Wilson and staggered fermion actions used in this work is stout smearing, which will be introduced shortly.

The first proposed smearing procedure was to replace each thin link by a weighted sum of staples. This is called APE smearing, and was introduced in [25]. This is illustrated in Figure 1.4. Usually, the original links are called thin links, while the smeared links are called fat links. The method can be extended to cover a whole hypercube that includes the link under consideration. This is called HYP smearing and was introduced in [24]. HYP smearing is illustrated in Figure 1.5

Using smearing is not unproblematic with Hybrid Monte Carlo, since one has to com-

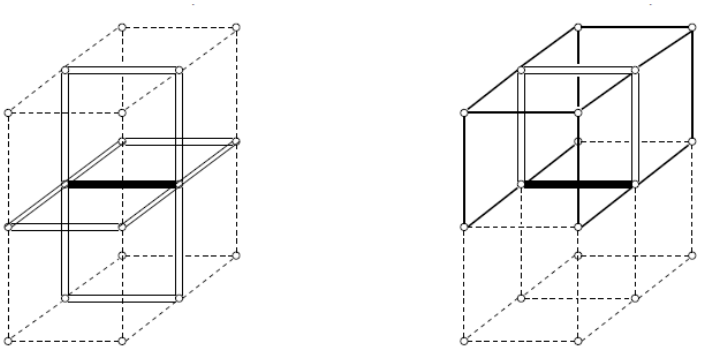

Figure 1.5: Illustration of HYP smearing in 3 dimensions from Ref. [24]. Each fat link is built from the four double line staples (left). Each double line link is built from two staples which only extend to the hypercube attached to the original link (right).

pute the derivative with respect to the thin links. The difficulty within e.g. APE smearing lies in the projection back to $SU(3)$, that one has to perform in the end (since the staple sum is no longer in $SU(3)$).

A method where this problem is not present is stout smearing, introduced in [26]. It consists of replacing the link at site x and in direction μ according to $V_{x,\mu} = e^{iQ_{x,\mu}}U_{x,\mu}$, where $Q_{x,\mu}$ is a traceless hermitian matrix constructed from staples, so that $e^{iQ_{x,\mu}}$ is manifestly in $SU(N)$, making the projection unnecessary. Also, this smearing method is analytic everywhere, and therefore there are no complications in taking the derivative with respect to the link variables. For details, see [26].

Smearing will be important in our determination of the static quark free energy and the electric and magnetic screening masses. The main point is: stout smearing is in the fermionic action of the Budapest-Wuppertal collaboration, therefore fields are generated with stout smearing in the fermionic part of the action. After the configurations are generated with HMC, before the measurement on the generated lattice, HYP smearing can be used on the gauge fields, to improve the statistical errors of some observables (in our case, the long distance tails of the correlators).

1.2 The naive potential picture of quarkonia at $T > 0$

Quarkonia are very non typical hadrons: the c and b quarks are heavy, and the mass of the $Q\bar{Q}$ bound state is largely determined by the bare c or b mass. Therefore one expects that a non-relativistic Schrödinger-equation:

$$\left(2M - \frac{\nabla^2}{M} + V(r)\right)\Psi = E\Psi,$$

with the potential roughly of the Cornell form[16]:

$$V(r) \approx \sigma r - \alpha_{\text{eff}}/r,$$

should describe the system to some approximation. Actually, if this Schrödinger equation is solved, the charmonium spectra is reasonably well reproduced even in this naive model. For a very basic exposition see the textbook [27]. For a modern treatment with effective field theoretical techniques see [28].

Matsui and Satz [13] assumed that such a potential picture still describes the $Q\bar{Q}$ system at $T > 0$. Then after deconfinement the string tension will be $\sigma = 0$ and the Coulombic part of the interaction will be screened:

$$V(r) \approx -\frac{\alpha_{\text{eff}}(T)}{r}\exp\left(-m_{\text{sc}}(T)r\right).$$

This Yukawa potential can still produce bound states. If $m_{\text{sc}} = 0$ we will have an infinite number of bound states like in the H atom. As the temperature increases, m_{sc} increases, and we will have less, and less bound states, until we will have none. One can obtain a quick estimate for the result by using an estimate for the ground state energy coming from the uncertainty relation $< p^2 >< r^2 > \approx 1$:

$$E \approx 2m + \frac{p^2}{2m} + V(r) \approx 2m + \frac{1}{2mr^2} + V(r).$$

Minimizing $E(r)$ we get $x(x+1) = (M\alpha_{\text{eff}}/m_{\text{sc}})^{-1}$ with $x = rm_{\text{sc}}$. This equation for x only has a solution if $(M\alpha_{\text{eff}}/m_{\text{sc}})^{-1} \leq 0.84$, giving us the maximum allowed value of the screening mass for a bound state to exist. Numerical solution of the Schrödinger equation leads to similar results [29]. What does this naive potential picture tell us? Exactly what

[16] Actually, this linear rise is only true for pure gauge theory. If there are dynamical quarks included, the potential flattens when there is enough energy to form a new quark-antiquark pair. This is called string breaking.

we would want for a thermometer. We will have for example the J/Ψ and Υ dissociations at quite different temperatures since the mass is quite different, but the potential is supposed to be the same.

There are theoretical problems with this model. At finite temperature, because of decoherence caused by random kicks from the media, it is not clear at all if such a potential picture can apply. In general, at finite temperature we do not have a bound state wave function, we have a density matrix for the subsystem $\bar{Q}Q$. If we insist on using a bound state wave function as an approximation, that means we have the underlying assumption that the J/Ψ is a tightly bound state, and it is unlikely, that a soft collision from the medium can break it. This may be a good approximation at low temperatures, but close to the dissociation temperature it surely breaks down, since then the J/Ψ should not be a tightly bound state anymore. This means that a reliable calculation of the J/Ψ dissociation from such a picture is problematic. Even if the naive potential picture is a good approximation, it is not clear what potential one should use[17]. The easiest way to frame this problem is: there are various thermodynamic potentials that reduce to the energy as $T \to 0$, which one should one put in such a model is not at all clear. It seems that the naive picture, where we have a bound state wave function even at finite temperature is not adequate. That does not necessarily mean that it does not give a good approximation for the dissociation temperature, but it does mean that a more careful theoretical investigation is needed.

1.3 The spectral function

For a more careful theoretical investigation, one first has to formulate the problem more precisely. Starting from QCD it is not at all clear what the meaning of the wave function in the naive potential picture could be. The problem can be formulated clearly in terms of real time correlators, or the spectral function (SF). In this section, we state the definition and the important properties of the spectral function, that will become important later in the text. The intent is for this part to be self-contained, however, we will not state the derivations for some of the statements here. For that I advise to look up the standard textbooks [4] and [5], and the review article [30]. Let us first define the following real

[17] More will be said about this question in Section 3.1.

time thermal correlators of two Heisenberg picture operators M and N:

$$G_{>}^{MN}(t) = Tr\left(\rho M(t)N(0)\right) \tag{1.51}$$

$$G_{<}^{MN}(t) = Tr\left(\rho N(0)M(t)\right) \tag{1.52}$$

$$G^{MN}(t) = iTr\left(\rho[M(t), N(0)]\right) = i\left(G_{>}^{MN}(t) - G_{<}^{MN}(t)\right) \tag{1.53}$$

$$G_{R}^{MN}(t) = G^{MN}(t)\theta(t) \tag{1.54}$$

We suppressed the spatial coordinates, to make the notation shorter. Lattice techniques can directly calculate correlators in imaginary time (Euclidean correlators), defined by analytic continuation:

$$G_{E}^{MN}(\tau) = G_{>}^{MN}(-i\tau). \tag{1.55}$$

A quantity of considerable interest is the spectral function, which is given by the Fourier transform of the correlator G^{MN}:

$$A^{MN}(\omega) \equiv -iG^{MN}(\omega) = -i\int_{-\infty}^{\infty} dt\, e^{i\omega t} G^{MN}(t) = \int_{-\infty}^{\infty} dt e^{i\omega t}\, \mathrm{Tr}\left(\rho\left[M(t), N(0)\right]\right). \tag{1.56}$$

Let us also introduce the Fourier-transform of the retarded correlator as:

$$G_{R}^{MN}(\omega) = \int_{-\infty}^{\infty} dt e^{i\omega t} G_{R}^{MN}(t) = \int_{0}^{\infty} dt e^{i\omega t} G_{R}^{MN}(t) = \int_{0}^{\infty} dt e^{i\omega t} G^{MN}(t). \tag{1.57}$$

We shall see shortly, this quantity has an important role to play in linear response theory.

After this series of definitions, we continue by a brief review of some properties of the spectral function and argue why it is of particular importance. First, time-translation invariance implies:

$$G_{<}^{MN}(t) = G_{>}^{NM}(-t), \tag{1.58}$$

$$G_{>}^{MN}(t) = G_{<}^{NM}(-t), \tag{1.59}$$

$$G^{MN}(t) = -G^{NM}(-t). \tag{1.60}$$

Next, let us consider an analytic continuation in t and allow the time argument to be complex as well. This will be useful in deriving relations between Euclidean and real time correlators. Using $N^{\dagger}(t) = e^{iHt}N^{\dagger}(0)e^{-iHt}$, the following reality properties can be easily shown:

$$G_{>}^{M^{\dagger}N^{\dagger}}(t) = G_{<}^{MN}(t^{*})^{*}, \tag{1.61}$$

$$G_{<}^{M^{\dagger}N^{\dagger}}(t) = G_{>}^{MN}(t^{*})^{*}, \tag{1.62}$$

$$G^{M^{\dagger}N^{\dagger}}(t) = G^{MN}(t^{*})^{*}. \tag{1.63}$$

The spectral function enjoys the following properties:

$$A^{MN}(\omega) = -A^{NM}(-\omega) \tag{1.64}$$

$$A^{M^\dagger N^\dagger}(\omega) = -A^{MN}(-\omega)^* = A^{NM}(\omega)^*, \tag{1.65}$$

where the first is a consequence of equations (1.58) - (1.60) and the second of equations (1.61) - (1.63), and we assumed a real ω. Using the cyclicity of the trace, it is also easy to show the so called Kubo-Martin-Schwinger (KMS) relation, valid for equilibrium thermal correlators:

$$\begin{aligned} G_>^{MN}(t) &= Z^{-1} \operatorname{Tr}\left(e^{-\beta H} M(t) N(0)\right) = Z^{-1} \operatorname{Tr}\left(N(0) e^{-\beta H} M(t) e^{\beta H} e^{-\beta H}\right) \\ &= Z^{-1} \operatorname{Tr}\left(e^{-\beta H} N(0) M(t + i\beta)\right) = G_<^{MN}(t + i\beta) = G_>^{NM}(-t - i\beta). \end{aligned} \tag{1.66}$$

In Fourier space this leads to:

$$G_<^{MN}(\omega) = e^{-\beta\omega} G_>^{MN}(\omega). \tag{1.67}$$

The KMS relation is of great importance in quantum statistical mechanics. In particular, we will use it to derive the relationship between the Euclidean correlators and the spectral function in the beginning of Chapter 2. As a special case of the KMS relation, the Euclidean correlator satisfies:

$$G_E^{MN}(\tau) = G_E^{NM}(\beta - \tau). \tag{1.68}$$

In this work, when studying the spectral functions, we will always have $N = M = M^\dagger$, M and N bosonic and $\rho = \frac{1}{Z} e^{-\beta H}$. This leads to important simplifications. Let us summarize them:

- By eq. (1.68), $N = M$ implies that G_E is symmetric around $\tau = \beta/2$. This means that if we have N_t points in the Euclidean time direction, only $N_t/2$ are independent.
- $N = M^\dagger$ implies that G_E is real. This can be derived easily using the reality properties of the correlators.
- $N = M^\dagger$ implies that A is real, courtesy of equation (1.65).
- From equation (1.60) and (1.63), we can show:

  $$A^{MN}(\omega) = \frac{1}{i}\left(G_R^{MN}(\omega) - G_R^{N^\dagger M^\dagger}(\omega)^*\right), \tag{1.69}$$

  in the special case of $N = M^\dagger$, this reduces to:

  $$A^{MM^\dagger}(\omega) = 2 \operatorname{Im} G_R^{MM^\dagger}(\omega). \tag{1.70}$$

This is an other way to see that A is real in this case. In the literature this special case is often presented as the definition of the spectral function.

With these simplifications in mind, a physical picture of the dissociation of bound states can be given:

- By inserting a complete set of states, and putting in the spatial variables as well, and letting x be the position four-vector, we have:

$$\begin{aligned}\frac{Z}{i}G^{MM^\dagger}(x) = Tr(e^{-\beta H}[M(x), M^\dagger(0)]) = \sum_n \langle n|\, e^{-\beta H}\left[M(x), M^\dagger(0)\right]|n\rangle = \\ = \sum_{m,n}\left(e^{-\beta E_n} - e^{-\beta E_m}\right)\langle n|\, M(x)\,|m\rangle\,\langle m|\, M^\dagger(0)\,|n\rangle = \\ = \sum_{m,n}\left(e^{-\beta E_n} - e^{-\beta E_m}\right)e^{i(p_n - p_m)x}\;|\;\langle n|\, M(0)\,|m\rangle\;|^2 \quad (1.71)\end{aligned}$$

  Taking the Fourier transform we get for the spectral function:

$$\begin{aligned}A(k) = \frac{1}{i}\int d^4x e^{ikx} G^{MM^\dagger}(x) = \\ = \frac{1}{Z}(2\pi)^4\sum_{m,n}\delta^{(4)}(k + p_n - p_m)\left(e^{-\beta E_n} - e^{-\beta E_m}\right)\;|\;\langle n|\, M(0)\,|m\rangle\;|^2 \quad (1.72)\end{aligned}$$

- At $T = 0$, we can only get a contribution if either $E_m = 0$ or $E_n = 0$. If $k_0 > 0$ the argument in the δ function can only be zero if $E_m > E_n$, which implies that $E_n = 0$. From this, we can see that at 0 temperature the spectral function reduces to the density of states:

$$A(k_0 > 0, \vec{k}; T = 0) = \frac{1}{Z}(2\pi)^4\sum_m \delta^{(4)}(k - p_m)\;|\;\langle 0|\, M(0)\,|m\rangle\;|^2 \quad (1.73)$$

  This means that the spectral function is a generalization of the density of states to finite temperature.

- Equation (1.72) also shows explicitly that for $k_0 > 0$ we have $A(k_0) > 0$ and for all k_0 we have $A(k_0) = -A(-k_0)$.

- The SF can be calculated exactly for free fields. E.g. for a free Klein-Gordon field we have

$$A^{\phi\phi}(k) = 2\pi\,\mathrm{sign}(k_0)\delta(k_0^2 - \omega_k^2), \quad (1.74)$$

  with $\omega_k^2 = m^2 + \vec{k}^2$. That is we get a δ peak at the energy of the relativistic particle. For this free field, the spectral function is independent of the density matrix. It is the same for all temperatures, chemical potentials, and even in non-equilibrium.

- For some interacting theory at $T = 0$ we get a δ peak for all the stable particles (or bound states) and a continuum for the scattering states. See a sketch on Figure 1.6
- For $T > 0$ the peaks get smeared, because of scattering with particles from the medium.
- But, if the peaks are well separated, they still behave like particles, e.g. they give contributions to thermodynamics quantities that one would expect from particles ([31, 32, 33]), and most importantly for us, the position of a peak will be (correlation length)$^{-1}$ of the Euclidean correlators.
- If the peaks get very wide, so that they are not well separated, then the quasi particle picture is not good anymore, and we can say that the given particle/bound state dissociated or melted.

With this, we have given a consistent framework for the melting of bound states at finite temperature. Of course the exact point at which the peaks get very wide and become not separate peaks is not well defined. It is clear however, that the ultimate goal would be to calculate the spectral functions of the different operators carrying the quantum numbers of the different meson states.

The operator, the SF of which is of particular importance in phenomenology is the electric current:

$$j_\mu^{EM} = \frac{2}{3}\bar{u}\gamma_\mu u - \frac{1}{3}\bar{d}\gamma_\mu d - \frac{1}{3}\bar{s}\gamma_\mu s + \frac{2}{3}\bar{c}\gamma_\mu c + ... \tag{1.75}$$

Correlators if these and other physical currents (like charged weak currents) show up often in calculations of different physical quantities. As an example at $T = 0$, let us consider e^+e^- annihilation to hadrons. It is standard textbook material [1] to show that, to leading order in the electromagnetic coupling, the standard R ratio is:

$$R(s) = \frac{\sigma(e^+e^- \to \text{hadrons})}{\sigma(e^+e^- \to \mu^+\mu^-)} = w(s), \tag{1.76}$$

where $w(s)$ is defined in terms of the the current-current correlators as:

$$w_{\mu\nu} = \int d^4x e^{iqx} \langle 0| \left[j_\mu^{EM}(x), j_\nu^{EM}(0)\right] |0\rangle = \left(q_\mu q_\nu - q^2\eta_{\mu\nu}\right) \frac{1}{6\pi} w(q^2), \tag{1.77}$$

where the last equation shows the most general form of $w_{\mu\nu}$ allowed by Lorentz symmetry and current conservation. It is straightforward to see from these formulas that the R ratio

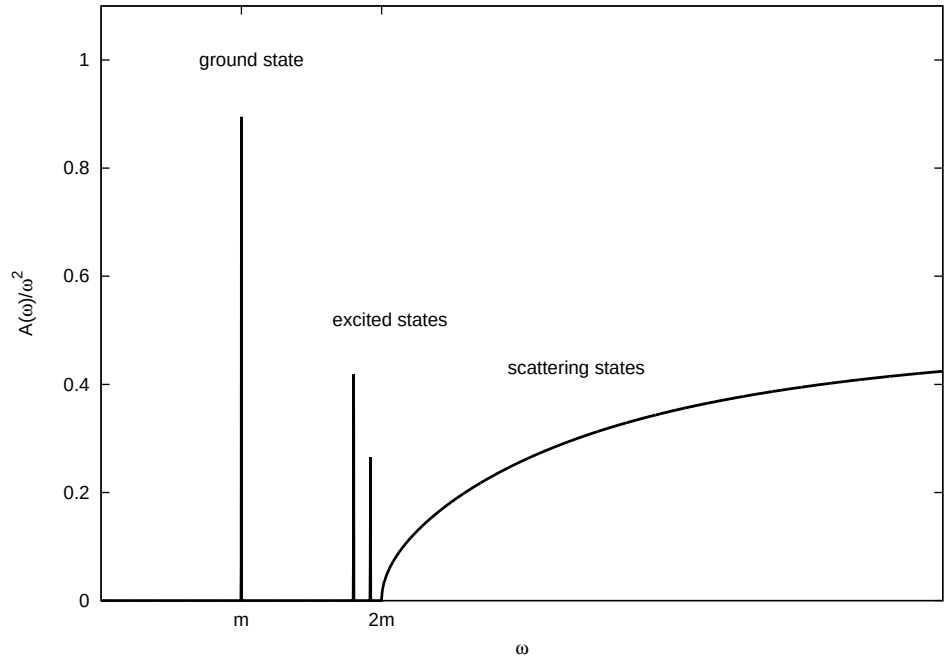

Figure 1.6: A sketch of a possible form of a spectral function in an interacting theory at $T = 0$. The peaks are Dirac δ like. The size of the peak is determined by the matrix element $\langle 0|O|n\rangle$, where O is the operator, whose correlator we are looking at. At finite temperature these delta like peaks will obtain a finite width, and the spectral function will be strictly positive. This finite width can lead to, for example the bound state peaks merging into the 2-particle continuum, making them no longer clearly distinguishable from the 2 particle scattering states. Note, that the onset of the continuum at $T = 0$ is restricted by the symmetry properties of the operators considered. For example, if the 2-particle state has some different symmetry as a one particle state, the continuum might no start at $2m$ but $3m$ instead. As an other example if a (massive)+(zero mass) state has the same quantum numbers as the (massive) state, then the continuum can start at the same spot where the Dirac delta peak is. This can be the case for theories without a mass gap, like QED.

- up to QED corrections - is given by the spectral function of the electromagnetic current as:

$$R(s) = -\frac{2\pi}{s}\left(A^{EM}\right)^{\mu}_{\mu}(s). \tag{1.78}$$

As an example at $T > 0$, let us mention the following important class of scenarios: A system consists of strongly and weakly interacting particle as well. The strongly interacting particles, because of these strong interactions, are in thermal equilibrium, but the weakly interacting particles are not. Therefore, they escape the system. This escape can be literal

(if the system is of finite size) or in an abstract sense (being still within the same volume but not interacting with the thermal particles). Examples of such processes include the decoupling of Dark Matter in cosmology, thermal photon and dilepton production in heavy ion collisions, and neutrino emission from neutron stars. In such scenarios, the particle production rate can be given in terms of the spectral function of physical currents in the thermal medium. For example, for dilepton production rate from hot QCD matter [34, 35, 36]:

$$\frac{dN_{l^+l^-}}{d^4x d^4k} = -\frac{\alpha_{EM}^2}{6\pi^3 k^2} \frac{1}{e^{\beta k_0} - 1} \left(A^{EM}\right)^{\mu}_{\mu}(k). \tag{1.79}$$

The mass of leptons is neglected in this formula for simplicity. Note that this equation is valid irrespective of the state of the system, i.e., whether it is hadronic or a quark-gluon plasma. Of course, to connect this with heavy ion experiments one also has to make some assumptions about the expansion of the fireball. We will not attempt that here. For a review, see Ref. [36].

1.3.1 Kubo formulas and heavy quark diffusion

Another important fact about the SFs is that the small frequency behavior is related to the transport coefficients in hydrodynamics. This relation is encoded in the Kubo formulas. For a set of pedagogical lectures concerning correlation functions in hydrodynamics see Ref. [37]. For a review on transport coefficients from a lattice QCD perspective, see Ref. [30].

In general, Kubo formulas need two ingredients to derive. The first one being hydrodynamics, the second being linear response. Matching the results of the two descriptions, we obtain a relationship between the phenomenological coefficients in the hydrodynamics prescription (transport coefficients) and the real time correlators, entering the formulas of linear response theory. Lots of different transport coefficients can be defined. The general feature is that in all cases, they will be related to the zero frequency behavior of real time retarded correlators.

Let us consider a simple diffusion process. Here let n be the density of some conserved four-current. Then to leading order in gradient expansion of the current $\mathbf{j}$ it will satisfy a

diffusion equation:

$$\partial_t n - D\nabla^2 n = 0 \tag{1.80}$$

this can be solved with a Laplace-transform in time and Fourier-transform in space. For the Fourier transform we define $n(t,\mathbf{k}) = \int \frac{d^3k}{(2\pi)^3} e^{i\mathbf{k}\cdot\mathbf{x}} n(t,\mathbf{k})$, and get:

$$n(t,\mathbf{k}) = e^{-D\mathbf{k}^2 t} n_0(t=0,\mathbf{k}) \equiv e^{-D\mathbf{k}^2 t} n_0(\mathbf{k}). \tag{1.81}$$

For the Laplace-transform we define $n(z,\mathbf{k}) = \int_0^\infty dt e^{izt} n(t,\mathbf{k})$. We get:

$$n(z,\mathbf{k}) = \frac{n_0(\mathbf{k})}{-iz + D\mathbf{k}^2}, \tag{1.82}$$

where $\operatorname{Im} z > 0$ is needed for convergence. For small fluctuations $n(t,\mathbf{x})$ can be written in terms of the source for the charge density n, which is just the corresponding chemical potential, as:

$$n(t,\mathbf{x}) = \left.\frac{\partial n}{\partial \mu}\right|_{\mu=0} \mu(t,\mathbf{x}) \equiv \chi\mu(t,\mathbf{x}), \tag{1.83}$$

giving

$$n(z,\mathbf{k}) = \frac{\chi\mu_0(\mathbf{k})}{-iz + D\mathbf{k}^2}. \tag{1.84}$$

This is the long-wavelength, late-time prediction on the number density from hydrodynamics. The diffusion constant gives the position of a pole at $-iD\mathbf{k}^2$, while the residue of the pole is given by the static susceptibility χ, that determines the initial conditions for the diffusion equation. From the point of view of hydrodynamics, D and χ are phenomenological parameters.

Let us now turn to linear response theory. Here the idea (or thought experiment) is that we apply a small disturbance to a system originally at equilibrium. If we apply the perturbing Hamiltonian δH and measure the physical quantity O, we will have:

$$\delta\langle O(t)\rangle = \langle O(t)\rangle - \langle O\rangle_{\mathrm{eq}} = -i\int_{-\infty}^{t} \mathrm{dt}'\,\langle[\mathrm{O(t)},\delta\mathrm{H(t')}]\rangle_{\mathrm{eq}}\,. \tag{1.85}$$

This formula is powerful because it relates an equilibrium expectation value to a (slightly) non-equilibrium process. In our case the perturbing Hamiltonian will be:

$$\delta H(t) = -\int d^3x \mu(t,\mathbf{x}) n(t,\mathbf{x}), \tag{1.86}$$

and the quantity we measure will be the density n, leading to:

$$\begin{aligned}\delta\langle n(t,\mathbf{x})\rangle = \langle n(t,\mathbf{x})\rangle = i\int_{-\infty}^{t} dt' \int d^3x' \,\langle[n(t,\mathbf{x}), n(t',\mathbf{x}')]\rangle_{\mathrm{eq}}\,\mu(t',\mathbf{x}') = \\ = \int_{-\infty}^{+\infty} dt' \int d^3x' G_R^{nn}(t-t',\mathbf{x}-\mathbf{x}')\mu(t',\mathbf{x}'),\end{aligned} \tag{1.87}$$

where we have used the definition of the retarded correlator (1.54). Taking the Fourier transform in $\mathbf{x}$, we get:

$$\langle n(t,\mathbf{k})\rangle = \int_{-\infty}^{+\infty} dt' G_R^{nn}(t-t',\mathbf{k})\mu(t',\mathbf{k}). \tag{1.88}$$

Next, we write in the Fourier representation of the retarded function in time:

$$G_R^{nn}(t-t',\mathbf{k}) = \int_{-\infty}^{\infty} \frac{d\omega}{2\pi} G_R^{nn}(\omega,\mathbf{k}) e^{-i\omega(t-t')}, \tag{1.89}$$

and get:

$$\langle n(t,\mathbf{k})\rangle = \int_{-\infty}^{+\infty} dt' \int_{-\infty}^{\infty} \frac{d\omega}{2\pi} G_R^{nn}(\omega,\mathbf{k}) e^{-i\omega(t-t')}\mu(t',\mathbf{k}). \tag{1.90}$$

At this point, we have to use a concrete form for the perturbation μ. We assume, that the perturbation we apply is switched on adiabatically at $t=-\infty$ and switched off rapidly at $t=0$:

$$\mu(t,\mathbf{x}) = e^{\epsilon t}\mu_0(\mathbf{x})\theta(-t). \tag{1.91}$$

In this case, the initial conditions, which in the language of hydrodynamics are given by the static susceptibility, in the language of correlators read as:

$$\begin{aligned}\langle n(t=0,\mathbf{k})\rangle &= \int_{-\infty}^{+\infty} dt' G_R^{nn}(-t',\mathbf{k})\mu(t',\mathbf{k}) = \\ &= \int_0^{\infty} dt' G_R^{nn}(t',\mathbf{k})\mu(-t',\mathbf{k}) = \int_0^{\infty} dt' G_R^{nn}(t',\mathbf{k}) e^{-\epsilon t'}\mu_0(\mathbf{k}) = \\ &= G_R^{nn}(z=i\epsilon,\mathbf{k})\mu_0(\mathbf{k})\end{aligned} \tag{1.92}$$

The induced density becomes:

$$\begin{aligned}\langle n(t,\mathbf{k})\rangle &= \int_{-\infty}^{+\infty} dt' \int_{-\infty}^{\infty} \frac{d\omega}{2\pi} G_R^{nn}(\omega,\mathbf{k}) e^{-i\omega(t-t')} e^{\epsilon t'}\theta(-t')\mu_0(\mathbf{k}) = \\ &= \mu_0(\mathbf{k}) \int_{-\infty}^{\infty} \frac{d\omega}{2\pi} G_R^{nn}(\omega,\mathbf{k}) \frac{e^{-i\omega t}}{i(\omega - i\epsilon)}.\end{aligned} \tag{1.93}$$

Now we do the Laplace transform in time (remember $\operatorname{Im} z > 0$):

$$\begin{aligned}\langle n(z,\mathbf{k})\rangle &= \mu_0(\mathbf{k}) \int_0^{\infty} dt e^{izt} \int_{-\infty}^{\infty} \frac{d\omega}{2\pi} G_R^{nn}(\omega,\mathbf{k}) \frac{e^{-i\omega t}}{i(\omega - i\epsilon)} = \\ &\mu_0(\mathbf{k}) \int_{-\infty}^{\infty} \frac{d\omega}{2\pi} G_R^{nn}(\omega,\mathbf{k}) \frac{1}{i(\omega - i\epsilon)} \frac{1}{i(\omega - z)}.\end{aligned} \tag{1.94}$$

To do the integral, we can close the contour in the upper ω half-plane, where the retarded correlator is analytic[18]. There are 2 poles, at $\omega = i\epsilon$ and $\omega = z$. We get:

$$\langle n(z,\mathbf{k})\rangle = \mu_0(\mathbf{k}) \frac{-G_R^{nn}(\omega = i\epsilon,\mathbf{k}) + G_R^{nn}(\omega = z,\mathbf{k})}{iz}. \tag{1.95}$$

[18]This is a consequence of $G_R(t) = 0$ for $t < 0$.

Which leads to

$$G_R^{nn}(z,\mathbf{k}) = G_R^{nn}(z=i\epsilon,\mathbf{k}) + iz\frac{\langle n(z,\mathbf{k})\rangle}{\mu_0(\mathbf{k})} = \frac{1}{\mu_0(\mathbf{k})}\left(\langle n(t=0,\mathbf{k})\rangle + iz\,\langle n(z,\mathbf{k})\rangle\right). \quad (1.96)$$

Up to this point in the linear response analysis, we have not used the previous hydrodynamics formulas. We use them at this point:

$$G_R^{nn}(z,\mathbf{k}) = \chi + iz\frac{\chi}{-iz+D\mathbf{k}^2} = \chi D\mathbf{k}^2\left(\frac{D\mathbf{k}^2+iz}{z^2+(D\mathbf{k}^2)^2}\right). \quad (1.97)$$

This is analytic for $\operatorname{Im} z > 0$, as it should be. We can define $G_R^{nn}(\omega,\mathbf{k})$ for all ω from $G_R^{nn}(z,\mathbf{k})$ by analytic continuation. Using eq. (1.70), this leads to the hydrodynamic prediction for the spectral function:

$$\frac{A^{nn}(\omega,\mathbf{k})}{\omega} = \frac{2\chi D\mathbf{k}^2}{\omega^2+(D\mathbf{k}^2)^2}. \quad (1.98)$$

The Kubo formula for the diffusion coefficient is given by:

$$\chi D = \frac{1}{2}\lim_{\omega\to 0}\lim_{\mathbf{k}\to 0}\frac{\omega}{\mathbf{k}^2}A^{nn}(\omega,\mathbf{k}). \quad (1.99)$$

Note here, that the order of the limits is important. An equivalent form of the Kubo-formulas is also sometimes given, that uses the correlator of the spatial part of the conserved currents, instead of the time-like one (the density). Let us call $A_{\mu\nu}(k)$ the spectral function corresponding to the Fourier transform of the correlator $\langle[j_\mu(x), j_\nu(0)]\rangle$. The Ward identity for current conservation reads:

$$k^\mu A_{\mu\nu}(k) = 0. \quad (1.100)$$

In the vacuum, current-conservation and Lorentz-invariance implies that the correlator is proportional to the projector:

$$P_{\mu\nu} = -\eta_{\mu\nu} + \frac{k_\mu k_\nu}{k^2}. \quad (1.101)$$

In thermal equilibrium state in canonical ensemble, we only have rotational symmetry, and therefore it is convenient to split the projector into transverse and longitudinal parts:

$$P_{\mu\nu} = P^T_{\mu\nu} + P^L_{\mu\nu}, \quad (1.102)$$

with

$$P^T_{0\mu} = 0 = P^T_{\mu 0} \qquad P^T_{ij} = \delta_{ij} - \frac{k_i k_j}{\mathbf{k}^2} \qquad P^L_{\mu\nu} = P_{\mu\nu} - P^T_{\mu\nu}. \quad (1.103)$$

These projectors satisfy $k^\mu P^L_{\mu\nu} = 0 = k^\mu P^T_{\mu\nu}$, and therefore any combination of them will automatically satisfy the Ward identity. Therefore, in general:

$$A_{\mu\nu}(k) = P^T_{\mu\nu}A^T(\omega,\mathbf{k}^2) + P^L_{\mu\nu}A^L(\omega,\mathbf{k}^2), \quad (1.104)$$

where, due to rotation invariance the $\mathbf{k} \to 0$ limit of A^L and A^T coincide[19] (at fixed ω):

$$\lim_{\mathbf{k}\to 0} A^L(\omega, \mathbf{k}^2) = \lim_{\mathbf{k}\to 0} A^T(\omega, \mathbf{k}^2). \tag{1.105}$$

This decomposition allows us to write this Kubo-formula in two other ways, as it allows us to write:

$$\lim_{\mathbf{k}\to 0} A^L(\omega, \mathbf{k}^2) = \lim_{\mathbf{k}\to 0} \frac{\omega^2}{\mathbf{k}^2} A^{00}(k) \equiv \lim_{\mathbf{k}\to 0} \frac{\omega^2}{\mathbf{k}^2} A^{nn}(k) \tag{1.106}$$

$$\lim_{\mathbf{k}\to 0} A^L(\omega, \mathbf{k}^2) = \frac{1}{3} \lim_{\mathbf{k}\to 0} \sum_{i=1}^{3} A^{ii}(k). \tag{1.107}$$

This leads to the following forms of the Kubo formula for diffusion:

$$\chi D = \frac{1}{2} \lim_{\omega\to 0} \lim_{\mathbf{k}\to 0} \frac{A^L(\omega, \mathbf{k})}{\omega} \tag{1.108}$$

$$\chi D = \frac{1}{6} \lim_{\omega\to 0} \lim_{\mathbf{k}\to 0} \sum_{i=1}^{3} \frac{A^{ii}(\omega, \mathbf{k})}{\omega}. \tag{1.109}$$

Equation (1.109) is the form of the Kubo formula that will directly apply to our lattice data. The current we will study corresponds to charm number conservation. If the transport coefficient D is nonvanishing, we expect some finite value of $\sum_i A^{ii}/\omega$ for small ω. This implies the presence of a transport peak in the SF. As we will see later, the only change we see in the spectral function of J/Ψ in our lattice data is the appearance of such a transport peak, up to temperatures of approximately $1.4T_c$. We will use the ratio G/G_{rec} in Section 2.6 to deduce this conclusion. Unfortunately, at the current level of statistics, we can not determine the diffusion constant (the zero intercept), because the reconstruction is only sensitive to the area of the transport peak.

[19] As the momentum goes to zero, there will be no distinction between transverse and longitudinal.

Chapter 2

Charmonium spectral functions from the lattice

We will start this chapter by deriving the formula connecting the spectral function to the Euclidean correlator. Combining the Fourier space KMS condition $G_<^{MN}(\omega) = e^{-\beta\omega}G_>^{MN}(\omega)$ with the definitions in equation (1.53) and (1.56) gives us:

$$A^{MN}(\omega) = G_>^{MN}(\omega) - G_<^{MN}(\omega) = (1 - e^{-\beta\omega})G_>^{MN}(\omega), \tag{2.1}$$

or

$$G_>^{MN}(\omega) = (1 + n_{\mathrm{B}}(\omega))A^{MN}(\omega) \quad \text{and} \quad \mathrm{G}_<^{\mathrm{MN}}(\omega) = \mathrm{n_B}(\omega)\mathrm{A}^{\mathrm{MN}}(\omega), \tag{2.2}$$

where $n_{\mathrm{B}}(\omega)$ is the Bose distribution. Then, we will also have:

$$G_E^{MN}(\tau) = G_>^{MN}(-i\tau) = \int_{-\infty}^{\infty} d\omega e^{-i\omega(-i\tau)}G_>^{MN}(\omega) = \int_{-\infty}^{\infty} d\omega \frac{e^{-\omega\tau}}{1 - e^{-\beta\omega}}A^{MN}(\omega). \tag{2.3}$$

This is the general formula that can be used to analytically continue the Euclidean correlators. We will use a different formula, valid when $M = N = M^\dagger$. First we write:

$$G_E^{MN}(\tau) + G_E^{MN}(\beta - \tau) = \int_{-\infty}^{\infty} d\omega \frac{\cosh(\omega(\tau - \beta/2))}{\sinh(\beta\omega/2)}A^{MN}(\omega). \tag{2.4}$$

If $M = N = N^\dagger$, the Euclidean correlator is symmetric around $\beta/2$, meaning $G_E^{MN}(\tau) + G_E^{MN}(\beta - \tau) = 2G_E^{MN}(\tau)$. Also, both the spectral function and the integral kernel $\frac{\cosh(\omega(\tau-\beta/2))}{\sinh(\beta\omega/2)}$ are odd functions of the frequency, so the integrand is even and we arrive at:

$$G_E^{MM^\dagger}(\tau) = \int_0^{\infty} d\omega \frac{\cosh(\omega(\tau - \beta/2))}{\sinh(\beta\omega/2)}A^{MM^\dagger}(\omega) \tag{2.5}$$

This will be the master formula for our determination attempt of the spectral function.

In this chapter we will deal with (connected) correlators between mesonic currents, and the corresponding mesonic SFs. These operators schematically look like[1]

$$J_H(t, \mathbf{x}) = \bar{q}(t, \mathbf{x})\Gamma_H q(t, \mathbf{x}), \tag{2.6}$$

where q is the quark field and $\Gamma_H = \gamma_5, \gamma_i$ for the pseudo-scalar and vector channels respectively. For the vector channel we will always mean a sum for the spatial components $i = 1, 2, 3$. We will measure charmonium correlators. The u, d, s quarks will be dynamical, while the charm quark will be included only in the quenched approximation.

We have just shown, that the SF is related to the Euclidean correlator – calculable on the lattice – by an integral transform

$$G(\tau, \vec{p}) = \int_0^\infty d\omega A(\omega, \vec{p}) K(\omega, \tau), \tag{2.7}$$

where we dropped the subscript H, and

$$K(\omega, \tau) = \frac{\cosh(\omega(\tau - 1/2T))}{\sinh(\omega/2T)} \tag{2.8}$$

is the integral kernel.

We will investigate the anticipated melting of the heavy meson states containing a charm quark and a charm antiquark: the J/Ψ (vector channel) and η_c (pseudoscalar channel) in the quark gluon plasma, which is supposed to happen somewhat above the transition temperature.

In the following, we will only be dealing with SFs at zero spatial momentum $A(\omega, \vec{0}) = A(\omega)$. In principle the determination of these spectral functions can give us the dissociation temperature and also the diffusion coefficient. We point out that the analysis of the non-zero spatial momentum SFs would go the same way, except one would need to start from non-zero spatial momentum correlators. There is no additional difficulty involved.

[1]Local currents of this form are not the conserved currents on the lattice. Writing down the Ward identities on the lattice([2]) it turns out that the conserved currents are non-local. Nevertheless, in the continuum limit, the local vector current correspond to the conserved current. However, because it is not a conserved current, at finite lattice spacing it has a finite renormalization. This does not concern us, since we don't attempt a continuum limit, and the renormalization is temperature independent.

2.1 The Maximum Entropy Method(MEM)

To get the SFs from a lattice study one has to invert equation (2.7). This equation however is notoriously hard to invert. A direct inversion is impossible, since the inverse is very strongly dependent on the noise in G_E. In the literature it is often said that the problem is that we want to reconstruct an approximation to a continuum function from a finite number of data points. That however is not accurate. For example, if one does a Fourier transform of a digital audio sample this is what actually happens. The difference is in the properties of the transformation itself. The number of data points vs. parameters is not the only problem when trying to reconstruct SFs. Even if one has a large number of data points (e.g. on anisotropic lattices), the Euclidean correlator is rather insensitive to fine details of the SF. Therefore the inversion introduces large uncertainties [38]. More on this will be said in the discussion of the mock data analysis.

To bypass this problem one wants to make a fit of some sorts for the spectral function. We could discretize A in ω space and have the fit parameters be $A(\omega_i)$. This fit however is ill-defined, since the typical number of frequencies for which one wants to reconstruct the SF is higher than the number of data points. In this case a χ^2 fit on the shape of the SF discretized to N_ω points is degenerate. One has to regularize the problem in some way.

The determination of hadronic SFs via the Maximum Entropy Method (MEM) was first suggested in [39], where it is introduced in detail. MEM is also treated in the standard textbook [40]. From a pragmatic point of view, the MEM is based on maximizing $-\frac{1}{2}\chi^2 + \alpha R$ where R is a regulator, which guarantees that there is a unique solution. There are various other regularizations possible (like the simplest possible regularization: a linear one), they are reviewed in the article [30], but MEM is still generally believed to be the most effective method when the spectral function exhibits sharp peaks, like in our case. Also, MEM is a regularization that has some justification from Bayesian probability theory. In the next subsection we will talk about inverse problems in general, then we will sketch the MEM procedure itself. The axiomatic construction for the entropy functional used in MEM is reviewed in the Appendix of Ref. [39].

2.1.1 Inverse problems and the use of prior information

Before presenting an outline of the MEM procedure, it can be illuminating to go through some preliminary remarks on inverse problems in general. Suppose $B(x)$ is some underlying or unknown process, that we wish to reconstruct by doing N noisy measurements c_i, where $i = 1, 2, 3, ..., N$. The relation between the measurements and the underlying function is assumed to be linear:

$$c_i = \int dx K_i(x) B(x) dx + \text{measurement error}. \tag{2.9}$$

This is a rather general formulation. In the simplest case, the c_i might approximate the $B(x)$ at certain locations x_i. In this case the kernels K_i are just narrow instrumental linear response functions centered around $x = x_i$. Alternatively, the c_i's might live in a completely different function space as $B(x)$, measuring different Fourier components of $B(x)$ for example. This is the case for our reconstruction of the spectral functions. The inverse problem is: knowing the c_i and their errors (covariance matrix), how do we find a good estimator of $B(x)$?

Now at this point the literature usually states that this is obviously an ill-posed problem. How could we reconstruct a whole function from only a finite number of noisy c_i? Truth is, we do that all the time. We always just measure/calculate enough points and then draw a curve through them. This seems quite intuitive in the case where the c_i are just approximations of $B(x_i)$, but even in this case, "connecting the points" is based on underlying assumptions, like the smoothness of $B(x)$ and the narrowness of the support of functions K_i for example. What does not seem so intuitive is the case where the c_i and $B(x)$ live in quite different function spaces. However, even in this case we are quite often not bothered by the problem of reconstructing an approximation to a continuum function from a finite number of data points. For example, this is what happens when we do a discrete Fourier transform of a digital audio sample, and it works absolutely fine. The goal of this discussion was to argue that the problem with lattice reconstruction of spectral functions is not only that we want to approximate a continuum function from a finite number of data points. The more serious problem is that the integral kernel $K_i(x) \Rightarrow K(\tau_i, \omega)$ in that case leads to a transformation that is very insensitive to details of $B(x) \Rightarrow A(\omega)$, so the transformation itself is hard to invert.

Of course, we cannot really want every point of the function $B(x)$, just some finite but

large number of points at x_k, with $k = 1, 2, 3, ..., M$. We will assume that neither $B(x)$, neither the kernels K_i vary much between x_k and x_{k+1}. Then the integral in equation (2.9) can be replaced by a sum:

$$c_i = \sum_{k=1}^{M} K_i(x_k) B(x_k) \Delta x_k + \text{measurement error} \qquad (\text{i} = 1, 2, ..., \text{N}). \tag{2.10}$$

If $M > N$, like in our case, the problem is, of course still ill-posed.

A quite general way of making it well-posed is the following. Let us take two functionals $\mathcal{A}$ and $\mathcal{B}$. We will:

$$\text{minimize} : \mathcal{A} + \alpha\mathcal{B}, \tag{2.11}$$

with α being some regularization parameter, $0 < \alpha < \infty$. This functional is supposed to have a unique minimum. Let $\mathcal{A}$ measure something like the agreement of the model $B(x)$ to the data c_i. This can be for example the χ^2. If we had no $\mathcal{B}$, this would be ill-posed, when $M > N$, the minimum of χ^2 would be degenerate, and a simple χ^2 would over-fit the data, making χ^2 unrealistically small, if not zero, and consequently, the reconstructed image in any of these minima of χ^2 is quite likely to overstate the importance of noise in the data points c_i. That is why $\mathcal{B}$ is needed. It can measure different things, for example:

- The smoothness of the desired solution
- The stability of the solution with respect to variations in data
- A priori judgment about the likelihood of the solution

Different methods differ in their choice of the functionals $\mathcal{A}$ and $\mathcal{B}$. The parameter α measures the trade-off between the minimums of the two functionals. In the next subsection we will outline the Maximum Entropy Method, motivating it's choice of $\mathcal{A}$ and $\mathcal{B}$ from Bayesian probability theory.

2.1.2 Outline of the MEM procedure

From Bayes' theorem the conditional probability of having an image[2] A, given the data D is:

$$P[A|D...] = \frac{P[D|A...]P[A|...]}{P[D|...]}, \tag{2.12}$$

[2]In physical terms, this image will correspond in our case to the spectral function, so we call it A. In the notation of the previous subsection the A here corresponds to B.

where $P[D|...]$ is just a normalization constant, $P[A|...]$ is called the prior probability, and $P[D|A...]$ is called the likelihood function and ... signifies possible other assumptions. The most probable image satisfies:

$$\frac{\delta P[A|D...]}{\delta A} = 0. \tag{2.13}$$

Assuming that the measurement errors are a multivariate Gaussian, the likelihood function is:

$$P[A|D...] = \frac{1}{Z_L} e^{-\frac{1}{2}\chi^2}, \tag{2.14}$$

where as usual

$$\chi^2 = \sum_{i,j=1}^{N_{\mathrm{data}}} (G_i^{\mathrm{fit}} - G_i^{\mathrm{data}}) \boldsymbol{\mathcal{C}}_{ij}^{-1} (G_j^{\mathrm{fit}} - G_j^{\mathrm{data}}), \tag{2.15}$$

with $\boldsymbol{\mathcal{C}}_{ij}$ being the covariance matrix of the data, calculated as:

$$\boldsymbol{\mathcal{C}}_{ij} = \sum_{k=1}^{N_k} \frac{1}{N_k(N_k-1)} \left(G_i^k - \bar{G}_i\right) \left(G_j^k - \bar{G}_j\right). \tag{2.16}$$

Here the sum goes over the lattices (field configurations) in the sample, N_k is the number of the lattices, and $\bar{G}_i$ means the average of the correlator at τ_i.

The prior probability[3] can be written with the auxiliary parameter α, and auxiliary function $m(\omega)$:

$$P[A|\alpha m...] = \frac{1}{Z_s} e^{\alpha S}, \tag{2.17}$$

where the Shannon–Jaynes entropy is

$$S = \int d\omega \left(A(\omega) - m(\omega) - A(\omega) \ln \left(\frac{A(\omega)}{m(\omega)} \right) \right), \tag{2.18}$$

where the so called prior function $m(\omega)$ is supposed to summarize our prior knowledge on the shape of the SF (such as the leading perturbation theory behavior). α will be averaged over, and will not be present in the final results. m will however be the main source of systematic uncertainty. Putting the prior probability and the likelihood function together we arrive at:

$$P[A|D\alpha m...] \propto \frac{1}{Z_S Z_L} e^{Q[A]}, \tag{2.19}$$

where

$$Q = \alpha S - \frac{1}{2}\chi^2. \tag{2.20}$$

[3]In the next section, we present a heuristic argument that shows why this form of the prior probability is plausible.

The most probable image for a given α and for a given prior function is at the maximum of Q. With the notation of the previous subsection $\mathcal{A} = \frac{1}{2}\chi^2$ and $\mathcal{B} = -S$. It can be proved [39], that the maximum of Q is unique.

2.1.3 Heuristic argument for the form of prior probability

What we need for MEM is a prior probability for the reconstruction (or image) A to be in a domain V:

$$P(A \in V) = \frac{1}{Z_S} \int_V [dA]\, \Phi\left(\alpha S(A)\right). \tag{2.21}$$

Here $[dA]$ is some integral measure and Z_S is a normalization constant and Φ is some function of the entropy $S(A)$, and α is a constant we will use later. In this equation we assumed locality, i.e. that the entropy $S(A)$ is a local functional of the image A, with no derivatives. We also assume that Φ is a monotonic function, so the most probable image, if there are no further constraints present, will be given by the maximum of the entropy.

The heuristic argument, known as the "monkey argument" gives us the explicit form of the prior probability. Let us first discretize the real line into cells, and so the image will also be discretized as A_i, with $i = 1, 2, ..., N$. Suppose a monkey throws M balls at the real line. We will assume M to be large. We will denote with p_i the probability of the ith cell to receive a ball (more precisely, the prior probability, i.e. our initial guess of the probability), and n_i the number of balls in the ith cell. Then the expectation value of the number of balls in the ith cell is simply $\lambda_i = Mp_i$, with normalization $\sum_i \lambda_i = M$.

The probability that the ith cell receives n_i balls is given by the binomial distribution, which in the limit of $M \to \infty$ with $\lambda_i =$ fixed is a Poisson distribution:

$$P_{M,p_i}(n_i) = \binom{M}{n_i} p_i^{n_i} (1-p_i)^{M-n_i} \xrightarrow[\lambda_i=\text{fixed}]{M\to\infty} P_{\lambda_i}(n_i) = \frac{\lambda_i^{n_i} e^{-\lambda_i}}{n_i!}. \tag{2.22}$$

The probability that a given $\vec{n} = (n_1, n_2, ...)$ is realized is:

$$P_{\vec{\lambda}}(\vec{n}) = \prod_{i=1}^{N} P_{\lambda_i}(n_i). \tag{2.23}$$

Next, we introduce a variable q that we will use to convert from a sum to an integral in this fashion:

$$q \sum_{n_i} \to \int dA_i, \tag{2.24}$$

and we introduce the notation $A_i = qn_i$ and $m_i = q\lambda_i$. With this notation, the prior probability becomes:

$$P(A \in V) = \sum_{\vec{n}} P_{\vec{\lambda}}(\vec{n}) \approx \int_V \prod_{i=1}^{N} dA_i q^{-N} \left(\prod_i \frac{\lambda_i^{n_i} e^{-\lambda_i}}{n_i!} \right) \tag{2.25}$$

Next we use Stirling's formula $n! \approx n^n e^{-n}\sqrt{2\pi n}$ and get:

$$P(A \in V) \approx \int_V \prod_{i=1}^{N} \frac{dA_i}{\sqrt{A_i}} \frac{e^{\frac{1}{q}S}}{(2\pi q)^{N/2}}, \tag{2.26}$$

where

$$S = \sum_{i=1}^{N} \left(A_i - m_i - A_i \ln\left(\frac{A_i}{m_i}\right) \right), \tag{2.27}$$

which, when compared with compared with equation (2.21), just gives:

$$\Phi = e^{\alpha S} \tag{2.28}$$

$$\alpha = q^{-1} \tag{2.29}$$

$$[dA] = \prod_{i=1}^{N} \frac{dA_i}{\sqrt{A_i}} \tag{2.30}$$

$$Z_S = \left(\frac{2\pi}{\alpha}\right)^{N/2} \tag{2.31}$$

$$\tag{2.32}$$

With this, we got the actual form of the prior probability and the entropy, as well as the integral measure and the normalization constant.

Is the entropy functional unique? No, it is not. There is nothing special about the functional form $-A\ln(A)$. There is no general agreement in the literature about the axioms the entropy functional has to satisfy. For example, in image reconstruction in radio astronomy, the entropy of the electromagnetic field in the limit of many photons per mode has the functional form $\ln(A)$ [41]. Even in lattice QCD, another form of the entropy functional has been proposed [42]. By all evidence, MEM seems as a useful nonlinear version of the scheme $\mathcal{A}+\alpha\mathcal{B}$, nothing more. From numerical tests, it seems that it is especially useful, when the "Fourier transform" we want to reconstruct is dominated by sharp peaks, which is exactly the case for quarkonium spectral functions.

2.1.4 Bayesian averaging over the regularization

After $Q = \alpha S - \frac{1}{2}\chi^2$ is maximized at a given value of α, and the optimal $A_\alpha(\omega)$ is obtained, the regularization parameter α has to be averaged over [39, 43]. The final output is defined

as a weighted average over α:

$$A(\omega) = \int [dA] \int d\alpha A_\alpha(\omega) P[A|D\alpha m...] P[\alpha|Dm...] \approx \int \mathrm{d}\alpha \mathrm{A}_\alpha(\omega) \mathrm{P}[\alpha|\mathrm{Dm...}], \quad (2.33)$$

We assumed the $P[A|D\alpha m...]$ is sharply peaked around a given value of $A_\alpha(\omega)$. Now, we can evaluate $P[\alpha|Dm...]$ using Bayes' theorem:

$$P[\alpha|Dm...] = \int [dA] P[D|A\alpha m...] P[A|\alpha m...] P[\alpha|m...] / P[D|m...]. \quad (2.34)$$

Using (2.19), we get

$$P[\alpha|Dm...] \propto P[\alpha|m...] \int [dA] \frac{1}{Z_S Z_L} e^{Q[A]}. \quad (2.35)$$

And finally, we assume that $P[\alpha|m...]$ is constant[4], and evaluate the integral in a Gaussian approximation:

$$P[\alpha|Dm...] \propto \exp\left(\frac{1}{2} \sum_k \log \frac{\alpha}{\alpha + \lambda_k} + \alpha S - \frac{1}{2}\chi^2 \right), \quad (2.36)$$

where the λ-s are the eigenvalues of the matrix:

$$\Lambda_{l,l'} = \frac{1}{2} \left(\sqrt{A_l} \frac{\partial^2 (\chi^2)}{\partial A_l \partial A_{l'}} \sqrt{A_{l'}} \right)_{A=A_\alpha}. \quad (2.37)$$

There is a trick for the efficient marginalization of α, involving Sylvester's determinant theorem. To arrive at this trick, we use the discretized version of the integral transform: $G(t_i) \equiv G_i = \sum_l K(\tau_i, \omega_l) A(\omega_l) \Delta\omega \equiv \sum_l K_{il} A_l$, and write:

$$\begin{aligned} 0 = \det\left(\Lambda - \lambda_k I_{N_\omega \times N_\omega}\right) = \det\left(\frac{1}{2} \sqrt{A_l} K_{il} \frac{\partial^2 \chi^2}{\partial G_i \partial G_j} K_{jl'} \sqrt{A_{l'}} - \lambda_k I_{N_\omega \times N_\omega} \right) = \\ = \det\left(\mathrm{diag}(\sqrt{A}) K^T \boldsymbol{\mathcal{C}}^{-1} K \,\mathrm{diag}(\sqrt{A}) - \lambda_k I_{N_\omega \times N_\omega} \right). \end{aligned} \quad (2.38)$$

Here $\mathrm{diag}(\sqrt{A})K^T$ is a matrix of size $N_\omega \times N_{\mathrm{data}}$, and $\boldsymbol{\mathcal{C}}^{-1} K \,\mathrm{diag}(\sqrt{A})$ is a matrix of size $N_{\mathrm{data}} \times N_\omega$. For non-zero eigenvalues λ_k, Sylvester's determinant theorem then implies that:

$$\begin{aligned} 0 = \det\left(\boldsymbol{\mathcal{C}}^{-1} K \,\mathrm{diag}(\sqrt{A}) \,\mathrm{diag}(\sqrt{A}) K^T - \lambda_k I_{N_{\mathrm{data}} \times N_{\mathrm{data}}} \right) = \\ = \det\left(\boldsymbol{\mathcal{C}}^{-1} K \,\mathrm{diag}(A) K^T - \lambda_k I_{N_{\mathrm{data}} \times N_{\mathrm{data}}} \right) \end{aligned} \quad (2.39)$$

Meaning that the matrix Λ can have only N_{data} nonzero eigenvalues, the eigenvalues of the matrix:

$$\tilde{\Lambda} = \boldsymbol{\mathcal{C}}^{-1} K \,\mathrm{diag}(A) K^T. \quad (2.40)$$

[4]This is not a strong assumption as long as the factor multiplying $P[\alpha|m...]$ is sharply peaked.

This matrix is not symmetric, but since its eigenvalues are the eigenvalues of the original symmetric matrix Λ they must also be real. The fact that a complex method gives real eigenvalues of the non symmetric matrix $\tilde{\Lambda}$ is a check of the numerical precision used in the calculations.

2.1.5 The method of maximizing Q

Q has a unique maximum. It can also be shown that the maximum of Q lies in an $N_{\rm data}$ dimensional subspace of the N_ω dimensional space of possible $A(\omega)$ vectors, that can be parametrized as:

$$A(\omega) = m(\omega) \exp\left(\sum_{i=1}^{N_{\rm data}} s_i f_i(\omega)\right). \tag{2.41}$$

The most widely used choice for basis functions involves a Singular Value Decomposition and is called the Bryan method. It was introduced in [44]. The particular choice of the basis for the subspace we use is $f_i(\omega) = K(\omega, \tau_i)$ and was introduced in Ref. [45]. In our experience this proved to be numerically more stable than the former one. The derivation of this method, (that also establishes that the solution is unique and lies in the aforementioned subspace) follows next. To maximize Q, we set

$$\frac{\delta}{\delta A(\omega)}\left(\frac{1}{2}\chi^2 - \alpha S\right) = 0. \tag{2.42}$$

This gives:

$$\sum_{i,j=1}^{N_{\rm data}} K(\omega, \tau_i) C_{ij}^{-1}\left(G_j^{\rm fit}[A] - G_j^{\rm data}\right) + \alpha \ln \frac{A(\omega)}{m(\omega)} = 0. \tag{2.43}$$

We introduce:

$$s_i = -\frac{1}{\alpha}\sum_{j=1}^{N_{\rm data}} C_{ij}^{-1}\left(G_j^{\rm fit}[A] - G_j^{\rm data}\right), \tag{2.44}$$

and rewrite this equation as

$$A(\omega) = m(\omega) \exp\left(\sum_{i=1}^{N_{\rm data}} s_i K(\omega, \tau_i)\right). \tag{2.45}$$

Since s_i depends on $A(\omega)$ this is a re-parametrization of the original problem. By substitution back in (2.43), we get:

$$\sum_{i=1}^{N_{\rm data}} K(\omega, \tau_i)\left[\sum_{j=1}^{N_{\rm data}} C_{ij}^{-1}\left(G_j^{\rm fit}[A] - G_j^{\rm data}\right) + \alpha s_i\right]. \tag{2.46}$$

Since the functions $K(\omega, \tau_i)$ are linearly independent, this equation can only hold if the expressions in the square brackets are zero. Multiplying by the covariance matrix, we get:

$$\alpha \sum_{j=1}^{N_{\rm data}} C_{ij} s_j + G_j^{\rm fit}[A] - G_j^{\rm data} = 0. \tag{2.47}$$

The second term in this sum is:

$$G_j^{\text{fit}}[A] = \int_0^{\omega_{\max}} d\omega K(\omega, \tau_j) m(\omega) \exp\left(\sum_{n=1}^{N_{\text{data}}} s_n K(\omega, \tau_n)\right). \tag{2.48}$$

Here, in the continuum theory $\omega_{\max} \to \infty$, on the lattice however, there is always a finite value, where the SF reaches zero, so the expression $\int_0^{\omega_{\max}} A(\omega) d\omega$ always makes sense, and we can write:

$$G_j^{\text{fit}}[A] = \frac{\partial}{\partial s_j} \int_0^{\omega_{\max}} d\omega m(\omega) \exp\left(\sum_{n=1}^{N_{\text{data}}} s_n K(\omega, \tau_n)\right) = \frac{\partial}{\partial s_j} \int_0^{\omega_{\max}} d\omega A(\omega). \tag{2.49}$$

We arrived at the result that the maximization of Q is equivalent to the minimization of

$$U = \frac{\alpha}{2} \sum_{i,j=1}^{N_{\text{data}}} s_i C_{ij} s_j + \int_0^{\omega_{\max}} d\omega A(\omega) - \sum_{i=1}^{N_{\text{data}}} G_i^{\text{data}} s_i, \tag{2.50}$$

since (2.47) can be rewritten as $\frac{\partial U}{\partial s_i} = 0$, and the positive definiteness of the covariance matrix also guarantees that $\frac{\partial^2 U}{\partial s_i \partial s_j}$ is also positive definite.

One can see from equation (2.41) that the shape of the subspace is strongly dependent on the choice of the prior function. This is the source of a systematic uncertainty, that has to be considered.

We also mention, that we use a modified version of the kernel and the spectral functions for the reconstruction [46, 47]:

$$\hat{K}(\tau, \omega) = \tanh(\omega/2) K(\tau, \omega), \tag{2.51}$$

and

$$\hat{A}(\omega) = \coth(\omega/2) A(\omega), \tag{2.52}$$

satisfying $KA = \hat{K}\hat{A}$. This "cures" the low frequency divergent $1/\omega$ behavior of the kernel, without spoiling the high ω behavior. In the rest of the chapter, we will only be dealing with Euclidean time, and we will simply denote it with t (changing the notation from τ).

2.1.6 Implementation

The statistics currently feasible for dynamical Wilson-fermion calculations are very small compared to quenched simulations, meaning additional care has to be taken in the MEM

analysis. We mention here some difficulties regarding MEM, that have not been pointed out in the literature before.

First of all, for realistic data double precision is not enough to make a reliable reconstruction of the SFs. Even in the case of the algorithm of Ref. [45], which does not involve a Singular Value Decomposition, the Hessian matrix of the function U has a big condition number, and arbitrary precision arithmetics is needed to find the correct minimum. Our implementation uses the Levenberg-Marquardt (or optionally the LBFGS) algorithm in arbitrary precision, implemeted by help of the GNU Multiple Precision Library. Using too low precision will generally lead to not finding the correct minimum. In practice, we have witnessed that using lower precision leads to broader peaks.

Also, even with the high precision one has to be very careful about the stopping criteria for the iteration. The general behavior is that after a rapid decrease of the function U, further iterations hardly improve it, i.e. it looks like hitting a plateau. Then after quite a few iterations, it starts improving fast once again, creating a step like pattern. With such a behavior, one has to choose a very strict stopping criterion.

If we work in the original N_ω dimensional space (here, we can use the LBFGS algorithm), and maximize Q instead, this situation is slightly better. In that space, the behavior is not step-like, but an iteration takes much more time, and whatever method one chooses, it takes lots of iterations to find the minimum, making the analysis computationally costly. This behavior is illustrated on Fig. 2.1.

We decided to follow the following procedure: minimize U in the N_{data} dimensional space to give us a head start, then after the iteration hits a plateau switch to the N_ω dimensional space and iterate there, to find the true minimum.

It can also be seen in Figure 2.1, that finding the correct minimum takes lots of iterations. This makes the MEM analysis itself computationally costly. Also note, that to perform a full analysis, with systematic and statistical error estimation, lots of MEM runs are needed. For this reason, the analysis was carried out on the computer cluster in Budapest, so that the different iterations can run in parallel. To do this efficiently I also wrote a queuing script for the MEM analysis on the cluster.

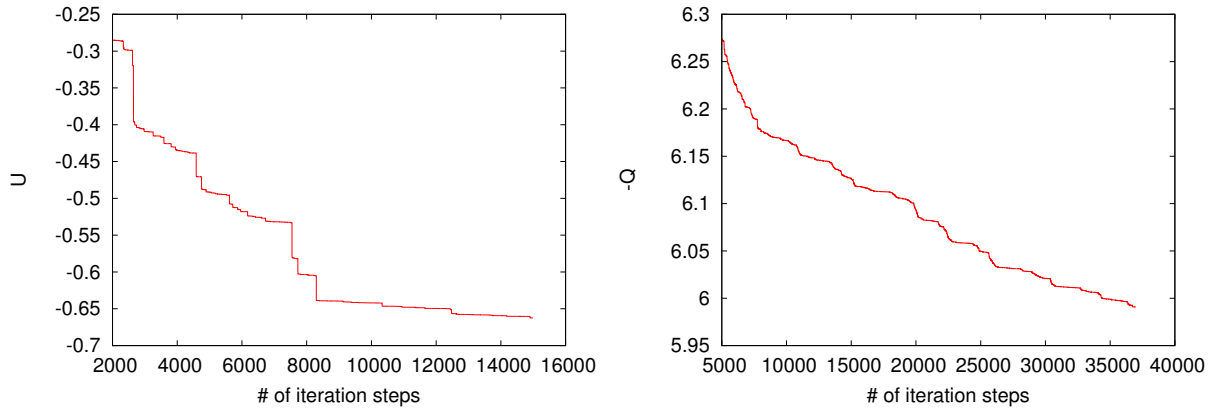

Figure 2.1: The behavior of the objective functions U and -Q (eqn. (2.20) and (2.50)) as a function of the iteration steps in the $N_{\rm data}$(left) and N_ω(right) dimensional spaces.

2.1.7 A comment on alternative methods

The use of MEM on smeared correlators[5] [48], and the use of variational methods at finite temperature [49] has also been suggested as a way to analyze charmonium properties at finite temperature. The problem with these propositions is the same: they enhance contributions from states that are known to be there already. However, the crucial question at finite temperature is not whether these state do contribute or not, they will always contribute to the thermal ensemble. The question is the magnitude of the contribution. The problem is that both of these methods change the magnitude of the contributions, and therefore drawing firm conclusions from them is difficult.

2.2 Mock data analysis

To test the feasibility of the MEM analysis, one can do mock data analysis. The general strategy is as follows:

- Write down an input spectral function $A_{\rm mock}(\omega)$
- Calculate correlators with $G_{\rm mock}(t) = \int K(t,\omega)A_{\rm mock}(\omega)d\omega$
- Add Gaussian noise to $G_{\rm mock}$, with variance $\sigma = b\tau G_{\rm mock}(\tau)$, where $b = 0.1...0.0001$ is a constant, setting the noise level, and generate mock configurations.
- Reconstruct spectral function with MEM and compare the reconstruction with $A_{\rm mock}$

[5] This means using not point sources, but sources with finite spatial extent: $\bar{\Psi}(\mathbf{x})\Gamma f(\mathbf{x},\mathbf{y})\Psi(\mathbf{y})$

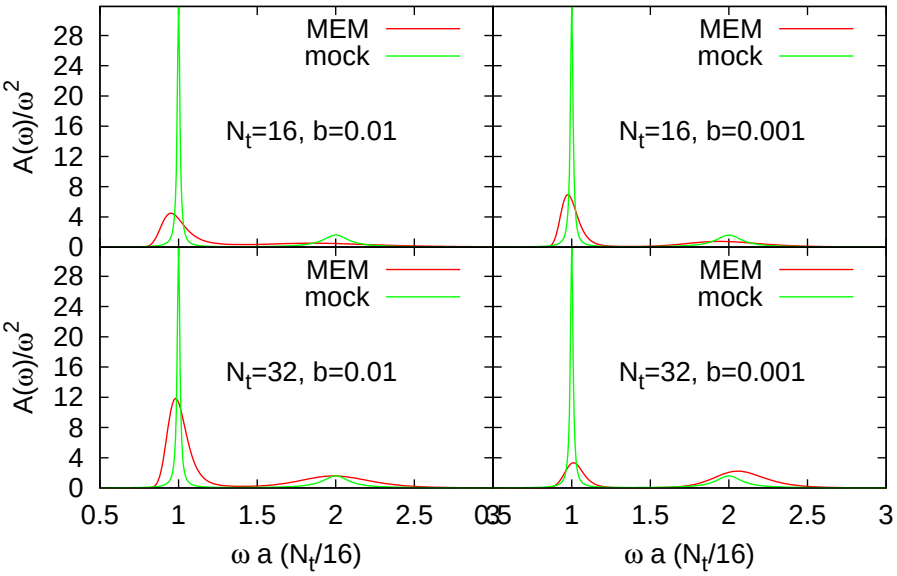

Figure 2.2: Mock data reconstruction with different data. Different values of N_t and noise level b are used, with the same prior function: $m(\omega) = \text{const.} = 0.1\text{a}^{-2}$. The input spectral function was scaled in such a way, as to be the same in physical units. So if there is a peak in the $N_t = 16$ lattice at $\omega a = 1$, there will be a peak in the $N_t = 32$ lattice at $\omega a = 0.5$, since in this case the lattice spacing is assumed to be half as big. This corresponds to the ratio $m/T = N_t = 16$. For $m = 3\text{GeV}$, like J/Ψ this corresponds to $T = 187.5\text{MeV}$, a relevant temperature for our purpose.

By doing this, we want to have a picture of how much we can believe from such a reconstruction, therefore we use the number of data points $(12 - 64)$ and the level of statistics (1000 configurations), that are feasible for lattice data. The mock spectral functions were assumed to be a sum of Lorentzian peaks[6]:

$$\frac{A(\omega)}{\omega^2} = \sum_{i=1}^{n_{\text{peaks}}} \frac{h_i}{\pi} \frac{\gamma_i}{(\omega - m_i)^2 + \gamma_i^2}. \tag{2.53}$$

The lessons learned from the mock data analysis, with some illustrations are the following:

1. MEM gives the correct qualitative features of the spectral function, but it is not a precise quantitative method.

2. More precisely, the peak positions are much better reconstructed than the shapes,

[6]Repeating the exercise with Gaussian peaks leads to similar results.

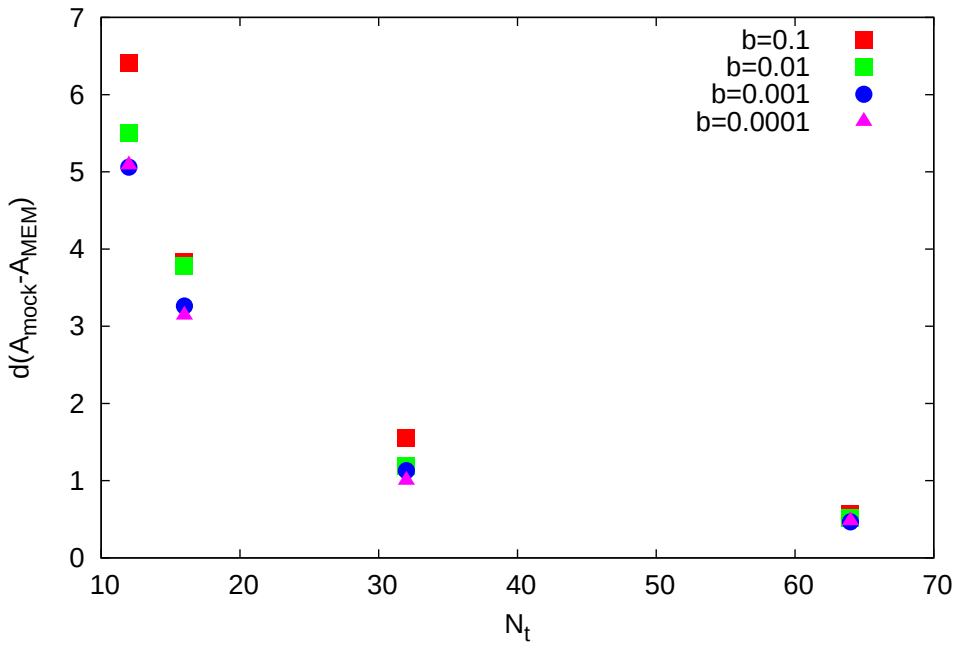

Figure 2.3: The quantity $\sqrt{\int d\omega (A_{\rm mock}(\omega) - A_{\rm MEM}(\omega))^2}$ as a function of N_t and b for the same mock spectral function and prior function that was used in Figure 2.2.

that have huge systematic errors. This is especially true for the position of the ground state peak, the most reliable quantity of the reconstructions I could identify.

3. As long as the data points are not too noisy, O(10) points are enough for the reconstruction of the bound state peak, with a relatively accurate determination of the peak position, but not the shape.

4. Of course, the quality of the reconstruction depends on the data. Both having more data points (higher N_t) and having more precise data points (less noise, i.e. smaller b) lead to a better determination of the spectral functions. Points 1-4 are illustrated on Figure 2.2, where we show reconstructions of spectral functions with different data.

5. To say something more concrete about the quality of the reconstruction let us define the quantity:

$$[\mathrm{d}\,(\mathrm{A_{mock}} - \mathrm{A_{MEM}})]^2 \equiv \int d\omega (A_{\rm mock}(\omega) - A_{\rm MEM}(\omega))^2. \tag{2.54}$$

This is one of the many possible ways one could measure the accuracy of the reconstruction. The smaller this number is, the better the reconstruction. We show the dependence of this quantity on N_t and b (in the case of the reconstructions in

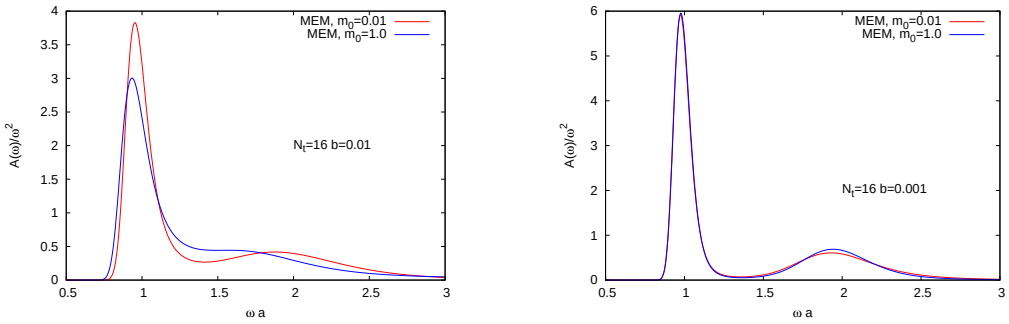

Figure 2.4: Mock data reconstruction illustrating the sensitivity on the normalization of the prior function. In both pictures we have $m(\omega) = m_0 a^{-2}$, but the noise level b is different. We can see that the noisier the data, the more sensitivity we have on the prior function. The mock spectral function used for this picture was the same as Figure 2.2 and 2.3

Figure 2.2) in Figure 2.3. There are claims in the literature ([39]), that it is more important to have low b than to have high N_t, but this is debatable. It depends on the measure of the goodness of the reconstruction one uses. In particular, the measure of the goodness of reconstruction we use here (which is different from that of Ref. [39]) does not support it[7] . All that can be said from such an analysis is that both increasing the number of data points and decreasing the noise level leads to a better determination, which is completely unsurprising.

6. The reconstruction is of course dependent on the prior function used. Moreover, the noisier the data, the more dependence we will have on the prior function. These point are illustrated in Figure 2.4.

7. Close lying can be merged into one broader, therefore non physical peak. This is illustrated in Figure 2.5. This is one of the main reasons that we do not deal with the higher excitations, and concentrate just on the ground state peak in our analysis.

2.2.1 A comment on anisotropic lattices

Mock data analysis suggests that anisotropic lattices are useful, since they make the reconstructions substantially more accurate. They also make the reconstruction possible at higher temperatures, since more points will be available at those higher temperatures

[7] An even more important difference is that the mock data analysis in Ref. [39] keeps the lattice spacing fixed, and not the temperature, when increasing N_t. This means that they change the physics.

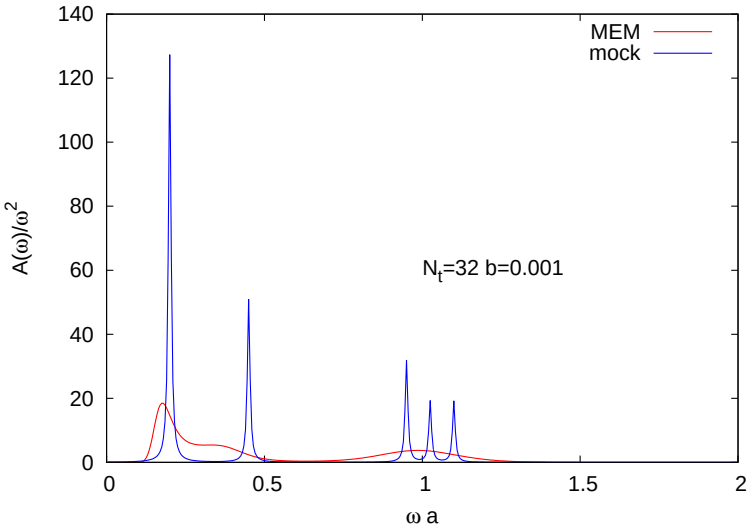

Figure 2.5: Mock data reconstruction illustrating unphysical peak merging.

for the reconstruction. Anisotropy tuning with dynamical fermions is a difficult task, but it can somewhat be made easier by the method described in [50]. This is one possible direction of future studies.

2.3 Error analysis

We discuss now the analysis of the actual lattice data. We don't carry out an error analysis of the full spectral function, since with the current statistics that would give huge errors. Instead, we only give errors to some physically interesting quantities related to the spectral function, that are more stable, namely: The position of the first peak and the quantity G_{rec} that will be defined later in the text.

The statistical error analysis is done with the usual jackknife method. For the sake of reducing computational cost, the statistical error estimate was only carried out on a given set of the parameters of the reconstruction algorithm.The systematic error analysis is carried out by varying the parameters of the reconstruction algorithm. Namely:

- the discretization of the frequency variable $\Delta\omega$
- the upper cut-off on the integral (2.7), $\omega_{\mathrm{max}} = N_\omega \Delta\omega$
- the shape and normalization of the prior function

A numerical check on the lattice data and mock data analysis show that as long as $\Delta\omega$ is sufficiently small to resolve the peaks and N_ω is such that $\omega_{\max}$ is sufficiently big, which means somewhere around 5 inverse lattice spacings, the results are not affected by the choice of the first two parameters. In this analysis we used $a\omega_{\max} = 5$ and $a\Delta\omega = 0.005$. The effect of the prior function however, can not be neglected. For the systematical error analysis we used 3 different shapes:

- m_0/a^2, motivated by the philosophy of "we know nothing".

- $m_0\omega^2$, motivated by continuum perturbation theory. We must stress however, that there is no reason to think that such an asymptotic behavior can actually be seen on the lattice. In fact, analytical calculations of the SFs with free Wilson quarks show a different behavior. (See [51] and [52]) There is nothing surprising about that, the lattice has an explicit cut-off, that means, the spectral function itself must have a cut-off at high frequency.

- $a^{-3}/(m_0/a + \omega)$, a theoretically unmotivated form, that has at least the desirable quality of going to zero at high ω. By using such a prior, we try to restrict the reconstructed shapes to the ones that are actually dictated by the lattice data.

- $m_0\omega/a$, motivated by the Kubo formula (1.109). This is the only prior function in the study that allows for a finite, nonzero diffusion constant, the others would imply either 0, or infinity. We have only used this prior in the vector channel, where the analysis with the other prior functions suggested a transport peak.

In all cases, a is the lattice spacing, and m_0 was varied between 10.0,1.0,0.1 and 0.01 to estimate the systematic errors. The systematic error was taken to be between the 17% and 83% percentiles of the sorted reconstructed parameters. The final error bars on the plots include both systematic and statistical errors.

We mention, that it has been suggested (see e.g. [53]), that the free Wilson fermion SFs should be used as the prior information, we see no reason to do this however, since the free results are expected to have huge corrections, and treat the prior as a source of uncertainty instead.

a[fm]	am_{ud}	am_s	m_π	N_s	N_t	$T = \frac{1}{N_t a}$	# confs.
0.057(1)	-0.00336	0.0050	545MeV	64	28	123MeV	151
0.057(1)	-0.00336	0.0050	545MeV	64	20	173MeV	95
0.057(1)	-0.00336	0.0050	545MeV	64	18	192MeV	328
0.057(1)	-0.00336	0.0050	545MeV	64	16	216MeV	254
0.057(1)	-0.00336	0.0050	545MeV	64	14	247MeV	411
0.057(1)	-0.00336	0.0050	545MeV	64	12	288MeV	300

Table 2.1: The different lattices used in the study. The configurations are separated by 5 trajectories. We have explicitly checked, that none of the covariance matrices $\boldsymbol{\mathcal{C}}_{ij}$ of the data we have display pathological spectra.

2.4 Simulation details

We use the same lattice configurations as in [15]. The gauge action used for the calculations was the Symanzik tree level improved gauge action [54, 17], defined in equation (1.15), with the parameters $c_0 = 5/3$ and $c_1 = -1/12$. The action for the fermionic sector was the clover improved [18] Wilson action[8]. Six steps of stout smearing [26] with smearing parameter $\varrho = 0.11$ were used. The clover coefficient was set to its tree level value, $c_{\mathrm{SW}} = 1.0$, which, for this type of smeared fermions, essentially leads to an $\mathcal{O}(a)$ improved action [55] with improved chiral properties [56]. The same action was first used in Ref. [57] where the excellent scaling properties of hadron masses were observed. The full hadron spectrum using this action was determined in Ref. [58].

The bare masses of the u and d quarks were taken to be degenerate, therefore the configurations were generated using an $N_f = 2 + 1$ flavor algorithm. The u and d quarks were implemented via the Hybrid Monte Carlo (HMC) algorithm [21], whereas the strange quark was implemented using the Rational Hybrid Monte Carlo (RHMC) algorithm [22]. In order to speed up the molecular dynamics calculations, the Sexton-Weingarten multiple time-scale integration scheme [59] combined with the Omelyan integrator [60] was employed. When all four extents of the lattice were even, the usage of even-odd preconditioning [61] gave an additional speed up factor of 2.

[8]For Maximum Entropy, staggered fermions are not practical, because of the lattice artifact of the odd and even sites behave differently, meaning that we would need to drop half of the points in the correlator.

J^P	m_i	name	ma	$ma/m_{D_s^*}a$	$m_{exp}[MeV]$	$m_{exp}/m_{D_s^*}$
0^-	m_s,m_c	D_s	0.54(1)	0.95(2)	1968.4	0.932
0^-	m_c,m_c	η_c	0.8192(7)	1.437(4)	2981.0	1.411
1^-	m_s,m_c	D_s^*	0.570(1)	1	2112.3	1
1^-	m_c,m_c	J/Ψ	0.8388(8)	1.472(2)	3096.916	1.466
$3/2^+$	$3m_s$	Ω	0.478(8)	0.84(2)	1672.45	0.791

Table 2.2: The different hadron masses, obtained by fitting $A\cosh(ma(t - N_t/2))$ to smeared correlators (in case of mesons, sinh in case of baryons) on 64^4 lattices.

From the study in [15], we only used the finest lattices, with gauge coupling $\beta = 3.85$, corresponding to a lattice spacing of $a = 0.057(1)$fm. The bare light quark masses where chosen to be $am_{ud} = -0.00336$ and $am_s = 0.0050$, which, when fixing the scale with a physical Ω baryon mass, corresponds to a pion mass $m_\pi \approx 545$MeV. A summary of the lattices used can be found in Table 2.1.

2.4.1 Charm mass tuning

From Ref. [62] the ratio $m_c/m_s = 11.85$. Since with Wilson fermions, there is an additive renormalization, it is not possible to use this ratio directly in setting the charm mass. However, we know that for ud and s the masses used in the simulation correspond to a mass ratio of 1.5 [63, 64], from this we get $(m_c - m_s)/(m_s - m_{ud}) = 35.55$ which gives the estimate for the charm mass that was used. To verify if this is approximately the correct charm mass, I checked the masses of the different mesons states containing s and c quarks, and they were indeed in the right ballpark. See Table 2.2.

2.4.2 Approximation of the pseudo-critical temperature

Since the simulation is done at a non-physical pion mass, instead of giving the temperature values in MeV, it is probably more appropriate to give temperatures in T_c units. Since with dynamical light quarks there is no phase transition, the transition is a cross-over, there is a multitude of possible definitions of T_c. We will use the temperature value where the tree-level improved strange quark number susceptibility is 0.5. One can obtain an estimate of this temperature from Figure 2 of Ref. [15] (copied here as Figure 2.6), where the continuum extrapolated strange quark susceptibility is plotted with systematic and

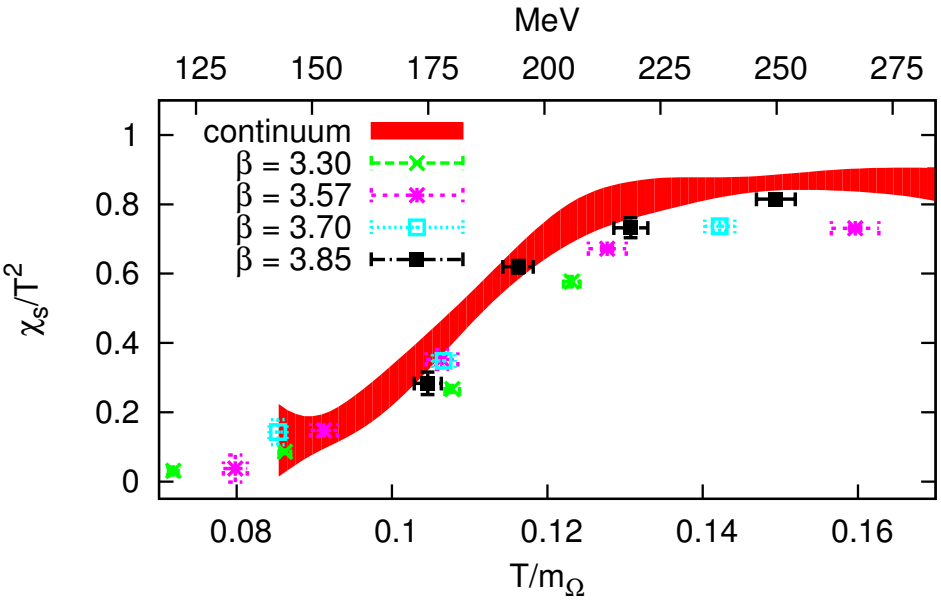

Figure 2.6: The tree-level improved (i.e. divided by the Stefan-Boltzmann limit) strange quark number susceptibility as a function of temperature from Ref. [15]

statistical errors. The transition temperature is $T/m_\Omega \approx 0.110$.

2.5 Maximum Entropy Analysis

First, we note, that lattice studies of charmonium SFs using the MEM have been carried out on numerous occasions in the literature ([45, 48, 65, 66, 67, 49, 53, 68, 69]), but so far not in 2+1 flavour QCD. A recent, detailed study of charmonium SFs in quenched QCD can be found in [53]. Results regarding spectral functions with 2 flavours of dynamical quarks can be found in Refs. [68, 69]. A recent study of electric conductivity using 2+1 flavors of anisotropic Wilson fermions can be found in [70]. Another interesting application of the spectral function reconstruction is the study of the melting bottomonium states in the context of Non-relativistic QCD [71]. The study of spectral functions in this PhD thesis is presented in Refs. [72, 73].

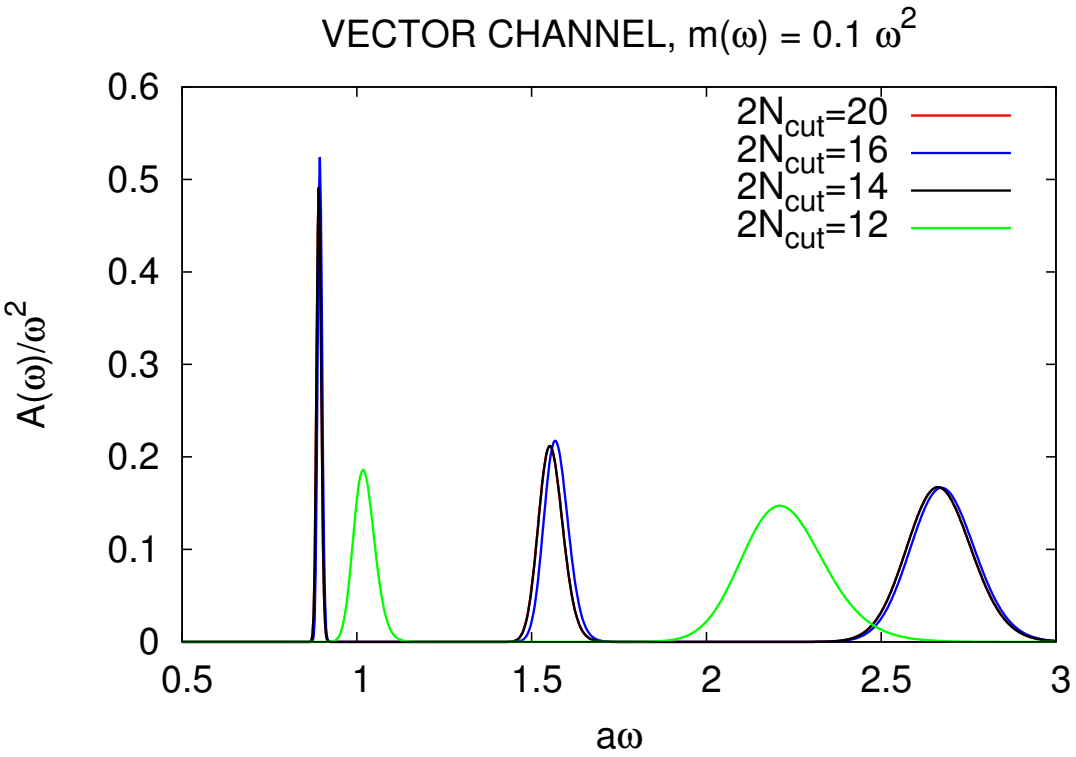

Figure 2.7: The results of dropping points from the zero temperature reconstruction. We dropped points starting from $t = 0$, using only the points closest to $t = N_t/2$. N_{cut} is the number of points used for reconstruction. For $2N_{\text{cut}} \leq 12$ one can no longer reconstruct the first peak.

2.5.1 Zero temperature analysis

Since the temperature is $T = 1/(N_t a)$, as the temperature increases we have less and less data points for our reconstruction of the SFs. That means that the reliability of the method decreases with increasing temperature. So we need an estimate of the highest temperature, where the MEM results are still likely to be trusted. To get such an estimate, we drop points from the lowest temperature correlators and do a MEM reconstruction with these limited number of points. We say that the reconstruction is no longer reliable when we can not reconstruct the first peak. The results are illustrated in Fig. 2.7. As we can see, $N_t = 12$ is already not reliable, meaning that the highest temperature[9] we can study with direct MEM reconstruction is corresponding to $N_t = 14$. This corresponds to $T/T_c \approx 1.3$. Early potential models of charmonium predicted the melting of J/Ψ already at this temperature.

[9]Of course, this is not an absolute criterion.

2.5.2 Finite temperature analysis

Reconstructions of the pseudoscalar (PS) SF with different prior functions can been seen in Fig. 2.8. Reconstruction of the PS spectral function with the same prior functions at different temperatures can be seen in Fig. 2.10. Looking at these pictures together one can draw the intuitive conclusion that the difference in the SFs at various temperatures is smaller than the reconstruction error coming from the variation of the reconstruction with different prior functions. So as far as our analysis can tell, the PS SF is temperature independent in the given range. This is further confirmed by Fig. 2.11, which shows a full error analysis of the peak position.

The situation is a little bit more complicated in the vector channel. Reconstructions of the vector SF with different prior functions can been seen in Fig. 2.9. Reconstruction of the vector SF with the same prior functions at different temperatures can be seen in Fig. 2.10. In this last plot the highest temperature seems to differ from the other temperatures. Due to some properties of the analysis (i.e. possible merging of adjacent peaks and problems with the resolution of the transport peak) using MEM alone one cannot draw any firm conclusions about the nature of the change in the SF - at least at the current level of statistical errors. At $N_t = 16$ the MEM reconstruction picks up a transport related low frequency peak, this can be seen in Figure 2.12. However at $N_t = 14$ the MEM is probably already not reliable in the vector channel. From mock data analysis, we observed that MEM can merge two close lying peaks to one peak between the two real peaks. We suspect that this is what is happening at $N_t = 14$. The $N_t = 14$ reconstruction also picks up a transport peak with some prior functions, but here we don't see three $\omega > 0$ peaks together with a transport peak. The first peak is always merged with the transport peak, or the second peak. This peak merging property makes the error bars on the first peak position at this temperature so big. Fig. 2.11 shows a full error analysis of the peak position. The actual physical picture will be clarified in the next point of our analysis.

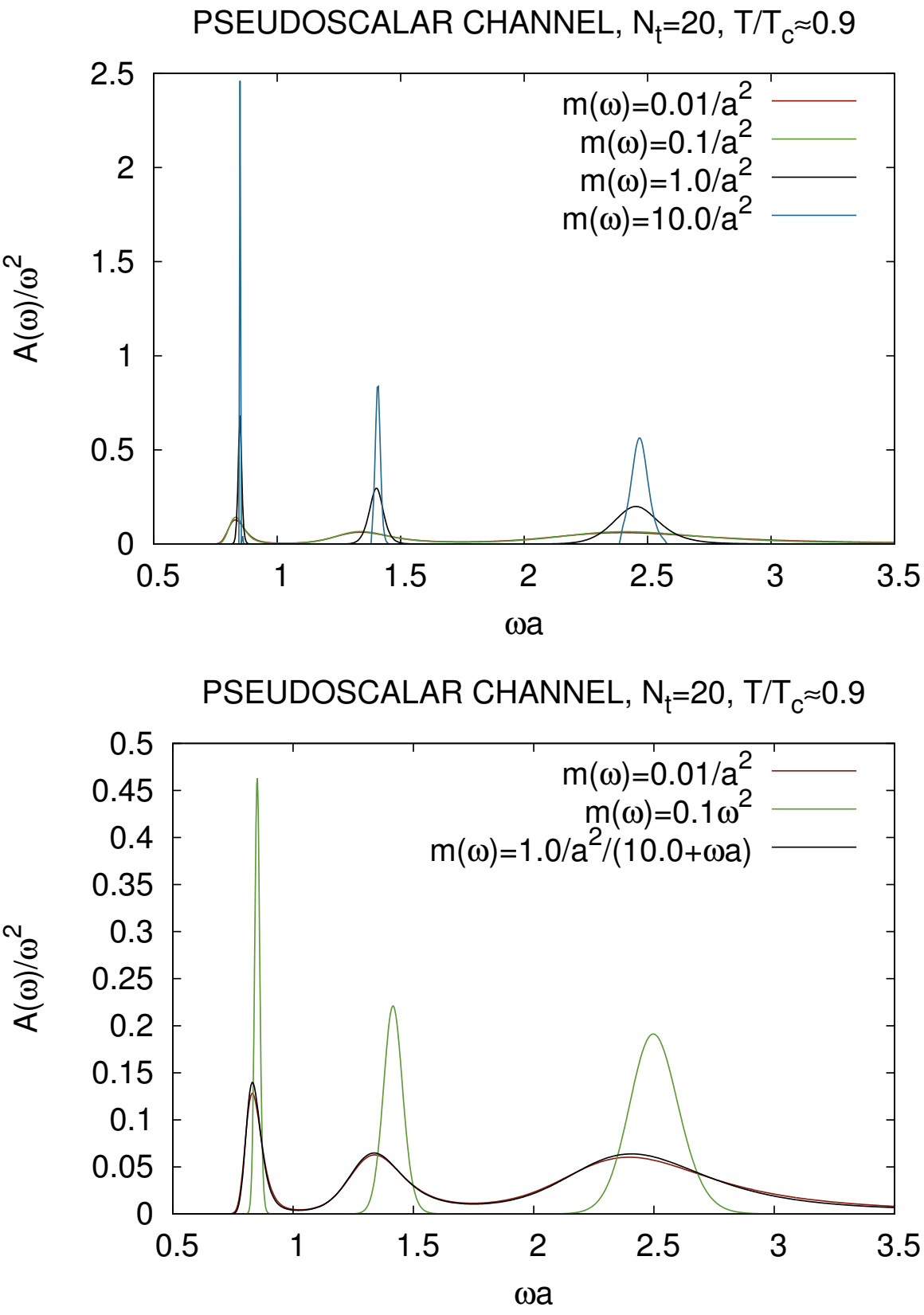

Figure 2.8: The sensitivity of the reconstruction on the prior function in the pseudoscalar channel. Note that the widths of the peaks have large systematic errors, as can be seen from the reconstruction with different prior functions.

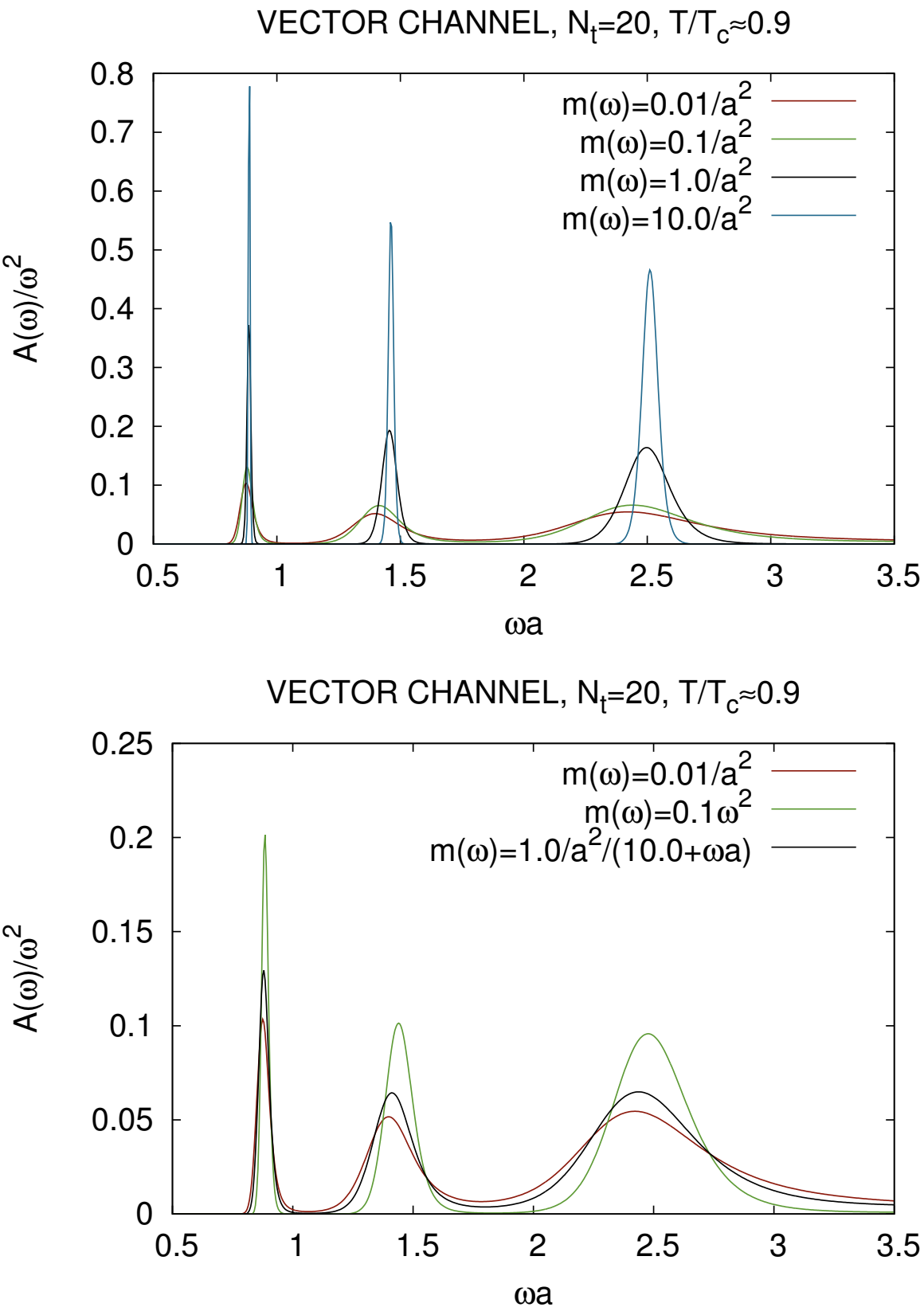

Figure 2.9: The sensitivity of the reconstruction on the prior function in the vector channel. Note that the widths of the peaks have large systematic errors, as can be seen from the reconstruction with different prior functions.

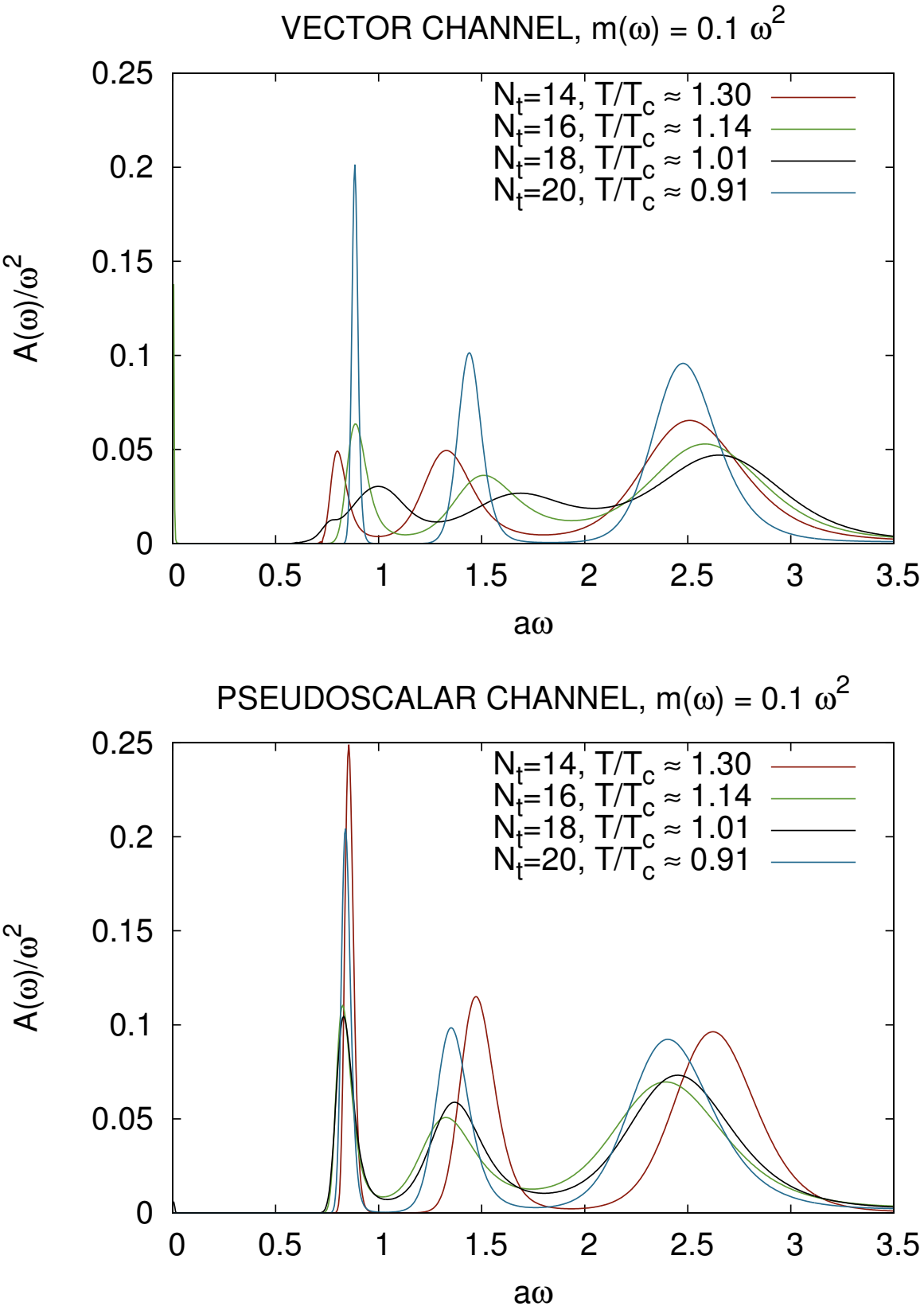

Figure 2.10: The temperature dependence of the reconstructed spectral functions.

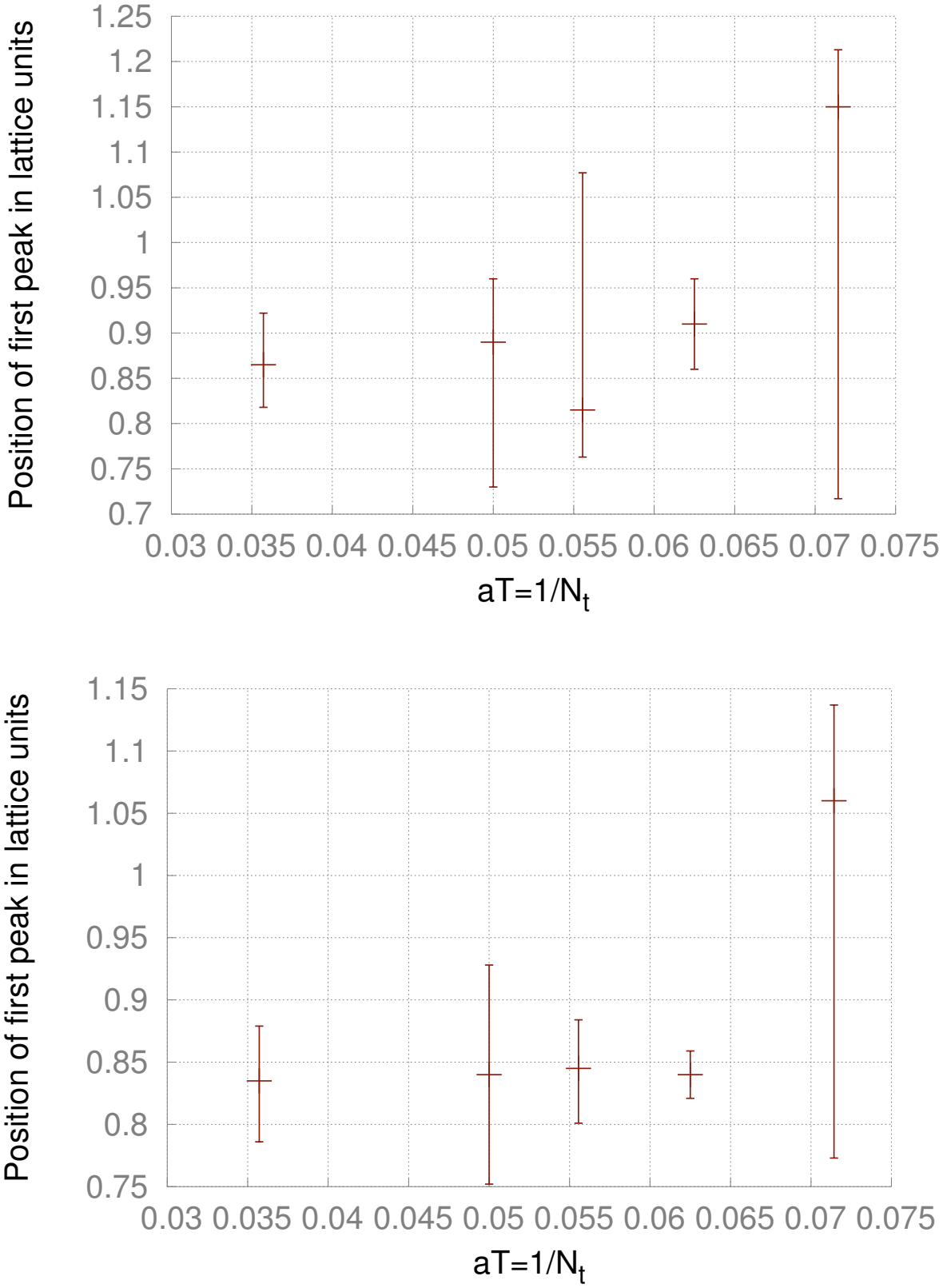

Figure 2.11: The position of the first vector(top) and pseudoscalar(bottom) peak as a function of temperature. The big error bars at the highest temperature, corresponding to $N_t = 14$ probably come from the fact that with so few data points, the MEM procedure merges the first two peaks sometimes (i.e. with some prior functions). Error bars include both systematic and statistical errors.

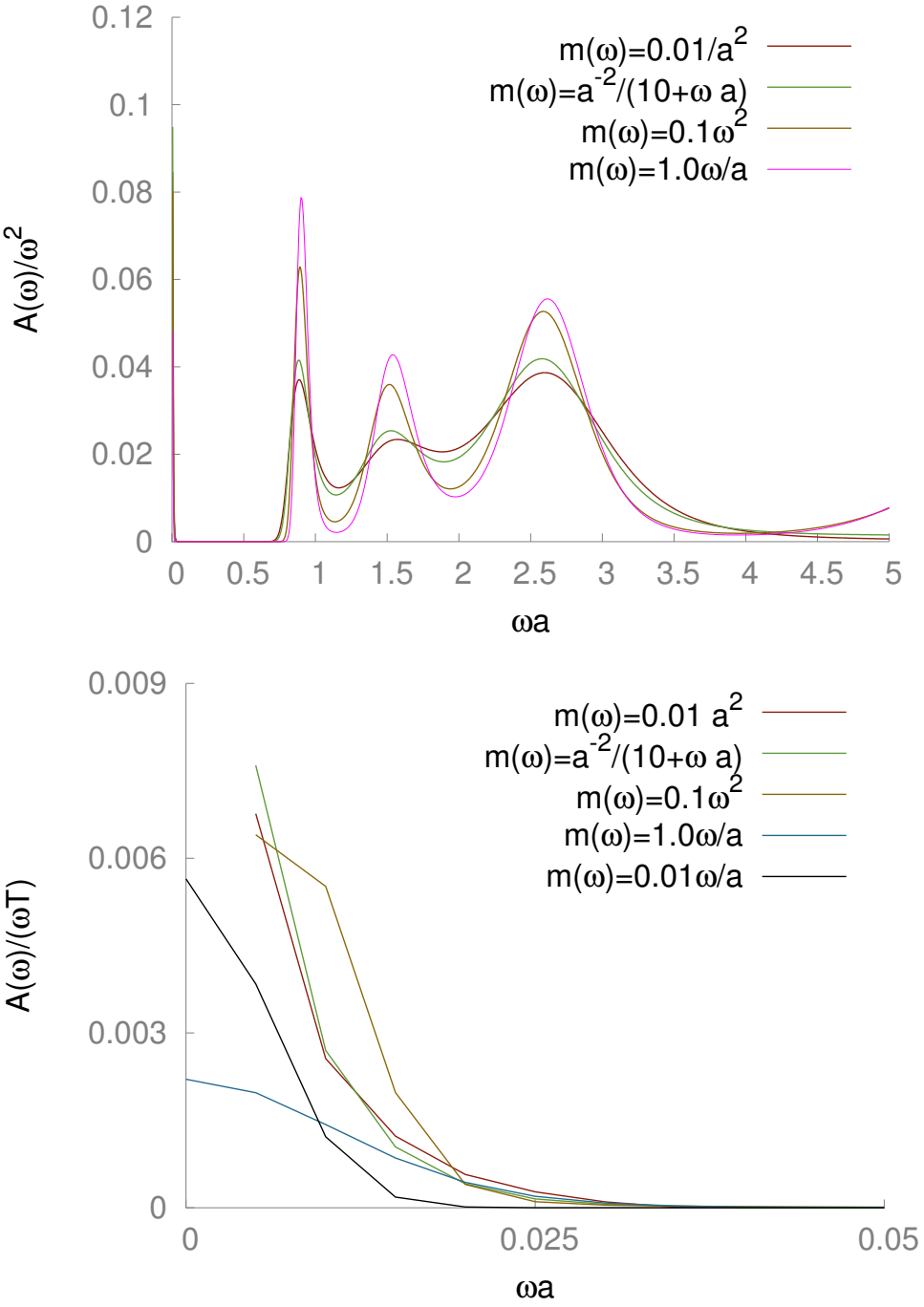

Figure 2.12: The MEM reconstructed vector SF at $N_t = 16$ in the vector channel. Notice the indication of a transport peak in the MEM analysis. With the prior functions $A(\omega) = m_0 a^{-2}$ or $\frac{a^{-2}}{m_0+\omega a}$ the zero frequency limit of $A(\omega)/\omega$ is always infinity, with $A(\omega) = m_0\omega^2$ it is always zero. To actually get a value for the transport coefficients, we need to use the prior function $A(\omega) = m_0\omega a^{-1}$. This way we can get an estimate, but as the results show, it has a big systematic uncertainty. As we will stress in the analysis of the "reconstructed" correlators, the data are not really sensitive to the zero frequency intercept, only the area of the transport peak.

2.6 The ratio G/G_{rec}

An alternative approach to study spectral functions was suggested in [74]. The ratio:

$$\frac{G\left(t,T\right)}{G_{\mathrm{rec}}\left(t,T\right)}=\frac{G(t,T)}{\int A(\omega,T_{\mathrm{ref}})K(\omega,t,T)\mathrm{d}\omega} \tag{2.55}$$

has a few advantages:

- MEM reconstruction is only needed at T_{ref}, where we have the most data points, and so a more reliable reconstruction. We use $N_t = 28$ as reference temperature.
- We can calculate this ratio even at high temperatures, where the MEM reconstruction is already unreliable.
- If the spectral function is temperature independent, then the trivial temperature dependence of the correlators, coming from the integral kernel will drop out, and the ratio will be $G/G_{\mathrm{rec}} = 1$.

It is also useful to study the same ratio with mid-point subtracted correlators [75]:

$$\frac{G^{-}}{G_{\mathrm{rec}}^{-}}=\frac{G\left(t,T\right)-G\left(N_t/2,T\right)}{G_{\mathrm{rec}}\left(t,T\right)-G_{\mathrm{rec}}\left(N_t/2,T\right)}= \\ =\frac{G\left(t,T\right)-G\left(N_t/2,T\right)}{\int A(\omega,T_{\mathrm{ref}})\left[K(\omega,t,T)-K(\omega,N_t/2,T)\right]\mathrm{d}\omega} \tag{2.56}$$

This way, one can drop the zero-mode (constant) contribution to the correlators. These have to do with transport coefficients, or (especially at very high temperatures) other low frequency ($\omega \ll T$) features of the spectral functions. If the ratio of G/G_{rec} is different from one, but the ratio with the middle-point subtracted correlators is not, that means that the temperature dependence of the SFs should be well described by just a zero-mode contribution $f(T)\cdot\omega\delta(\omega-0^{+})$.

The results of such an analysis can be seen in Figs. 2.13 and 2.14. As one can see, the results in the pseudoscalar channel are consistent with a temperature independent SF, while the results in the vector channel show a temperature dependent zero mode/low frequency contribution in the SF. We can also try to extract the zero mode contribution itself by considering the difference $G - G_{\mathrm{rec}}$. This is only plotted in the vector channel, in Fig. 2.15 (in the pseudoscalar channel it is always consistent with zero). The difference has big errors, but on the two highest temperatures it is non zero within 1σ. At every temperature it is consistent with a time separation independent constant. With

the ansatz $A(\omega, T) = f(T)\omega\delta(\omega - 0^+) + A(\omega, T_0)$ we get $f(T)T \approx (3 \pm 1.5) \cdot 10^{-5}$ at $1.5T_c$ in lattice units [10]. This ansatz, taken strictly, would imply a diverging diffusion constant. However, the data do not restrict the shape of the transport peak, they are only sensitive to the area. By using this ansatz, we do not mean to say that the diffusion constant diverges, we simply extract that area of the transport peak. To get a diffusion constant additional information is needed. (The width or the height of the peak, which is too narrow to resolve at this point.) The survival of J/Ψ up to such high temperatures is consistent with previous results in quenched and 2 flavour QCD (see eg. [49, 53, 69]).

We can now summarize the main results of this Chapter:

- Direct MEM reconstruction was performed up to a temperature of $1.3T_c$. In this range we see no clear indication of either η_c or J/Ψ melting.
- Moreover, from the MEM analysis, the positions of the first peaks are consistent with a constant, with an error of approximately 30% at the highest temperature.
- The analysis of the ratio G/G_{rec} was performed up to a temperature of $1.4T_c$, a slightly higher temperature than MEM. Up to this temperature range, we see no indication of either η_c or J/Ψ melting. In fact, the pseudoscalar SF shows no temperature dependence at all, up to our error bars.
- The temperature dependence of the vector channel spectral function is consistent with the appearance of a temperature dependent transport peak at $\omega \approx 0$ and a temperature independent part at $\omega > 0$.
- At the current level of statistics, the diffusion constant can not be extracted, since our reconstruction is only sensitive to the area of the transport peak.

[10] Since we are not using the conserved current on the lattice, but a local current, this will have a finite, lattice spacing dependent renormalization constant of $\mathcal{O}(1)$. We neglect this fact, since we don't do a continuum limit, and the renormalization is temperature independent.

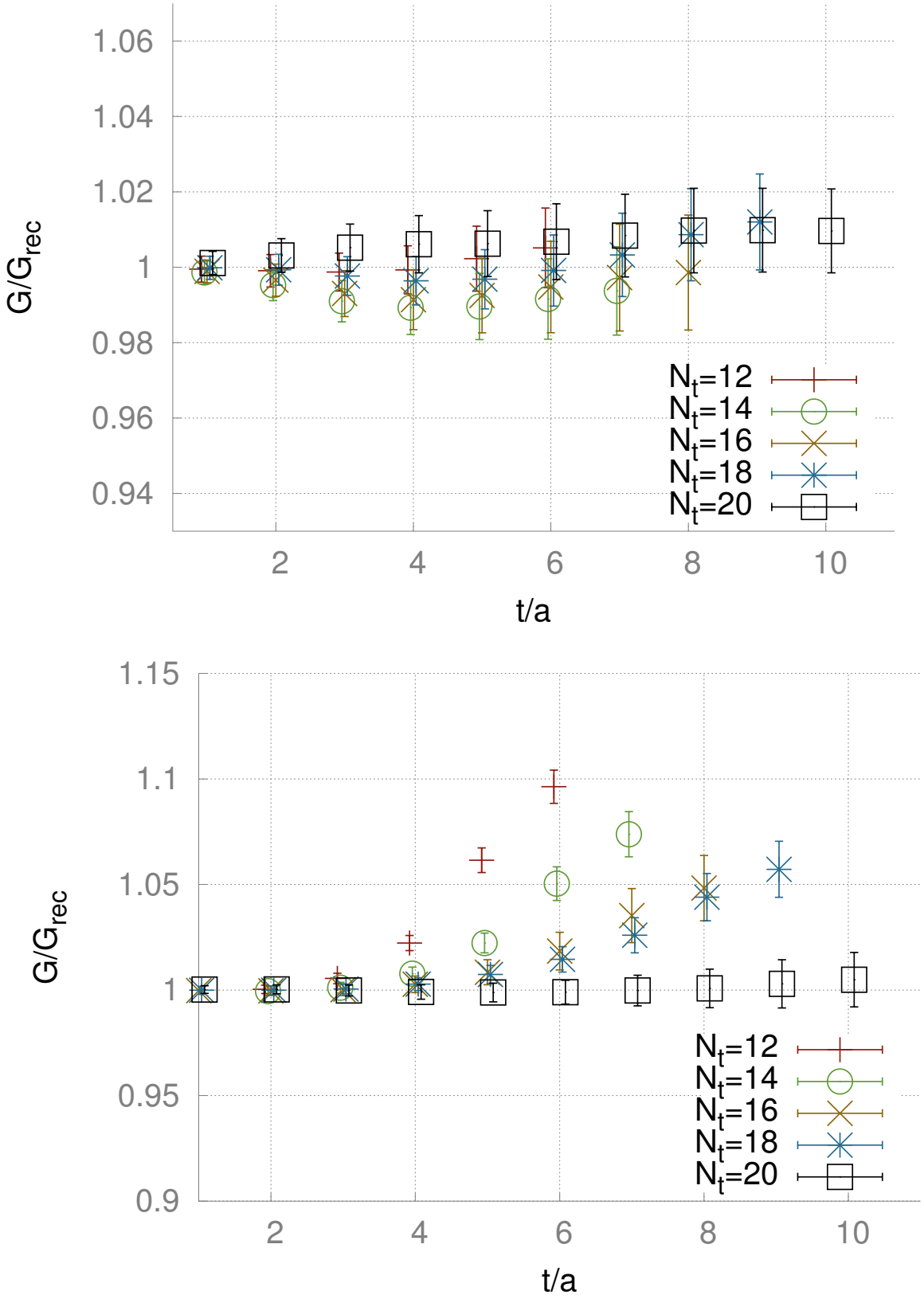

Figure 2.13: The ratio G/G_{rec} in the pseudoscalar(top) and vector(bottom) channels. Error bars include both systematic and statistical errors.

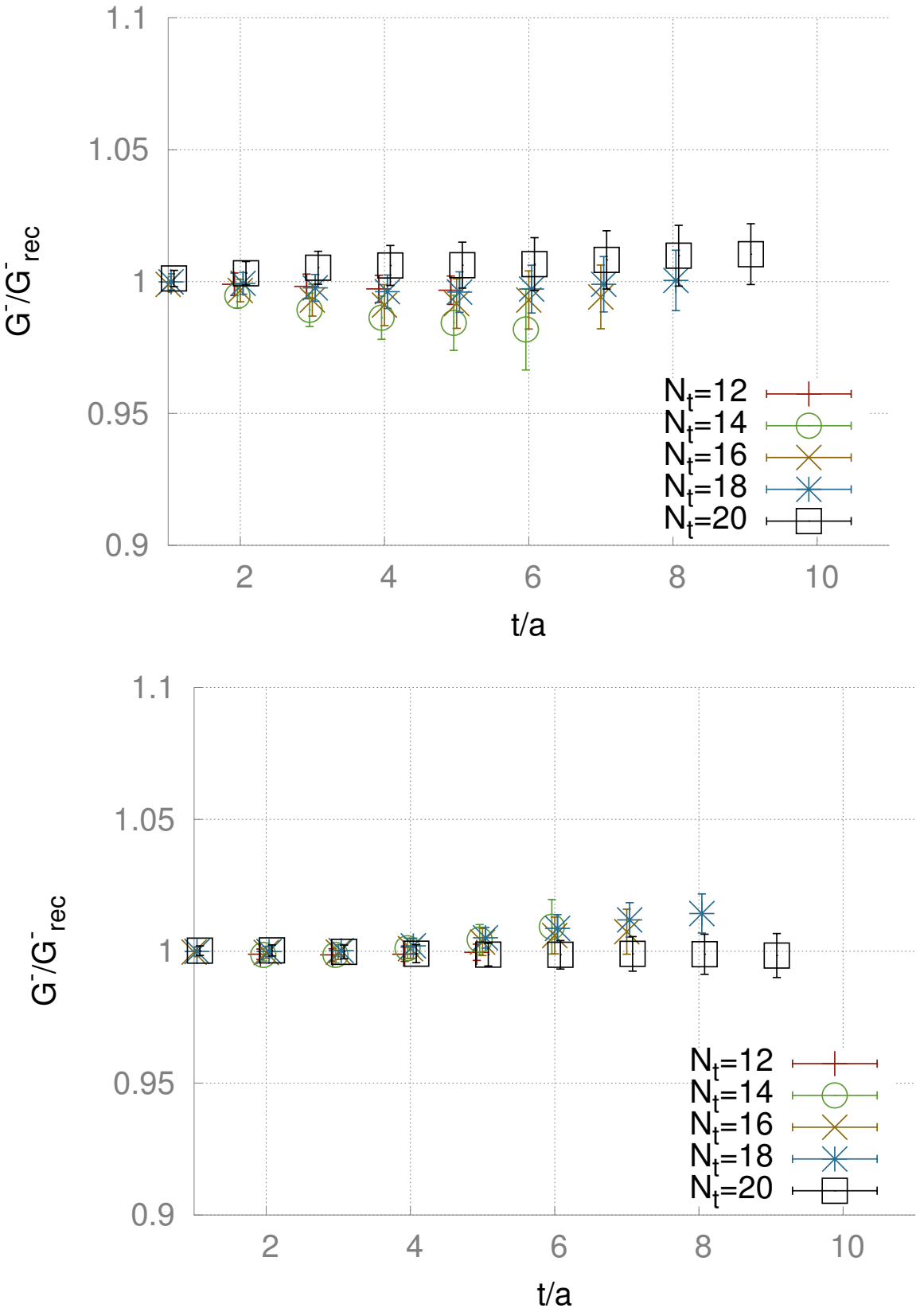

Figure 2.14: The ratio $G^{-}/G^{-}_{\mathrm{rec}}$ in the pseudoscalar(top) and vector(bottom) channels. Error bars include both systematic and statistical errors.

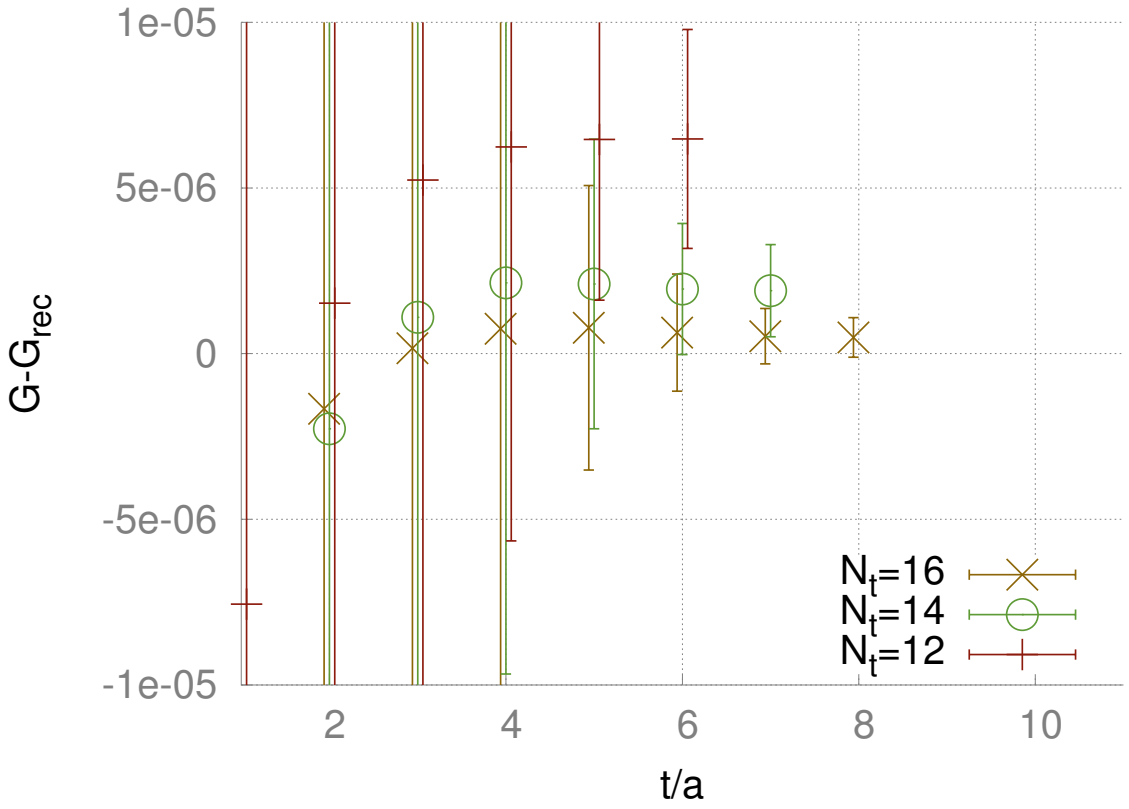

Figure 2.15: The difference $G - G_{\mathrm{rec}}$ in the vector channel at the 3 highest temperatures. If we assume the ansatz $A(\omega, T) = f(T)\omega\delta(\omega - 0^+) + A(\omega, T_{\mathrm{ref}})$ the difference is equal to $f(T)T/2$. Error bars include both systematic and statistical errors.

2.7 What do we expect in the case of melting?

Even though we see no indication of melting in any of the channels, it is instructive to see how G/G_{rec} would look like (qualitatively) in the case of melting states. In particular, it is important to consider the question: If the peak actually did melt, how big an effect would that have on G/G_{rec}? One might suspect, that the effect is quite small, because of the experience with MEM reconstruction. For example, we have noted several times already, that the widths of the peaks are often not well reconstructed by MEM. This means that the Euclidean correlator is not really sensitive to the width. So, it could be, that the width already increased considerably at finite temperature, but we just don't see it in the correlator. So the question is: how big an effect are we looking for? Looking at Figure 2.13, we see that at the current level of statistics an accuracy of $\approx 2\%$ is feasible in G/G_{rec}, that can improve somewhat, but if the effect we are looking for is smaller than, say 1%, we probably won't be able to see it in lattice simulations for quite a while. So

with that in mind, we go on to look at some scenarios of the spectral function changing in a variety of ways.

Let us consider a very simple model of the spectral function, the sum of a Lorentzian peak and a continuum contribution that goes to const. $\times\, \omega^2$ as $\omega \to \infty$:

$$\frac{A(\omega)}{\omega^2} = \frac{h}{\pi} \frac{\gamma}{(\omega - m)^2 + \gamma^2} + K \frac{1}{1 + \exp\left(\frac{m_{\mathrm{th}} - \omega}{\delta}\right)} \tag{2.57}$$

Since the UV physics should be temperature independent, there should be a high ω part in the spectral function that does not change significantly. We will assume that the continuum contribution does not change with temperature. The melting can take place in various forms (and the combinations thereof):

- The position of the ground state peak (m) goes up
- The width of the ground state peak (γ) increases
- The area of the peak (h) diminishes

The effect of these variations can bee seen on Figure 2.16. The most important feature to take note of, is that the ratio G/G_{rec} is much more sensitive to m and h, than to the width γ. A factor of 2 change in the thermal width in this example leads to an approximately 4% change in G/G_{rec}. That is small, but it should already be visible.

We also look at a different scenario, where the peaks are not so well separated, but we have a comb of melting peaks (multiply Lorentzian peaks in the ansatz). Similarly as before, the effect of the thermal width doubling should already be noticeable in G/G_{rec}. It seems therefore, that substantial, nontrivial changes of the spectral function should most likely lead to G/G_{rec} being significantly different from 1, even with our current error bars. We also note, that the different scenarios of the ground state peak melting (Fig. 2.16) more often than not tend to decrease G/G_{rec}, which is the opposite of what happens when a diffusion peak appears in the spectral function (see Fig. 2.13). If the two phenomena occur at the same time, it is difficult to disentangle the two effects.

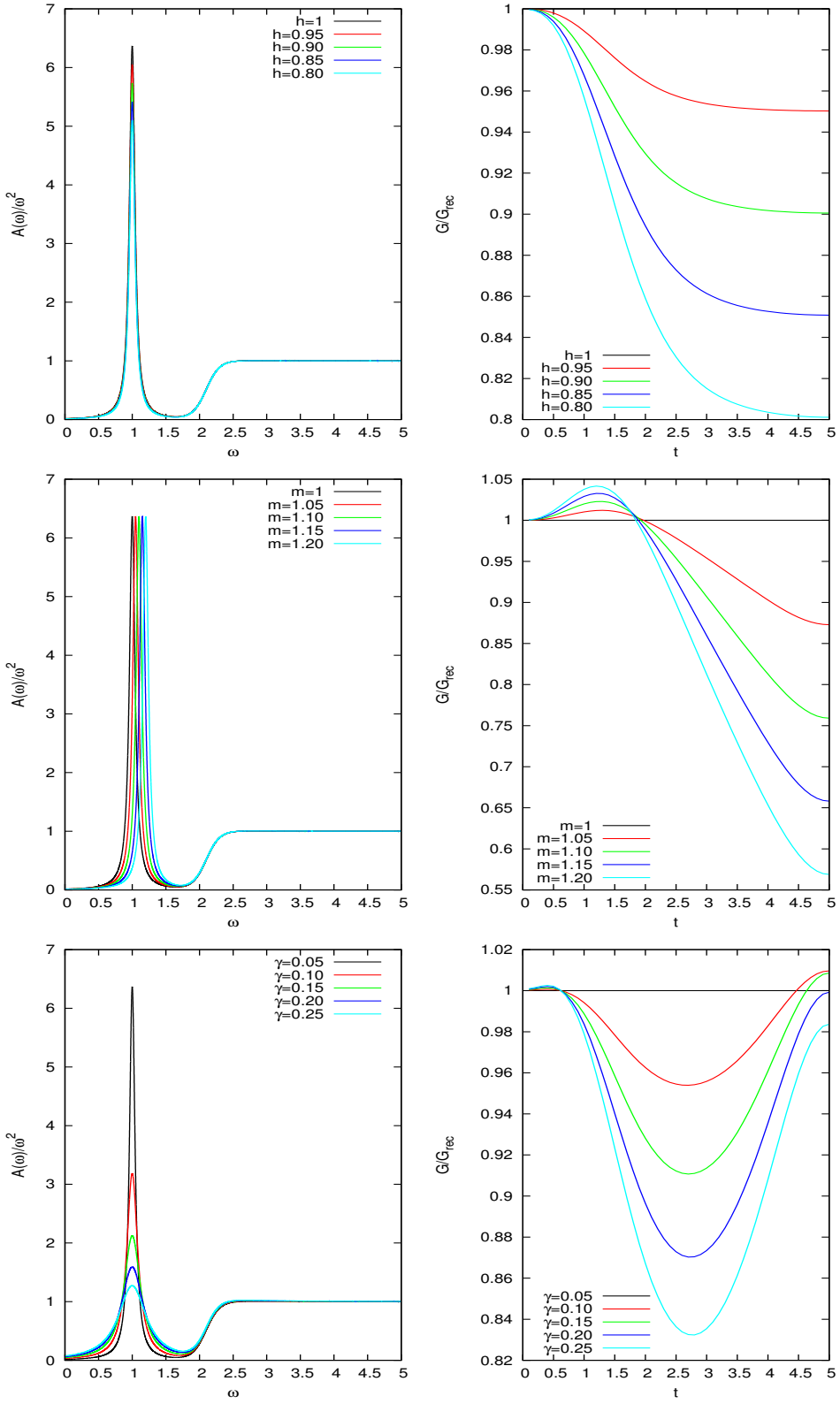

Figure 2.16: Illustrating the effect of the change of the peak position, width or area. On the left we can see the different spectral functions. On the right we have G/G_{rec}. Here, G_{rec} is calculated from the black spectral function, while G is calculated from the spectral function with the corresponding color.

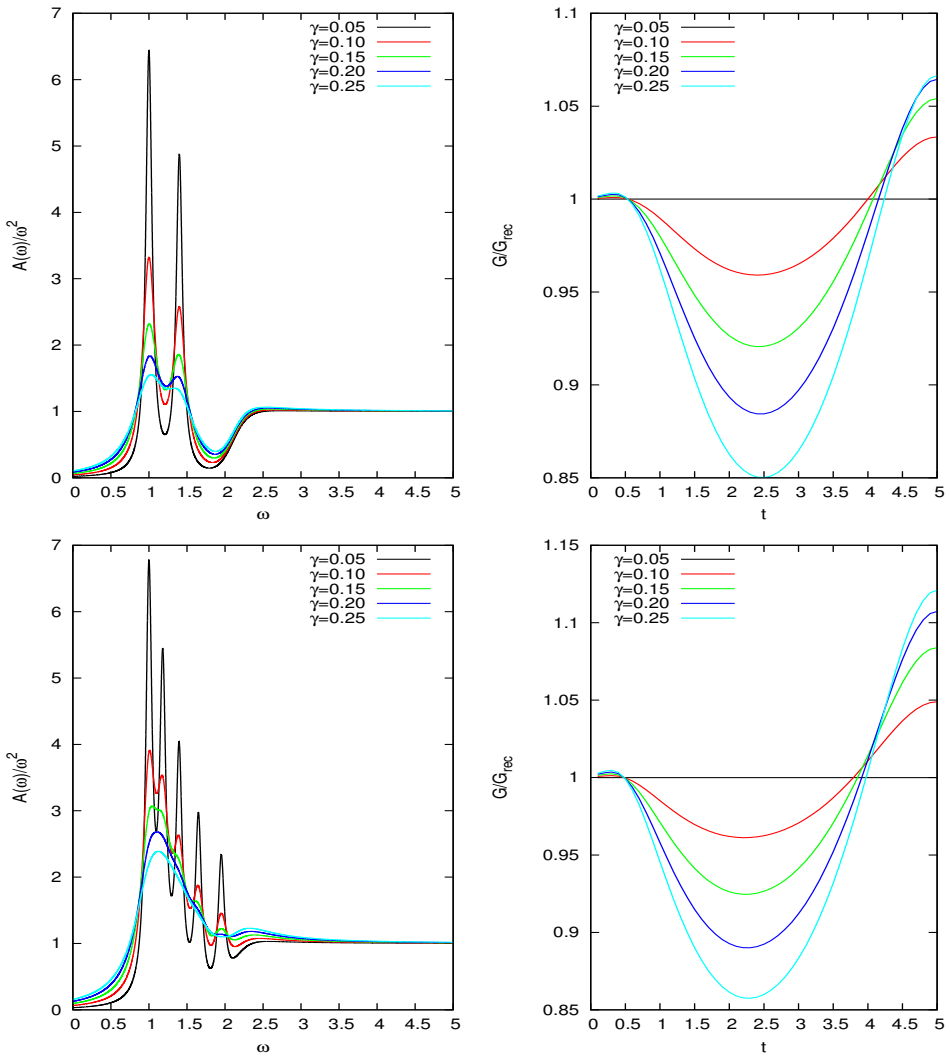

Figure 2.17: Illustrating the effect of a comb of melting peaks for 2 and 5 peaks. On the left we can see the different spectral functions. On the right we have G/G_{rec}. Here, G_{rec} is calculated from the black spectral function, while G is calculated from the spectral function with the corresponding color.

Chapter 3

The static $Q\bar{Q}$ free energy and screening masses

As we have seen in the previous sections, even though in principle the spectral function contains the important physical information, calculating it directly is difficult. For this reason, it is customary to use potential models to deduce some physical conclusions regarding quarkonium systems. This was already mentioned in the introduction where we talked about the naive potential model that historically first motivated the investigations of charmonium at finite temperature. In this section we start by giving a short introduction to the potentials proposed in the literature. This is important, because we have a long history of mutually inconsistent definitions of the static $Q\bar{Q}$ potential at finite temperature. Next, we discuss our results on the static $Q\bar{Q}$ pair free energies. These results were published in Ref. [76].

3.1 An introduction to static potentials

3.1.1 Static potential in non-relativistic QM

The notion of a static potential in non-relativistic quantum mechanics is quite simple. Let's start with the relative coordinate part of the 2-body problem, with the Hamiltonian:

$$H_{\text{rel}} = \frac{P^2}{2\mu} + V(r), \tag{3.1}$$

where $\mu = \frac{m_1 m_2}{m_1+m_2}$ is the reduced mass. In the limit $\mu \to \infty$ the kinetic term vanishes and the wave function Ψ satisfies the static Schrödinger equation:

$$i\partial_t \Psi = V(r)\Psi, \tag{3.2}$$

which can be immediately integrated to give:

$$\Psi(r,t) = e^{-iV(r)t}\Psi(r,0), \tag{3.3}$$

meaning that in the static limit the only change in the wave function with time consists in the accumulation of a phase. Analytically continuing this to Euclidean times we get

$$\Psi(r,-i\tau) = e^{-V(r)\tau}\Psi(r,0), \tag{3.4}$$

meaning that we can read off the potential from the exponential fall off of the wave function in Euclidean time. Another way to look at this is to consider the transition amplitude:

$$\langle r|e^{-iHt}|r'\rangle \xrightarrow{m\to\infty} \delta(r-r')e^{-iV(r)t}, \tag{3.5}$$

or, in the Euclidean case:

$$\langle r|e^{-H\tau}|r'\rangle \xrightarrow{m\to\infty} \delta(r-r')e^{-V(r)\tau}. \tag{3.6}$$

Let us also briefly discuss how things look in the second quantized formalism, but still at zero temperature. Let us introduce two field operators ϕ and χ. We will think about these as corresponding to Q and $\bar{Q}$, but not in QCD, but a naive non-relativistic potential model. Then the Hamiltonian is of the form:

$$\begin{aligned} H = \int d^3x\phi^\dagger(\mathbf{x})(-\frac{\Delta}{2M})\phi(\mathbf{x}) + \int d^3x\chi^\dagger(\mathbf{x})(-\frac{\Delta}{2M})\chi(\mathbf{x}) + \\ + \int d^3xd^3y\phi^\dagger(\mathbf{x})\chi^\dagger(\mathbf{y})V(\mathbf{x}-\mathbf{y})\chi(\mathbf{y})\phi(\mathbf{x}). \end{aligned} \tag{3.7}$$

Let us also introduce the $Q\bar{Q}$ correlator:

$$G_>\left(t,\mathbf{r}_1;t,\mathbf{r}_2|0,\mathbf{r}_1^{'};0,\mathbf{r}_2^{'}\right) = \langle 0|\,\chi(t,\mathbf{r_2})\phi(t,\mathbf{r_1})\phi^\dagger(0,\mathbf{r}_1^{'})\chi^\dagger(0,\mathbf{r}_2^{'})\,|0\rangle\,, \tag{3.8}$$

where $|0\rangle$ is the Fock-vacuum of the fields, i.e. $\chi\,|0\rangle = 0 = \phi\,|0\rangle$. Then, from the Heisenberg equations of motion of the field operators, i.e. $i\partial_t\phi = [H,\phi]$, one can deduce:

$$i\partial_t\phi(t,\mathbf{r_1}) = -\frac{\Delta_{\mathbf{r}_1}}{2M}\phi(t,\mathbf{r}_1) + \int d^3y\chi^\dagger(t,\mathbf{y})V(\mathbf{r}_1-\mathbf{y})\chi(\mathbf{y})\phi(\mathbf{r}_1), \tag{3.9}$$

and similarly, for χ, from which one arrives (using the canonical commutation relations, like $\{\chi(t,\mathbf{x}),\chi^\dagger(t,\mathbf{y})\} = \delta(\mathbf{x}-\mathbf{y})$ and the fact the $|0\rangle$ is the vacuum state) at the equation of motion for the correlator:

$$\left(i\partial_t + \frac{\Delta_{\mathbf{r}_1}}{2M} + \frac{\Delta_{\mathbf{r}_2}}{2M} - V(\mathbf{r}_1-\mathbf{r}_2)\right)G_>\left(t,\mathbf{r}_1;t,\mathbf{r}_2|0,\mathbf{r}_1^{'};0,\mathbf{r}_2^{'}\right) = 0, \tag{3.10}$$

which is just a Schrödinger equation. Once again, in the infinite mass limit the kinetic terms disappear, and the potential will lead to an accumulation of a phase in the correlator. Now, unlike the formalism of the previous paragraph, this has a chance of being generalizable to finite temperature as well. At $T > 0$ the quarkonium system does not have a wave function, but the correlator exists and is well defined, as a thermal expectation value.

3.1.2 Static potential in gauge theory at $T = 0$

In this subsection we will mostly follow Ref. [2]. The reason for repeating some textbook material here is to emphasize what we mean precisely by a static quark (intuitively, it is of course just an external charge). In pure gauge theory in the continuum Minkowski space, the action is:

$$S = -\frac{1}{4}\int d^4x F^a_{\mu\nu}F^{\mu\nu a}. \tag{3.11}$$

In the canonical formalism (similarly to the case of QED) there is no conjugate momentum for A_0, and the corresponding constraint $\pi_0 = 0$ is most easily solved by choosing the temporal gauge:

$$A_0 = 0. \tag{3.12}$$

The momenta conjugate to the remaining fields A^{ia} are:

$$\pi^a_i = \frac{\delta S}{\delta(\partial_0 A^{ia})} = -F^a_{0i} = F^{0ia} = -E^a_i, \tag{3.13}$$

where we introduced the chromoelectric fields E^a_i. If we also introduce the chromomagnetic fields as:

$$B^a_i = -\frac{1}{2}\epsilon_{ijk}F^{jka}, \tag{3.14}$$

then the Hamiltonian is:

$$H = \frac{1}{2}\int d^3x (E^a_i E^a_i + B^a_i B^a_i). \tag{3.15}$$

Now, the important point is that the Gauss-law:

$$D^i E_i = 0, \tag{3.16}$$

is not part of the Hamiltonian equations, it has to be imposed as an initial condition. It is then valid for all times because $\partial_0(D^i E_i) = 0$ follows from the equations of motion.

Now, if we consider the coordinate representation wave functional $\psi[A]$, i.e. a functional of the gauge fields at time zero, then the electric field becomes an operator acting

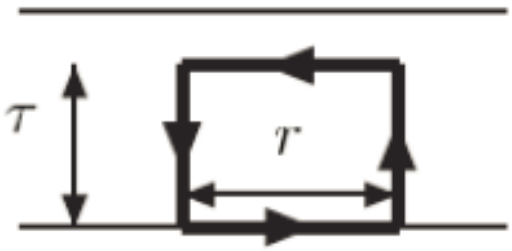

Figure 3.1: The Wilson loop $\mathcal{C}_{RT}$.

on the wave functional as $i\frac{\delta}{\delta A^{ia}}$, and the quantity in the Gauss-law $D^i E_i$ becomes the generator of local gauge transformations acting on the wave functional. Thus the Gauss-law, which expresses the absence of external charges, is equivalent to the gauge invariance of the wave functional. In order to introduce external charges, we have to consider non-invariant wave functionals. If the wave functional transforms according to the fundamental representation of the gauge group:

$$\psi_\alpha \to \Lambda_{\alpha\beta}(\mathbf{x})\psi_\beta, \tag{3.17}$$

then the divergence of E acts on these wave functionals as:

$$D^i E_i^a = gT^a\delta^{(3)}(\mathbf{x}). \tag{3.18}$$

This is what we call a static quark. A state with a static quark at $\mathbf{x}$ and a static antiquark at $\mathbf{y}$ transforms as:

$$\psi_{\alpha\beta} \to \Lambda_{\alpha\gamma}(\mathbf{x})\Lambda^{-1}_{\delta\beta}(\mathbf{y})\psi_{\alpha\beta}. \tag{3.19}$$

Because of the gauge invariance of the Hamiltonian, states with different configurations of static charges completely decouple, meaning that states with a static quark at $\mathbf{x}$ and a static antiquark at $\mathbf{y}$ form a Hilbert space of their own $\mathcal{H}_{\mathbf{xy}}$. We can then define the static quark potential as:

$$V(R = |\mathbf{x} - \mathbf{y}|) = \min_{\mathcal{H}_{\mathbf{xy}}} \langle \mathrm{H} \rangle . \tag{3.20}$$

On a Euclidean lattice, the above considerations can be repeated, but the wave function will depend on the link variables U, not the continuum gauge fields A at time zero. We can give the recipe for computing the potential on the lattice, as the logarithm of the Wilson loop for large T time extents (see Fig. 3.1):

$$V(R) = -\lim_{T\to\infty} \frac{1}{T} \ln \langle 0| \operatorname{Tr} \left(U \left(\mathcal{C}_{RT} \right) \right) |0\rangle \tag{3.21}$$

It does not take long to derive this result. For any state $\Psi \in \mathcal{H}_{\mathbf{xy}}$ we have after inserting a complete set of states:

$$\langle \Psi| e^{-TH} |\Psi\rangle = \sum_n |\langle n|\Psi\rangle|^2 e^{-TE_n} \xrightarrow[T\to\infty]{} |\langle 0_{\mathbf{xy}}|\Psi\rangle|^2 e^{-TV(R)}, \tag{3.22}$$

where $|0_{\mathbf{xy}}\rangle$ is the ground state of $\mathcal{H}_{\mathbf{xy}}$, procided that the overlap $\langle 0_{\mathbf{xy}}|\Psi\rangle$ is not zero. Notice, that this equation is analogous[1] to eqs. (3.4) and (3.6). Now, if we choose a test function in $\mathcal{H}_{\mathbf{xy}}$:

$$\Psi_{\alpha\beta}[U] = U_{\alpha\beta}(\mathbf{x},\mathbf{y})\Omega[U], \tag{3.23}$$

where $U(\mathbf{x},\mathbf{y})$ is the parallel transporter for a straight path between $\mathbf{x}$ and $\mathbf{y}$, and $\Omega[U]$ is the gauge invariant vacuum wave function, and we use the lattice version of the temporal gauge which makes the time-like transporters 1, we have:

$$\begin{aligned}\langle\Psi|\, e^{-TH}\,|\Psi\rangle &= \frac{1}{Z}\int \mathcal{D}U\bar{U}_{\alpha\beta}(\mathbf{x}+T\hat{4},\mathbf{y}+T\hat{4})U_{\alpha\beta}(\mathbf{x},\mathbf{y})e^{-S} = \\ &= \frac{1}{Z}\int \mathcal{D}U\,\mathrm{Tr}\left(U\left(\mathcal{C}_{RT}\right)\right)e^{-S} = \langle 0|\,\mathrm{Tr}\left(U\left(\mathcal{C}_{RT}\right)\right)|0\rangle\,,\end{aligned} \tag{3.24}$$

which is exactly what we wanted to show.

3.1.3 Real-time static potential at $T > 0$

Generalizing the previous result to finite temperature is not straightforward. As we have already argued in the case of non-relativistic QM, the considerations with the wave function cannot be directly generalized to finite temperature. However, similarly to equation (3.10), we can look at the Schrödinger equation satisfied by thermal correlators (if there is one). To do this let us start with the correlator:

$$G_{>}^{M_R M_R^\dagger}(t,r,T) \equiv \left\langle M_R(t)M_R^\dagger(0)\right\rangle \quad (t>0), \tag{3.25}$$

where the operator $M_R(t)$ is defined as:

$$M_R(t) = \bar{Q}(x)\Gamma U(x,y)Q(y), \tag{3.26}$$

where the coordinate four-vectors are taken at the same time: $x = (t,\mathbf{x})$ and $y = (t,\mathbf{y})$, the space-like separation is $R = |\mathbf{x}-\mathbf{y}|$, U is a parallel transporter, and Γ is some γ matrix depending on the channel. This is then analogous to to operator defined in equ. (3.8) in the case of non-relativistic quantum mechanics. The difference is that for relativistic fields

[1] There is an important difference, so it is not a complete analogy. In non-relativistic QM the position eigenstate $|r\rangle$ is an eigenstate of the Hamiltonian in the $M\to\infty$ limit. This is not true to our test function, but we can still use it to project out the energy we are interested in. A more complete analogy would be there if we considered the state $|r\rangle$, but at a finite mass M. In this case the propagation amplitude would not simply be (3.6), but we would have $\langle r|e^{-HT}|r'\rangle \xrightarrow{T\to\infty} \delta(r-r')\,\langle r|0\rangle\,\langle 0|r'\rangle\, e^{-E_0 T}$. instead.

Q and $\bar{Q}$ are not described by independent fields and that we have introduced a parallel transporter to respect gauge invariance. Ref. [77] proposed the following definition of the static potential at finite temperature. Assume that in the static quark limit

$$(i\partial_t - V(t,r,T))G_>(t,r,T)_{M\to\infty} = 0, \tag{3.27}$$

where we have dropped the superscripts $M_R M_R^\dagger$. Calculate $G_>(t,r,T)$ in some approximation, then plug it into this formula to calculate:

$$V(t,r,T) = \left(\frac{i\partial_t G_>(t,r,T)}{G_>(t,r,T)}\right)_{M\to\infty}. \tag{3.28}$$

Note, that whatever $G_>$ is, this can always be done, so equation (3.27), that says the correlator in the static quark limit satisfies a Schrödinger equation just gives the definition of V, equ. (3.28). To go on, one needs an additional assumption for the case of a finite, but heavy quark mass:

$$(i\partial_t + \frac{\Delta}{2M} - V(t,r,T))G_>(t,r,T)_{M=\text{heavy, finite}} = 0, \tag{3.29}$$

This assumption is far from trivial, and in fact has not been systematically derived from QCD with well defined approximations so far. Still, it is the best guess we have of a good potential model of quarkonia at finite temperature. If a potential model is really adequate for the thermal correlator, there is a good chance that this is how the potential has to be computed. We can also see that equ. (3.28), as a definition of the static potential, does not bypass our greatest difficulty in calculating the quarkonium spectral functions. Since it is defined in terms of real time quantities, it needs analytical continuation, just like the direct determination of spectral functions does, it is just that the correlator we have to analytically continue is different, and is defined in the infinite quark mass limit. Ref. [77] also noted that the real time static potential defined this way is complex, after calculating the late time behavior of the correlator $G_>$ in hard thermal loop approximation at high temperature.

Let us try to motivate this statement about the imaginary part of the real time potential in general terms. Let us call eigenstates of the Hamiltonian without heavy quarks or antiquarks $|n\rangle$, with eigenvalue E_n, and eigenstates with a heavy quark-antiquark pair separated by a distance R, with eigenvalue $E_{n'}(R)$ $|n';R\rangle$. Clearly, the operator M_R, when acting on an energy eigenstate of type n can be expanded on the energy eigenvectors as:

$$M_R^\dagger |n\rangle = \sum_{m'} A_{n,m'} |m';R\rangle\,, \tag{3.30}$$

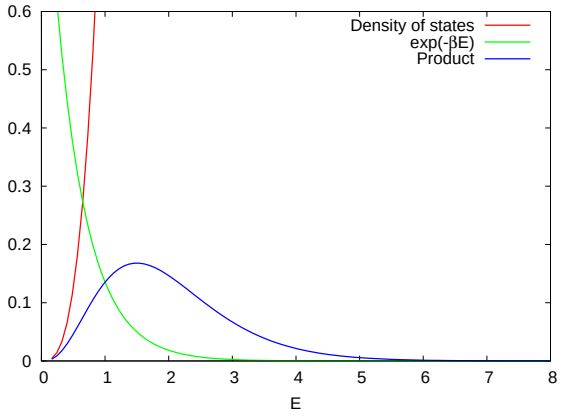

Figure 3.2: A sketch of the density of states vs the Boltzmann weight.

where the $A_{n,m'}$ are some complex coefficients. Let us expand the correlator $G_>$ in the energy eigenbasis. Here we make the following approximation: Since we are interested in $T \ll M$, no states of type $|n'; R\rangle$ have to be put next to $e^{-\beta H}$, since they are suppressed by a factor of $e^{-2M/T}$. For similar reasons we do not have to put in states with 1,2,3,... heavy quarks:

$$G_>(t) \approx \frac{1}{Z} \sum_n \langle n|e^{-\beta H} e^{iHt} M_R(0) e^{-iHt} M_R^\dagger(0)|n\rangle \,. \tag{3.31}$$

Next, we put in a complete set of states, and use that (as we discussed previously) the sectors of the Hilbert space with no heavy quarks is orthogonal to the sector with a heavy $\bar{Q}Q$ pair at distance r, also this sector is orthogonal to the sector with a heavy $\bar{Q}Q$ pair at some distance other distance:

$$\begin{aligned} G_>(t) \approx \frac{1}{Z} \sum_{n,n'} \langle n|e^{-\beta H} e^{iHt} M_R(0) e^{-iHt}|n'; R\rangle \, \langle n'; R|M_R^\dagger|n\rangle = \\ = \frac{1}{Z} \sum_{n,n'} e^{-\beta E_n} e^{i(E_n - E_{n'}(R))t} \left|\langle n'; R|M_R^\dagger|n\rangle\right|^2 . \end{aligned} \tag{3.32}$$

Consider first $T \to 0$. In this case the sum over n is dominated by the ground state $n = 0$. The sum over n' has many states, however the excited states lead to a more rapid oscillation than the ground state (of this subspace), so the static potential can be unambiguously defined as the smallest oscillation frequency, irrespective of the operator M_R chosen (irrespective of the path we use for the parallel transporter). The motion remains periodic, or coherent, at all times, given that only the discrete part of the string spectrum is excited. At $T > 0$ however, the sum is not trivial. For any given n', the contributions with $n > 0$ make the oscillations slower. How they do that exactly depends of the matrix elements of M_R. If some state n dominates the sum, then the oscillation

frequency will be reduced from $E_{n'}(R) - E_0$ to $E_{n'}(R) - E_n$. This phenomenon can be referred to as screening. Now, at high temperatures, say $T > 2m_\pi$ scattering states will also be excited. The density of states will rapidly increase in this case, and we may expect to find a kind of "resonance", the density of states $\tilde{\rho}$ will be rapidly increasing, while $e^{-\beta E_n}$ will be rapidly decreasing. The product can have a peak in this case. This is illustrated in Fig. 3.2. We model this peak by a Breit-Wigner form, then the sum over n is given by the Fourier transform of the Breit-Wigner function:

$$\begin{aligned}\sum_n e^{-\beta E_n + iE_n t} \left|\langle n'; R|M_R^\dagger|n\rangle\right|^2 &\to \int dE_n \tilde{\rho}(E_n) e^{-\beta E_n + iE_n t} \left|\langle n'; R|M_R^\dagger|n\rangle\right|^2 \\ &\approx \int dE_n e^{iE_n t} \frac{K(n', R, T)}{(E_n - \epsilon(n', R, T))^2 + \gamma^2(n', R, T)} \\ &\propto \exp\left(i\epsilon(n', R, T)t - \gamma(n', R, T)t\right). \quad (3.33)\end{aligned}$$

We observe that apart from the energy shift, represented by ϵ, the absolute value of the correlator also decreases. This means that the static potential has an imaginary part. This can be referred to as decoherence. In the finite temperature case, both screening and decoherence are dependent on n', R, T and the choice of the operator M_R. To summarize: at finite temperature the real-time static potential should have an imaginary part, but both the real and the imaginary part depends on the choice of the operator M_R. Also, whatever the choice of the operator we make, to get the potential we have to do an analytic continuation. An attempt at such an analytic continuation with MEM from quenched lattice data is performed in Ref. [78].

3.2 Static quark free energy

We have seen, that the determination of the spectral functions, both directly and with potential models, runs into the great difficulty of analytic continuation. It is therefore useful, to consider a related, but simpler problem, the determination the excess free energy we get by inserting two static quarks in the plasma. This is not the potential governing the time evolution of the correlator defined in the previous section, since it is real. It is however a well defined gauge-invariant quantity, and it carries non-trivial information on the confinement properties of the medium, and unlike the real-time potential, it can be effectively calculated on the lattice. We briefly review the derivation of the free energy expressed from the Polyakov-loop, first proposed in Ref. [79]. The excess free energy for

1 static quark and 1 static antiquark can be expressed as:

$$e^{-\beta F_{\bar{Q}Q}} = \sum_{|s\rangle} \langle s|e^{-\beta H}|s\rangle \,, \tag{3.34}$$

where the summation runs over states $|s\rangle$ containing a static quark at $\mathbf{r}$ and static antiquarks at $\mathbf{r}'$. Let us introduce the operators $Q_a(t,\mathbf{r})^\dagger$ and $Q_a(t,\mathbf{r})$ creating and eliminating the static quarks with color index a and space-time position $x=(t,\mathbf{r})$, and let us denote the charge conjugate of $Q_a(t,\mathbf{r})$ with $Q^c_a(t,\mathbf{r})$. Then:

$$\begin{aligned}
e^{-\beta F_{\bar{Q}Q}} &= \sum_{|s'\rangle} \left\langle s' \left| \sum_{a,a'} Q_a(0,\mathbf{r}) Q^c_{a'}(0,\mathbf{r}') e^{-\beta H} Q^\dagger_a(0,\mathbf{r}) Q^{c\dagger}_{a'}(0,\mathbf{r}') \right| s' \right\rangle = \\
&= \sum_{|s'\rangle} \left\langle s' \left| \sum_{a,a'} e^{-\beta H} e^{\beta H} Q_a(0,\mathbf{r}) e^{-\beta H} e^{\beta H} Q^c_{a'}(0,\mathbf{r}') e^{-\beta H} e^{\beta H} e^{-\beta H} Q^\dagger_a(0,\mathbf{r}) Q^{c\dagger}_{a'}(0,\mathbf{r}') \right| s' \right\rangle = \\
&= \sum_{|s'\rangle} \left\langle s' \left| \sum_{a,a'} e^{-\beta H} Q_a(\beta,\mathbf{r}) Q^c_{a'}(\beta,\mathbf{r}') Q^\dagger_a(0,\mathbf{r}) Q^{c\dagger}_{a'}(0,\mathbf{r}') \right| s' \right\rangle = \\
&= \sum_{|s'\rangle} \left\langle s' \left| \sum_{a,a'} e^{-\beta H} Q_a(\beta,\mathbf{r}) Q^\dagger_a(0,\mathbf{r}) Q^c_{a'}(\beta,\mathbf{r}') Q^{c\dagger}_{a'}(0,\mathbf{r}') \right| s' \right\rangle ,
\end{aligned} \tag{3.35}$$

where $|s'\rangle$ denotes states without static quarks. This can be further simplified by utilizing the static Dirac equation satisfied by the heavy quarks:

$$(\frac{1}{i}\partial_t - gA^0(t,\mathbf{r}))Q(t,\mathbf{r}) = 0, \tag{3.36}$$

where A^0 is a Lie-algebra valued variable. Integrating this equation, we have:

$$Q(t,\mathbf{r}) = \mathcal{P}\exp\left(ig\int_0^t dt' A^0(t',\mathbf{r})) \right) Q(0,\mathbf{r}). \tag{3.37}$$

Introducing the Polyakov-loop as a path ordered exponential:

$$L(\mathbf{r}) = \mathcal{P}e^{ig\int_0^\beta dt A^0(t,\mathbf{r})}, \tag{3.38}$$

we arrive at:

$$e^{-\beta F_{\bar{Q}Q}} = \sum_{|s'\rangle} \langle s'|e^{-\beta H} \operatorname{Tr} L(\mathbf{r}) \operatorname{Tr} L^\dagger(\mathbf{r}')|s'\rangle = \langle \operatorname{Tr} L(\mathbf{r}) \operatorname{Tr} L^\dagger(\mathbf{r}')\rangle \tag{3.39}$$

This is the main formula for our determination of the free energy. The lattice version of the Polyakov loop is:

$$L(\mathbf{x}) = \prod_{x_4=0}^{N_t-1} U_4(\mathbf{x},x_4). \tag{3.40}$$

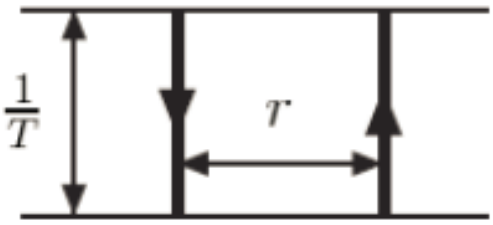

Figure 3.3: The Polyakov loop, measured at two different point in 3-space gives the correlator, from which we can calculate the static $Q\bar{Q}$ pair free energy.

After calculating this the gauge invariant $\bar{Q}Q$ free energy is given by:

$$F_{\bar{Q}Q}(r) = -T \ln C(r,T) = -T \ln \left\langle \sum_{\mathbf{x}} \mathrm{Tr} L(\mathbf{x}) \mathrm{Tr} L^{+}(\mathbf{x}+\mathbf{r}) \right\rangle . \tag{3.41}$$

This derivation can be repeated for any number of static quarks, the free energy of n static quarks is given by the expectation value of n Polyakov loops. We finish this section with two comments:

- The so-called singlet and octet free energies have been proposed [80, 81, 82, 83, 84], as a decomposition of the free energy. It was customary to use the singlet free energy as input for potential models, with the single free energy being:

  $$F_1 = -T \ln \left(\mathrm{Tr} \left(L(\mathbf{r}) L(\mathbf{0}) \right) \right) . \tag{3.42}$$

  The problem is that this is not gauge invariant, therefore extracting physical information from it is not straightforward [85].

- The relation between the free-energy and the potential to be inserted in a Schrödinger equation remains an open question. Thus, the effective potential has been identified alternatively with the $\bar{Q}Q$ free energy [86, 87], the internal energy [88, 89] or even with a linear combination of both [90, 91], leading to different dissociation temperatures for the J/Ψ, depending on the choice made. None of these choices can be the potential governing the time evolution of the real time correlator however, since they contain no imaginary part. After this was realized by the community, one approach became identifying the free energy with the real part of the potential [92]. This hypothesis is probably not true in general, as shown by the explicit perturbative calculation in Ref. [93]. Even though these different potential model calculations contain input from the lattice, none of them are derived from QCD itself. Calculations using the real-time static antiquarks potentials can be found in Refs. [77, 94].

- We also note that the literature sometimes includes a factor of $1/N_c = 1/3$ in the definition of the Polyakov loop. This would lead to an additional term in the single static quark free energy that is linear in the temperature.

3.2.1 Simulation details

The simulations were performed by using the tree level Symanzik improved gauge, and stout-improved staggered fermion action, that was used in [95]. We worked with physical quark masses, and fixed them by reproducing the physical ratios m_π/f_K and m_K/f_K [95].

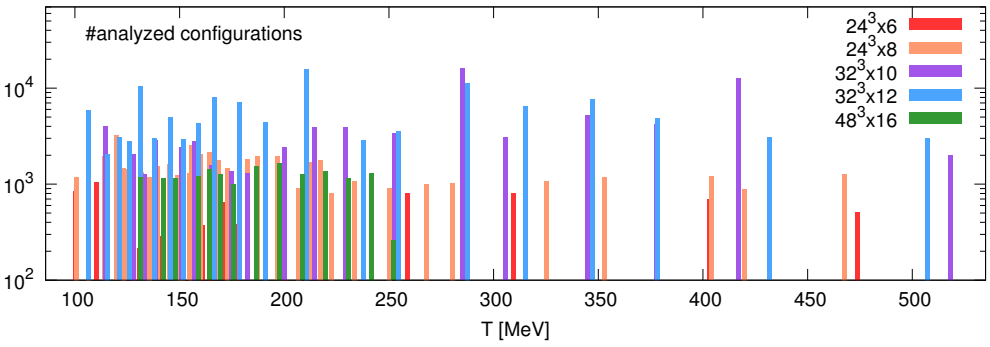

Figure 3.4: Number of the analyzed lattice configurations.

Compared to previous investigations of the Polyakov loop correlators by the Budapest-Wuppertal group, reported in the conference proceedings [96], here we used finer lattices, namely we carried out simulations on $N_t = 12$ and 16 lattices as well as on $N_t = 6, 8, 10$ lattices. Our results were obtained in the temperature range 150 MeV $\leq$ T $\leq$ 450 MeV. We use the same configurations as in Ref. [7] and [97]. Figure 3.4 summarizes our statistics.

3.2.2 Renormalization procedure and continuum extrapolation

After measuring the Polyakov loop correlator $C(r,T)$ at $T = 1/(N_t a)$ temperature, we computed the unrenormalized free energy according to $F_{\bar{Q}Q} = -T \ln C(r,T)$. The $a(\beta)$ function was taken from the line of constant physics, along which we kept the ratios of the physical values of m_π, f_K and m_K fixed at zero temperature. Detailed description of the determination of the line of constant physics can be found in Ref. [97].

Approaching the continuum limit, the value of the unrenormalized free energy diverges. In order to eliminate the additive divergence of the free energy renormalization is needed.

There are various proposals in the literature for this renormalization procedure:

- Earlier works [81, 82, 83] matched the short distance behavior to the $T = 0$ static potential. This is wrong. While it is certainly true, that UV physics should be temperature independent, this is an asymptotic statement, and therefore leaves the renormalization constant undefined. The reason for that is very simple: $1/r$ is asymptotic to $1/r + C$ as $r \to 0$ for any constant C, so C cannot be determined from such an asymptotic matching.

- A more precise definition is to require that the $T = 0$ potential (calculable from the Wilson loop) vanishes at some distance [98, 96]. Although this is a correct procedure, it requires a precise determination of the potential at $T = 0$. This makes the extension of the temperature range of the continuum extrapolation exceedingly difficult, as it requires $T = 0$ simulations at lots of different values of the gauge coupling β, and the determination of the Wilson loop in the limit of large temporal size.

- Here, we use a renormalization procedure based entirely on our $T > 0$ data, similarly to Refs. [99] and [15]. The data contains a temperature independent divergent part from the ground state energy. The difference between the value of free energies at different temperatures is free of divergences. We will argue, that this procedure is not only more efficient computationally (as no $T = 0$ determinations of the Wilson loop are needed), but also allows for the extension of the temperature range for the continuum extrapolation. In an earlier paper of the Budapest-Wuppertal collaboration [15], this prescription was adopted for Wilson fermions, where it is more straightforward to implement. In this work, we introduce an implementation of this prescription, that is suited for staggered fermions.

We define the renormalized free energy as:

$$F^{ren}_{\bar{Q}Q}(r, \beta, T; T_0) = F_{\bar{Q}Q}(r, \beta, T) - F_{\bar{Q}Q}(r \to \infty, \beta, T_0), \tag{3.43}$$

with a fixed T_0. This renormalization prescription corresponds to the choice that the free energy at large distances goes to zero at T_0. For Wilson fermions, where the temperature is usually controlled by N_t, and the the continuum limit by the gauge coupling β the implementation of this prescription is straightforward: at each β only one interpolation

is needed, in temperature, to the reference temperature T_0. For staggered fermions, the temperature is usually controlled by the gauge coupling β, and the continuum limit by N_t. However, the subtraction (3.43) still has to be done at fix β, and not at fix N_t, which makes the implementation of the renormalization prescription more complicated. We will perform it in two steps.

Since the divergence in the free energy is independent[2] of r, it is sufficient to remove it in the $r \to \infty$ limit. Because of the cluster decomposition principle, this limit corresponds to twice the single heavy quark free energy. Therefore in the first step we renormalize the single static quark free energy, which satisfies:

$$2F_Q(\beta, T) = F_{\bar{Q}Q}(r \to \infty, \beta, T) = -T \log \left| \langle \mathrm{Tr}\, L \rangle \right|^2 . \tag{3.44}$$

We define its renormalized counterpart as:

$$F_Q^{ren}(\beta, T; T_0) = F_Q(\beta, T) - F_Q(\beta, T_0). \tag{3.45}$$

In the second step the full renormalized $\bar{Q}Q$ free energy can be written as:

$$F_{\bar{Q}Q}^{ren}(r, \beta, T; T_0) = \tilde{F}_{\bar{Q}Q}(r, \beta, T) + 2F_Q^{ren}(\beta, T; T_0), \tag{3.46}$$

where

$$\tilde{F}_{\bar{Q}Q}(r, \beta, T) = F_{\bar{Q}Q}(r, \beta, T) - F_{\bar{Q}Q}(r \to \infty, \beta, T) = F_{\bar{Q}Q}(r, \beta, T) - 2F_Q(\beta, T), \tag{3.47}$$

Note, that this second step of the renormalization procedure is completely straightforward to implement, at each simulation point in N_t and β we just subtract the asymptotic value of the correlator, that can be computed simply from the Polyakov loop. Doing the renormalization in two steps like this has a technical reason that will be explained shortly.

Let us also mention that the Polyakov loop correlator behaves similarly to baryon correlators in imaginary time[3]: at large values of r we can get negative values of C at some configurations, even though the ensemble average should in principle be positive definite. For this reason, it is highly desirable to use gauge field smearing which makes for a much better behavior at large r, at the expense of unphysical behavior at small r.

[2]This is equivalent to the statement, that once we renormalize the Polyakov-loop itself, there is no additional renormalization needed for the correlator of Polyakov-loops.

[3]They both have a (mild) sign problem.

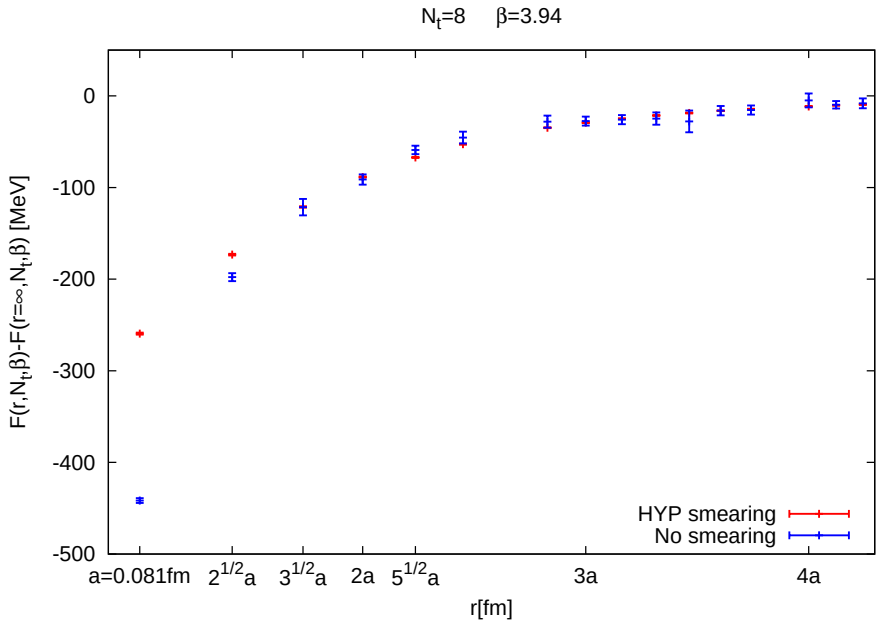

Figure 3.5: The smeared and unsmeared free energies at a given β and N_t, after the first step of the renormalization procedure.

For this reason, we measured the correlators both without and with HYP smearing. We expect that outside the smearing range (i.e. $r \geq 2a$) the two correlators coincide. This is supported by Figure 3.5. Therefore we use the smeared correlators for $r \geq 2a$ and the unsmeared ones for $r < 2a$.

Single heavy quark free energy

First, we discuss the implementation of the renormalization of the single heavy quark free energy, equation (3.45). Notice that if we implemented the renormalization condition (3.43) directly, then we would just need to subtract $2F_Q(\beta, T_0)$ from the unrenormalized free energy, so at first sight it looks like we are doing some unnecessary rounds by doing this in two steps. What we gain by this is that we can extend the temperature range, at which we can do the continuum limit. To understand this statement let us look at Figure 3.6 (top). The dotted black symbols are bare values of $2F_Q$ at given values of N_t and β. The colored symbols are interpolations of these curves, in β to the value of β_0 corresponding to the temperature T_0 at each N_t. If we take for example $T_0 = 200$MeV, corresponding to the green line in the figure, this gives us 5 points from the curve $F_Q(\beta, T_0)$. According

to equation (3.45) this is what we have to subtract from the bare free energy at this value of β to get the renormalized single quark free energy. The disadvantage of the green curve, is that the β range it covers is rather limited. So, if we want to be able to make a continuum limit from say the $N_t = 8, 10, 12$ lattices, the temperature range we can cover is rather limited as well. The lowest temperature we will be able to do a continuum limit at will be $(6/8) \times 200\text{MeV} = 150\text{MeV}$, and the highest temperature will be $(16/12) \times 200\text{MeV} = 266\text{MeV}$. To do a continuum limit at higher temperatures, we need the $F_Q(\beta, T_0)$ curve at higher values of β, and at first, it looks as like that would need runs at higher values of N_t. This is not computationally feasible, but there is a simple trick to extend the temperature range. Clearly, if we call the continuum limit of the single quark free energy

$$F_Q^{\text{ren}}(T; T_0) = \lim_{\beta \to \infty} F_Q^{\text{ren}}(\beta, T; T_0), \tag{3.48}$$

then, for any value of T:

$$F_Q^{\text{ren}}(T; T_0) - F_Q^{\text{ren}}(T; T_1) = F_Q^{\text{ren}}(T_1; T_0) \tag{3.49}$$

is just a number[4]. We can use this fact to extend the temperature range of the continuum limit by using different values of T_0, that is different renormalization prescriptions, and shift them together by the value of the RHS of equ. (3.49). This is the procedure that we will follow.

To implement equation (3.45), we first calculate $F_Q(\beta, N_t)$ or equivalently $F_{\bar{Q}Q}(r \to \infty, \beta, N_t)$ from equation (3.44). Then at each N_t we interpolate to the β value corresponding to the temperature T_0, giving us some points of the function $F_Q(\beta, T_0)$. Finally, we interpolate these $F_Q(\beta, T_0)$ points in β, obtaining the final curve we can use for the renormalization. This procedure is illustrated in Figure 3.6 (top). When doing this interpolation we take into account the error on the data points of $F_Q(\beta, N_t)$ via the jackknife method. The statistical errors of the single quark free energy are very small, meaning that the interpolation method gives a comparable error to the final interpolated value. We estimate the systematic error of the interpolations by constructing different interpolations. For interpolations of the $F_Q(\beta, N_t)$ curves we use linear and cubic spline interpolations (for each value of N_t), and for the interpolation of $F_Q(\beta, T_0)$ we use different polynomial

[4]This statement is only true in the continuum. At finite lattice spacing there is also a lattice spacing dependent artifact in this difference.

interpolations (order 1,2), cubic spline and barycentric rational function interpolation. In total this means $2^5 \times 4 = 128$ different interpolations, then for interpolating the bare F_Q we use spline and linear interpolations, so for the final renormalized values we have in total $128 \times 2 = 256$ different interpolations. All interpolations are taken to have the same weight. We use the median of this as the estimate, and the symmetric median centered 68% as the 1σ systematic error estimate [100]. The statistical and systematic errors turn out to be of the same order, and are then added in quadrature.

After doing this procedure, the β range in which we can interpolate the $F_Q(\beta, T_0)$ curve is limited, therefore, the temperature range where we can do the continuum extrapolation is limited. To extend the temperature range where we can calculate the single heavy quark free energy, we use the fact that the single heavy quark free energies at different temperatures differ only by an additive constant in the continuum. Therefore we use different values of T_0 to do the continuum extrapolation, and shift all those curves to the position of the 200MeV curve. We used 5 different values of T_0, namely, 170 MeV, 200 MeV, 240 MeV, 320 MeV, and 390 MeV. The results of this analysis can be found in Figure 3.6 (bottom). For the continuum limits, we use the $N_t = 8, 10, 12$ lattices, that are available at all temperatures. We use the $N_t = 16$ lattice to estimate the systematic error of the continuum extrapolation, where it is available. If:

$$d_1 = |\text{cont. lim.}(8, 10, 12)| - |\text{cont. lim.}(8, 10, 12, 16)|$$
$$d_2 = |\text{cont. lim.}(8, 10, 12)| - |\text{cont. lim.}(10, 12, 16)|\,,$$

then the systematic error of the continuum extrapolation is taken to be $\max(d_1, d_2)$. Where the $N_t = 16$ lattices are not available, we approximate the relative systematic error by the average of the systematic errors at the parameter values where we had the $N_t = 16$ lattices available. This corresponds to an error level of approximately 10%. The systematic and statistical errors of the continuum extrapolations are then added in quadrature. The linear fits of the continuum limit extrapolations all have good values of χ^2.

Finally, we mention that the determination of the continuum limit of the Polyakov loop, or equivalently, the single static quark free energy is already available in the literature. For two recent determinations of the Polyakov loop see Refs. [7, 101]. The difference is that here we take the continuum limit at significantly higher temperatures.

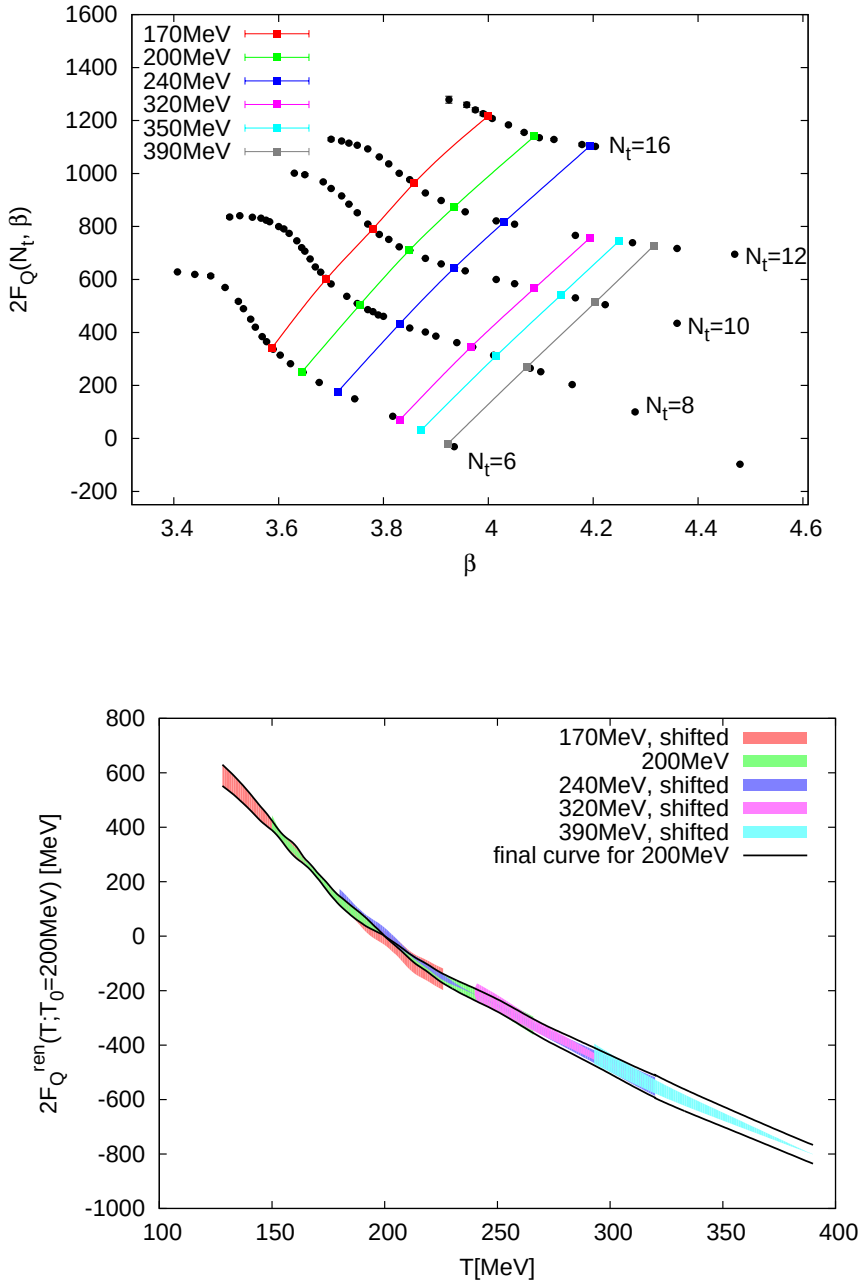

Figure 3.6: Top: Determining $F_Q(\beta, T_0)$ for different values of T_0 with interpolation. The bare $2F_Q$ values for different values of N_t are the black symbols. The colored symbols correspond to different fixed T_0 values for each N_t. The colored lines are interpolations between these points in β. Bottom: $2F_Q^{ren}(T;T_0)$ values in the continuum, calculated for different values of T_0. For the final curve, all of the curves have been shifted to the position of the $T_0 = 200$MeV curve. The errors of each piece decrease as we approach the corresponding T_0. For the final curve, we used linear error propagation, assuming independent errors. We also mention that calculating the continuum limit of $2F_Q^{ren}(T;T_0)$ without HYP smearing leads to results consistent with the one presented here.

Heavy $\bar{Q}Q$ pair free energy

Next, we turn to the determination of $\tilde{F}_{\bar{Q}Q}$ defined in equation (3.47). This quantity is UV finite, and goes to 0 as $r \to \infty$. Similarly to the single quark free energy, the determination of $\tilde{F}_{\bar{Q}Q}$ at a given value of T and r requires two interpolations. At first we are given $\tilde{F}_{\bar{Q}Q}$ at several values of T, at each T we have a different value of the lattice spacing. If we want to know the value of $\tilde{F}_{\bar{Q}Q}$ at $(T, r) = (T^*, r^*)$ at some value of N_t, first we do an interpolation in the r direction to the value r^* at each given T, then we do an interpolation in the T direction, where the node points for the interpolations are the interpolated values in the previous step. The statistical error then can be estimated by constructing these interpolations for every jackknife sample. For systematic error estimation we try different interpolations in the r and T directions. In the r direction we have: polynomials of order 1,2,3,...,7 and a cubic spline, in the T direction we have polynomials of order 1,2,3 and cubic spline. This is in total $4 \times 8 = 32$ different interpolations. Just as before, we use the median of these values as the estimate, and the symmetric median centered 68% as the 1σ systematic error estimate. Like in the case of the single heavy quark free energies, the statistical and systematic errors turn out to be of the same order, and are then added in quadrature.

Next, we do the continuum extrapolation. Here we also take a similar approach as in the previous subsection. For the continuum extrapolations, we use the $N_t = 8, 10, 12$ lattices, that are available at all temperatures. We use the $N_t = 16$ lattice to estimate the systematic error of the continuum extrapolation, exactly like before. Also, where the $N_t = 16$ lattices are not available, we estimate the systematic error, as in the previous section, by the average of the systematic error at the points where we do have $N_t = 16$ lattices (approximately 7%). The linear fits of the continuum limit extrapolations all have good values of χ^2. Figure 3.7 shows a few examples of continuum extrapolations at various temperatures and distances.

Next, we add the values of $2F_Q$, determined in the previous subsection, and visible in Figure 3.6 to the free energy values to obtain the final results in Figure 3.8 (errors are added in quadrature). Note, that the $N_t = 6$ lattices were only used in the whole analysis to extend the β range of the renormalization condition for the single quark free energy.

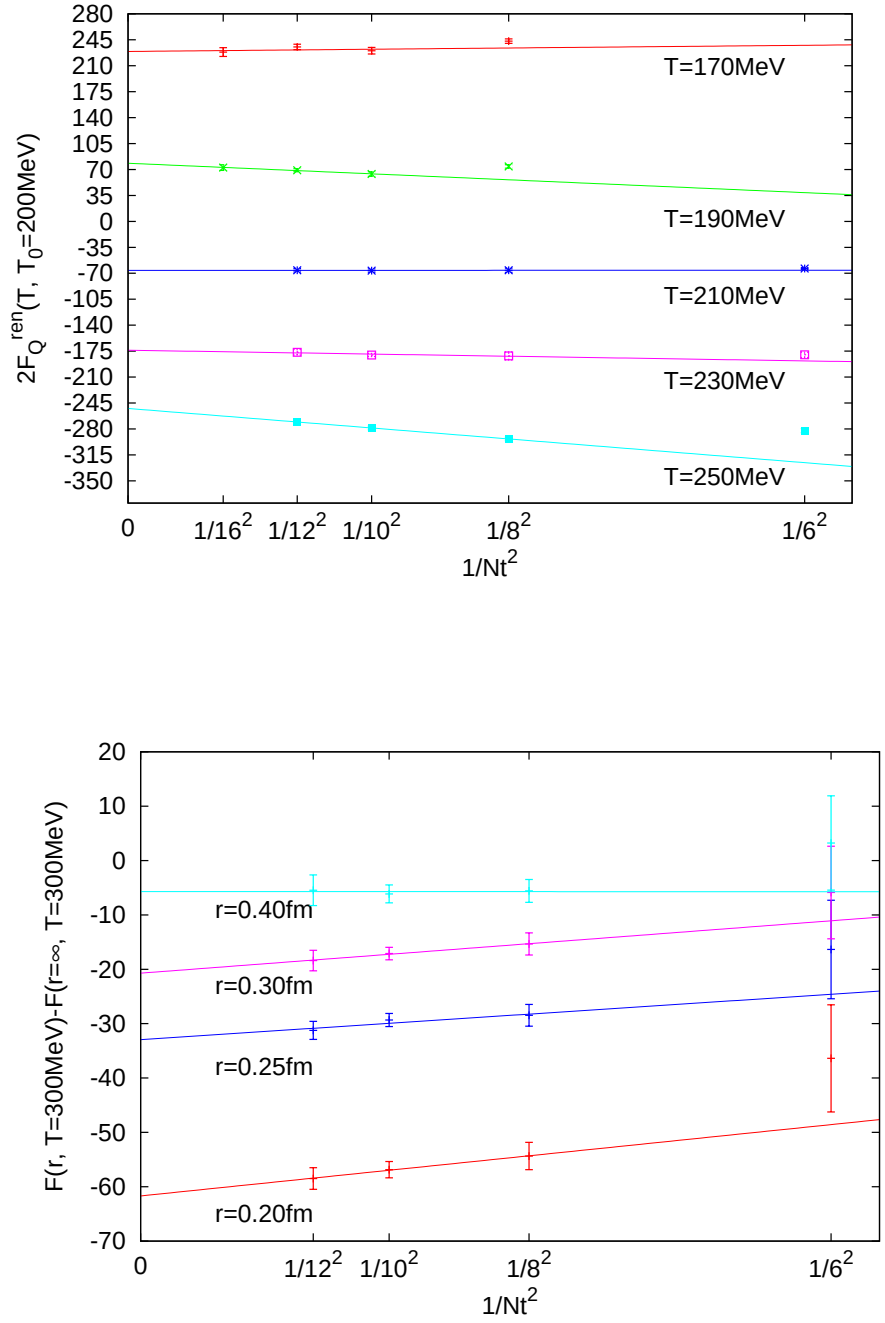

Figure 3.7: Cut-off effects in the free energy. On the top, we see an illustration of the continuum extrapolation of the renormalized single heavy quark free energy, with $T_0 = 200$ MeV, at different temperature values. As can be seen from a closer inspection of this figure, the cut-off error in this quantity, at these lattice spacings is approximately $5-10\%$. On the bottom, we can see a continuum extrapolation of $\tilde{F}_{\bar{Q}Q}(r,\beta,T) = F_{\bar{Q}Q}(r,\beta,T) - F_{\bar{Q}Q}(r\to\infty,\beta,T)$ at $T = 300$ MeV, for different values of r. Cut-off effects have a similar magnitude here as well.

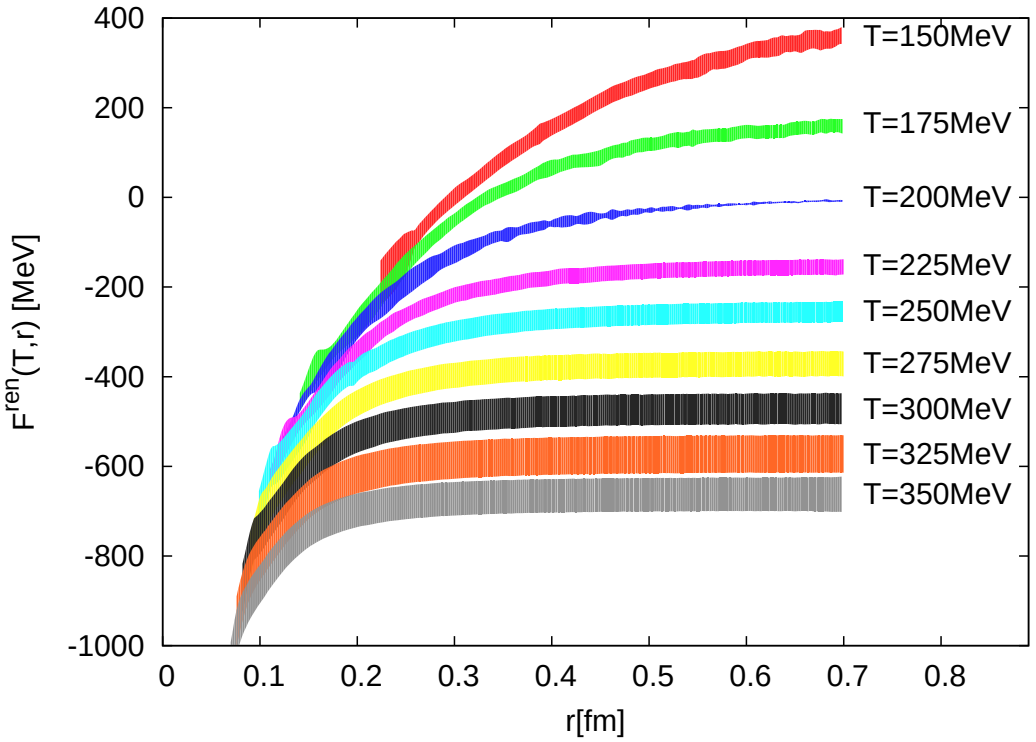

Figure 3.8: Continuum values of the static $\bar{Q}Q$ free energy at different temperatures. Note that the curves seem to tend to the same curve as $r \to 0$, corresponding to the expectation that UV physics is temperature independent.

3.3 Screening masses

In the following, we will study the large r behavior of the correlator of Polyakov loops. We start by defining two screening masses, that can be extracted from this large distance behavior.

3.3.1 Non-perturbative definition

Let us first summarize what is known perturbatively about the correlator of Polyakov loops:

- The leading order term to the correlator of Polyakov loops is a two gluon exchange diagram. It was first calculated at next-to-leading order in the dimensionally reduced effective theory (EQCD_3) [102]. This effective field theory assumes the scale hierarchy $T \gg 1/r \sim m_D$, where $m_D \sim gT$ is the Debye-mass, defined as a pole in

the gluon propagator. The result looked parametrically like:

$$C(r,T) \sim \frac{e^{-2m_D}}{r^2} \qquad (T \gg 1/r \sim m_D), \tag{3.50}$$

where the factor of two before the Debye mass comes from 2 gluon exchange. This result can be interpreted, due to the assumed hierarchy of scales, as an intermediate distance behavior at very high temperatures. Note, the m_D can only be calculated to leading $\mathcal{O}(gT)$ order in perturbation theory, as perturbation theory breaks down at $\mathcal{O}(g^2T)$ order because of infrared divergences.

- A calculation in the magnetic regime, i.e. the effective field theory $MQCD_3$, assuming $m_D \gg 1/r$ was done in Ref. [103]. Here it was understood, that 3.50 is not the correct asymptotic behavior at $r \to \infty$, and that at large r, the exponential decay of the Polyakov loop correlator is dominated by a magnetic screening mass:

  $$C(r,T) \sim e^{-m_M r}/r \qquad (T \gg m_D \gg 1/r), \tag{3.51}$$

  The magnetic mass is parametrically $m_M \sim g^2T$, but the coefficient can not be calculated perturbatively, it is essentially non-perturbative, and corresponds to a glueball mass in the 3D effective field theory. Figure 3.9 shows examples of diagrams, that indirectly couple the Polyakov-loop correlator to magnetic gluons. The dominance of magnetic screening at large distances was confirmed by 2 flavour lattice simulations (using a somewhat heavy pion) in [104].

- A perturbative calculation at NNLO, assuming the scale hierarchy $1/r \gg T \gg m_D \gg \frac{g^2}{r}$, can be found in Ref. [93].

- Ref. [93] also examines the problem with effective field theory techniques in other regimes of the parameters. In particular, after integrating out just the scale $1/r$, it argues, that the short distance behavior of the correlator, when $\frac{g^2}{rT} \gg 1$ is $1/r$.

For our purpose, the most important of these results is [103], for the following reason: To fit the correlation lengths in a lattice calculation, one needs the large r behavior, which is essentially non-perturbative, even at high temperatures. The reason is simple: even in the weak coupling limit, at distances larger than $(g^2T)^{-1}$ the physics of magnetic screening becomes dominant.

A related fact is that - as I already mentioned - for the gluon self-energy, perturbation theory itself breaks down at the $\mathcal{O}(g^2T)$ order because of infrared divergences. This term

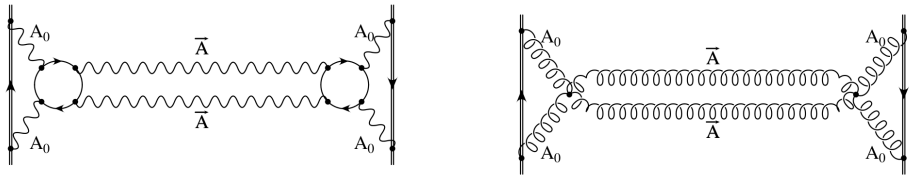

Figure 3.9: Examples of Feynman diagrams that indirectly couple magnetic gluons with the Polyakov loop correlator. The diagram on the left is already present in QED. The diagram on the right shows an even more direct coupling with magnetic gluons. This diagram is only present in nonabelian gauge theories. The presence of diagrams such as these leads to the fact that, even though the Polyakov-loop correlator does not couple directly to magnetic gluons, its large distance behavior is nevertheless dominated by them.

contains contributions from magnetic gluons. Therefore, the perturbative definition of a screening mass, as a pole in the gluon propagator, is of limited use, since perturbation theory itself breaks down ([105]). It is better to define the screening masses as inverse correlation lengths in appropriate Euclidean correlators. In order to investigate the effect of electric and magnetic gluons separately, one can use the symmetry of Euclidean time reflection[5] [105], that we will call $\mathcal{R}$. The crucial property of electric versus magnetic gluon fields A_4 and A_i is that under this symmetry, one is intrinsically odd, while the other is even:

$$A_4(\tau, \mathbf{x}) \xrightarrow{\mathcal{R}} -A_4(-\tau, \mathbf{x}), \quad \mathrm{A_i}(\tau, \mathbf{x}) \xrightarrow{\mathcal{R}} \mathrm{A_i}(-\tau, \mathbf{x}) \tag{3.52}$$

Under this symmetry the Polyakov loop transforms as $L \xrightarrow{\mathcal{R}} L^\dagger$. One can easily define correlators that are even or odd under this symmetry, and thus receive contributions only from the magnetic or electric sector, respectively [105, 104]:

$$L_M \equiv (L + L^\dagger)/2 \tag{3.53}$$

$$L_E \equiv (L - L^\dagger)/2. \tag{3.54}$$

[5]This is equivalent to real time TC, meaning that this definition is only useful in theories where this symmetry holds. This does not include the electroweak sector of the standard model, or QCD at finite chemical potential.

We can further decompose the Polyakov loop into $\mathcal{C}$ even and odd states, using $A_4 \xrightarrow{\mathcal{C}} A_4^*$ and $L \xrightarrow{\mathcal{C}} L^*$ as:

$$L_{M\pm} = (L_M \pm L_M^*)/2 \tag{3.55}$$

$$L_{E\pm} = (L_E \pm L_E^*)/2. \tag{3.56}$$

Next, we note that $\mathrm{Tr}\, L_{E+} = 0 = \mathrm{Tr}\, L_{M-}$, so the decomposition of the Polyakov loop correlator to definite $\mathcal{R}$ and $\mathcal{C}$ symmetric operators contains two parts[6]. We define the magnetic correlation function as:

$$C_{M+}(r,T) \equiv \left\langle \sum_{\mathbf{x}} \mathrm{Tr} L_{M+}(\mathbf{x}) \mathrm{Tr} L_{M+}(\mathbf{x}+\mathbf{r}) \right\rangle - \left| \left\langle \sum_{\mathbf{x}} \mathrm{Tr} L(\mathbf{x}) \right\rangle \right|^2, \tag{3.57}$$

and the electric correlator as[7]:

$$C_{E-}(r,T) \equiv - \left\langle \sum_{\mathbf{x}} \mathrm{Tr} L_{E-}(\mathbf{x}) \mathrm{Tr} L_{E-}(\mathbf{x}+\mathbf{r}) \right\rangle. \tag{3.58}$$

Then, from the exponential decay of these correlators, we can define the magnetic and electric screening masses. Note that with our definition $\mathrm{Tr} L_{M+} = \mathrm{Re}\,\mathrm{Tr} L$ and $\mathrm{Tr} L_{E-} = i\,\mathrm{Im}\,\mathrm{Tr} L$, and:

$$C(r,T) - C(r\to\infty,T) = C_{M+}(r,T) + C_{E-}(r,T), \tag{3.59}$$

from which it trivially follows that if the magnetic mass screening mass is lower than the electric mass, we will have $C(r,T) - C(r\to\infty,T)$ asymptotic to $C_{M+}(r,T)$ as $r\to\infty$, or equivalently, the highest correlation length in C equal to that of C_{M+}.

As for the asymptotic form of these correlators, similar arguments apply as with the full Polyakov loop correlator. In the high temperature limit the asymptotic behavior will be dominated by a glueball mass in the 3D effective Yang-Mills theory [105, 103], but because of the symmetry properties, the quantum numbers carried by the glueballs will be different. We will therefore fit the ansatz:

$$C_{M+}(r,T) \xrightarrow{r\to\infty} K_M(T) \frac{\mathrm{e}^{-m_M(T) r}}{r}, \tag{3.60}$$

$$C_{E-}(r,T) \xrightarrow{r\to\infty} K_E(T) \frac{\mathrm{e}^{-m_E(T) r}}{r}, \tag{3.61}$$

[6]Note that the Polyakov loop correlator does not overlap with the $\mathcal{R}(\mathcal{C}) = +(-)$ and $\mathcal{R}(\mathcal{C}) = -(+)$ sectors. To access these sectors, other operators are needed.

[7]Here our definition differs from that used in [104] in a sign.

to extract screening masses, noting that the ansatz in principle is only motivated at high temperatures, where the effective field theory applies. Nevertheless we find that even close to T_c the ansatz describes the large r tails of our lattice data well.

Note, that the correlation lengths (or screening masses) extracted this way are directly related to the static $\bar{Q}Q$ free energy. Since as we will see $m_M < m_E$, the magnetic screening mass determines the long distance behavior of the free energy.

Let us make one last comment. As we already mentioned, the leading weak coupling behavior of the Debye mass can be calculated from one-loop thermal perturbation theory. Subleading corrections depend on nonperturbative g^2T scale physics. Now, in the weak coupling regime, screening masses in the different $\mathcal{R}$ odd symmetry channels are only different by these $\mathcal{O}(g^2T)$ nonperturbative amounts. At asymptotically high temperature, these masses should approach each other. At not asymptotically high temperatures, it is a matter of convention which of these inverse correlation lengths is called the Debye mass. I do not commit to the channel calculated here, and therefore I do not call the electric screening mass calculated here a Debye mass. Also, from dimensionally reduced effective field theory simulations [106] it seems that the longest correlation length is not in this sector, but in $\mathcal{R}(\mathcal{C}) = -(+)$.

3.3.2 Lattice determination

We continue with the discussion of the electric and magnetic screening masses obtained from the correlators (3.57) and (3.58). For this analysis we only use lattices above the (pseudo)critical temperature, since that is the physically interesting range for screening. Next, we mention that for this analysis, we only use the data with HYP smearing, since we are especially interested in the large r behavior. Before going on to the actual fitting procedure of the screening masses let us first illustrate some simple relations, with the raw lattice data of the electric and magnetic correlators. First is that the screening masses in both channels are approximately proportional to the temperature. This can be seen on Figure 3.10. The next observation is that the electric screening mass is larger than the magnetic one. This can be seen on Figure 3.11. Both of these facts are expected to hold at high temperatures, from the dimensionally reduced effective theory, but these lattice results suggest that they hold at lower temperatures as well.

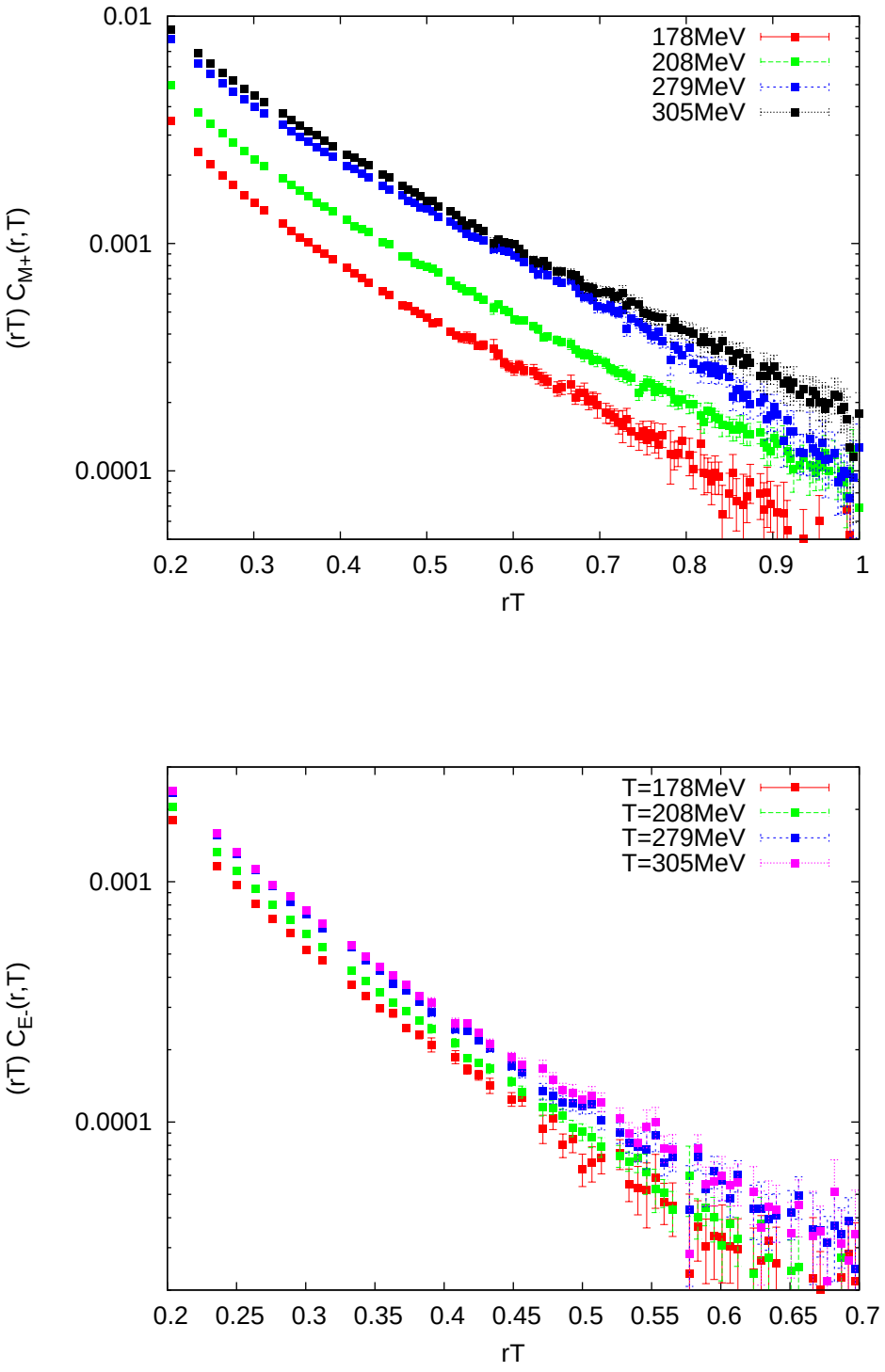

Figure 3.10: Illustrating that the screening masses are approximately proportional to the temperature. Since the x axis of this plot is rT, if one assumes a Yukawa form of the correlator, then the slopes of these curves are just m_M/T and m_E/T respectively. The fact that the graphs are approximately parallel straight lines suggests that these ansatzes are approximately correct, and that the masses are approximately proportional to the temperature.

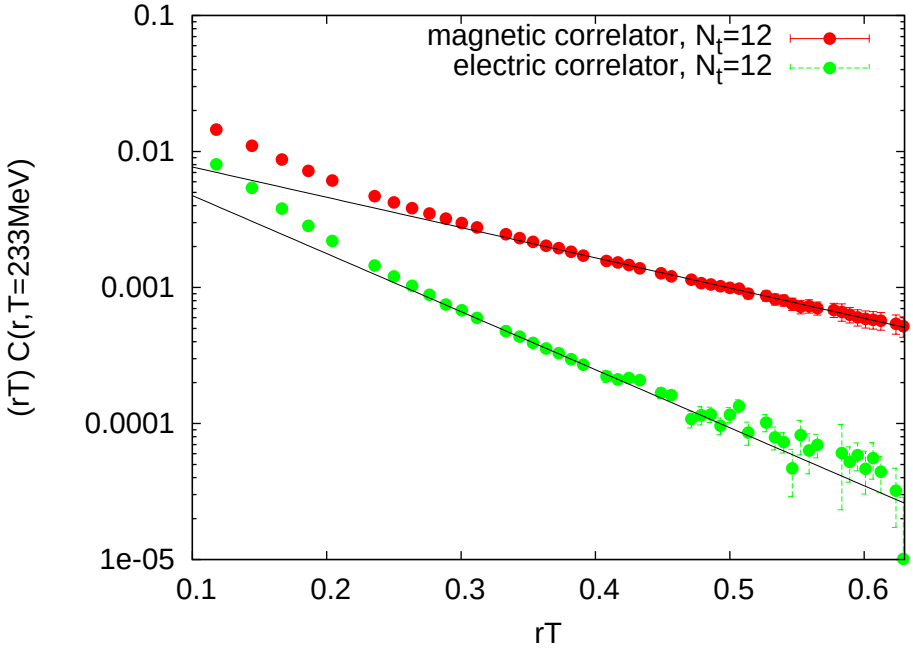

Figure 3.11: Illustrating $m_E > m_M$ with the lattice data at $N_t = 12$ and $T = 233$ MeV (32^3 lattices with HYP smearing). It can be clearly seen that the electric correlator drops faster. To lead the eye, we included on the plot the Yukawa fits to the tails of the correlators.

3.3.3 Correlated fitting and continuum extrapolation

Next, we turn to the actual determination of the screening masses. So far there has been one determination of electric and magnetic screening masses on the lattice using the non-perturbative definition given by Ref. [105]. That study used 2 flavours of Wilson fermions with a somewhat heavy pion, and did not attempt a continuum extrapolation [104].

The basic strategy of the determination of the screening masses is as follows: first we perform fits using the ansatz (3.60) and (3.61) at finite lattice spacing, then we carry out a continuum extrapolation of the screening masses. We first discuss the fitting procedure. Since the masses are expected to be proportional to the temperature, the natural distance unit in this problem is rT. This is confirmed by Figure 3.10. We therefore give limits on the range of the fits in these units. For the correct determination of the screening masses, special care is needed in the choice of the fit interval. To find the proper minimum rT

value of the fits, we use hypothesis testing, similar to that in Ref. [16]. If the fits are good, then the value of χ^2, defined as:

$$\chi^2 = \sum_{i,j} (C_i^{\text{fit}} - C_i^{\text{data}}) \boldsymbol{\mathcal{C}}_{ij}^{-1} (C_j^{\text{fit}} - C_j^{\text{data}}), \tag{3.62}$$

should have a χ^2 distribution, with the appropriate degrees of freedom. Here $\boldsymbol{\mathcal{C}}_{ij}$ is the covariance matrix. In this case the quantity

$$Q = \int_{\chi^2}^{\infty} \left(\text{Probability density of } \chi^2\right)(x)dx, \tag{3.63}$$

should have a uniform distribution on $[0, 1]$. If we fix the range of all the fits in rT units, each fit (at some value of N_t and β) gives one pick from a supposed uniform distribution in Q. This is equivalent to having multiple picks from the same uniform distribution. We will test this hypothesis with a Kolmogorov-Smirnov test [40] for the uniform distribution. Here one determines the maximum value of the absolute difference between the expected and measured cumulative probability distributions. This is then used to define a significance level or probability that the measured distribution can indeed be one originating from the expected uniform distribution. These probabilities are listed in Table 3.1. We will only use value of $(rT)_{\text{min}}$ where the Kolmogorov probability is at least 0.3. This test tells us, that for systematic error estimation, we will have, for the magnetic correlator $(rT)_{\text{min}}$ going from 0.465 to 0.61, and for the electric correlator we have $(rT)_{\text{min}}$ going from 0.35 to 0.43. $(rT)_{\text{max}}$ was fixed in both cases[8].

At this point we mention that for the continuum limit we will not use the $N_t = 16$ lattices, because the mass fits there have huge error bars. Nevertheless, when the continuum limit is done, we will see that the values of the masses at the $N_t = 16$ lattices are consistent with the continuum estimates. Also, if we use them, we get the same results, because they do not give a contribution to the continuum limit, due to the big errors.

Now that we have estimated the proper rT range of the fits, we go on to the fitting of the masses. The results of the fits at different values of N_t can be seen in Figures

[8]Increasing $(rT)_{\text{max}}$ results in a less precise covariance matrix and correspondingly, somewhat worse χ^2 values, but consistent screening masses. For example, if for the magnetic correlator we choose $(rT)_{\text{max}} = 1$ instead of 0.9, the final value of the Kolmogorov-Smirnov probability in Table 3.1 will not be 96%, but 38% instead. Nevertheless the growing trend in the probabilities will be the same. Also, we will get the same results within uncertainties.

Correlator type	$(rT)_{\min}$	$(rT)_{\max}$	$Pr\,(\mathrm{KS}, \mathrm{uniform})$
Magnetic	0.43	0.9	0.007
Magnetic	0.45	0.9	0.016
Magnetic	0.465	0.9	0.30
Magnetic	0.5	0.9	0.38
Magnetic	0.61	0.9	0.96
Electric	0.3	0.65	$3 \cdot 10^{-7}$
Electric	0.32	0.65	0.018
Electric	0.35	0.65	0.31
Electric	0.43	0.65	0.94

Table 3.1: Hypothesis testing, using fits at all values of $N_t = 8, 10, 12$ and all values of β. This means 33 sampled values in total, with fixed values of the low range of the fit $(rT)_{\min}$. One can see a rather sharp increase in the probabilities for the magnetic correlator at $(rT)_{\min} = 0.465$ and for the electric correlator at $(rT)_{\min} = 0.35$. This table justifies our choice for the ranges of $(rT)_{\min}$ values used in our systematic error estimation.

3.12 and 3.13. The systematic errors come from changing the lower limit of the fit, in the case of the magnetic correlator, from $(rT)_{\min} = 0.465$ to $(rT)_{\min} = 0.61$, and in the case of the electric correlator, from $(rT)_{\min} = 0.35$ to $(rT)_{\min} = 0.43$. The results coming from different values of $(rT)_{\min}$ are weighted using the Akaike Information Criterion(AIC) [107]. The median of the weighted histogram gives the central value, and the central 68% the systematic error estimate. Note that using the Q values as weights or uniform weights gives a very similar result. The statistical error comes from a jackknife analysis with 20 jackknife samples. The two errors turn out to be of similar magnitude (with the statistical error being somewhat bigger) and are then added in quadrature.

Next, we fit linear functions in T to all screening masses at all values of N_t, and use these to do a continuum extrapolation from the $N_t = 8, 10, 12$ lattices. Taking into account the errors of the linear fits, all χ^2 values of the continuum limits are very good. The continuum limit, in addition to the statistical error, also has a systematic error estimated, from doing a 2 point linear extrapolation from the $N_t = 12, 10$ lattices, and taking the difference of the extrapolated value from fitted value to the $N_t = 8, 10, 12$ lattices[9]. The

[9]In the previous section, we used the $N_t = 16$ lattices for systematic error estimation, here however, we do not use them since they do not improve the statistical accuracy of the continuum limits.

statistical and systematic errors are added in quadrature. The continuum limits of the screening masses can be seen in Figure 3.14.

It is somewhat surprising that the screening mass normalized by the temperature, even close to T_c is only weakly temperature dependent. It is also surprising that the Yukawa ansatz used for the fits, although only motivated at higher temperatures, still describes the data at T just above T_c. In order to demonstrate this we include here the reduced χ^2 values of the fits at the lowest temperatures used in the study. For the magnetic masses, when fitting with $(rT)_{\rm min} = 0.465$ and $(rT)_{\rm max} = 0.9$ we get at the lowest temperatures (different at the different N_t values, but around 160 MeV in each case) $\chi^2/N_{\rm dof} = 1.23, 1.28, 1.19$ for $N_t = 8, 10, 12$, respectively. For the electric masses, when fitting with $(rT)_{\rm min} = 0.35$ and $(rT)_{\rm max} = 0.65$ we obtain: $\chi^2/N_{\rm dof} = 0.80, 1.16, 0.86$ for $N_t = 8, 10, 12$, respectively.

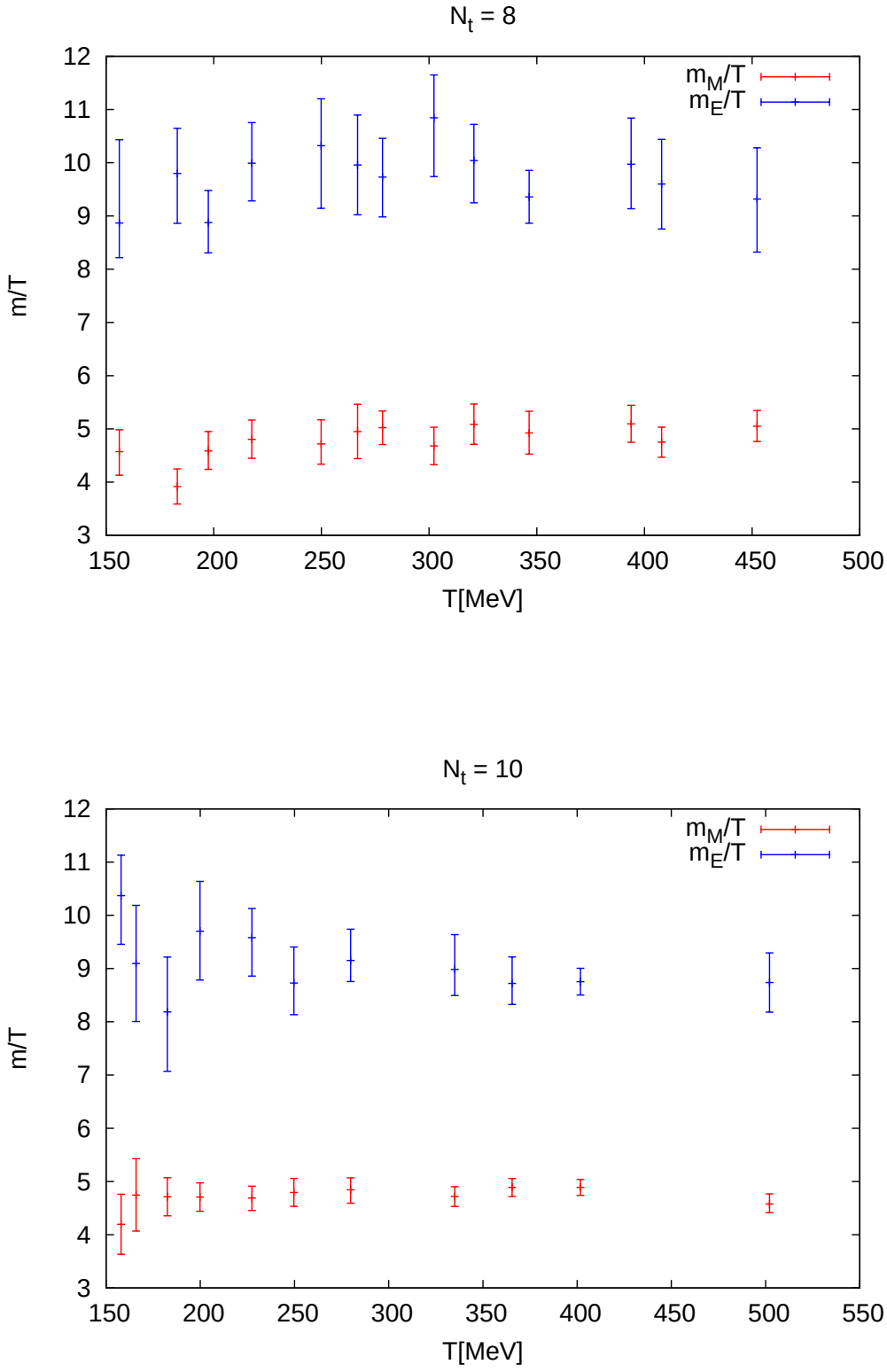

Figure 3.12: The fitted values of electric and magnetic screening masses at $N_t = 8, 10$.

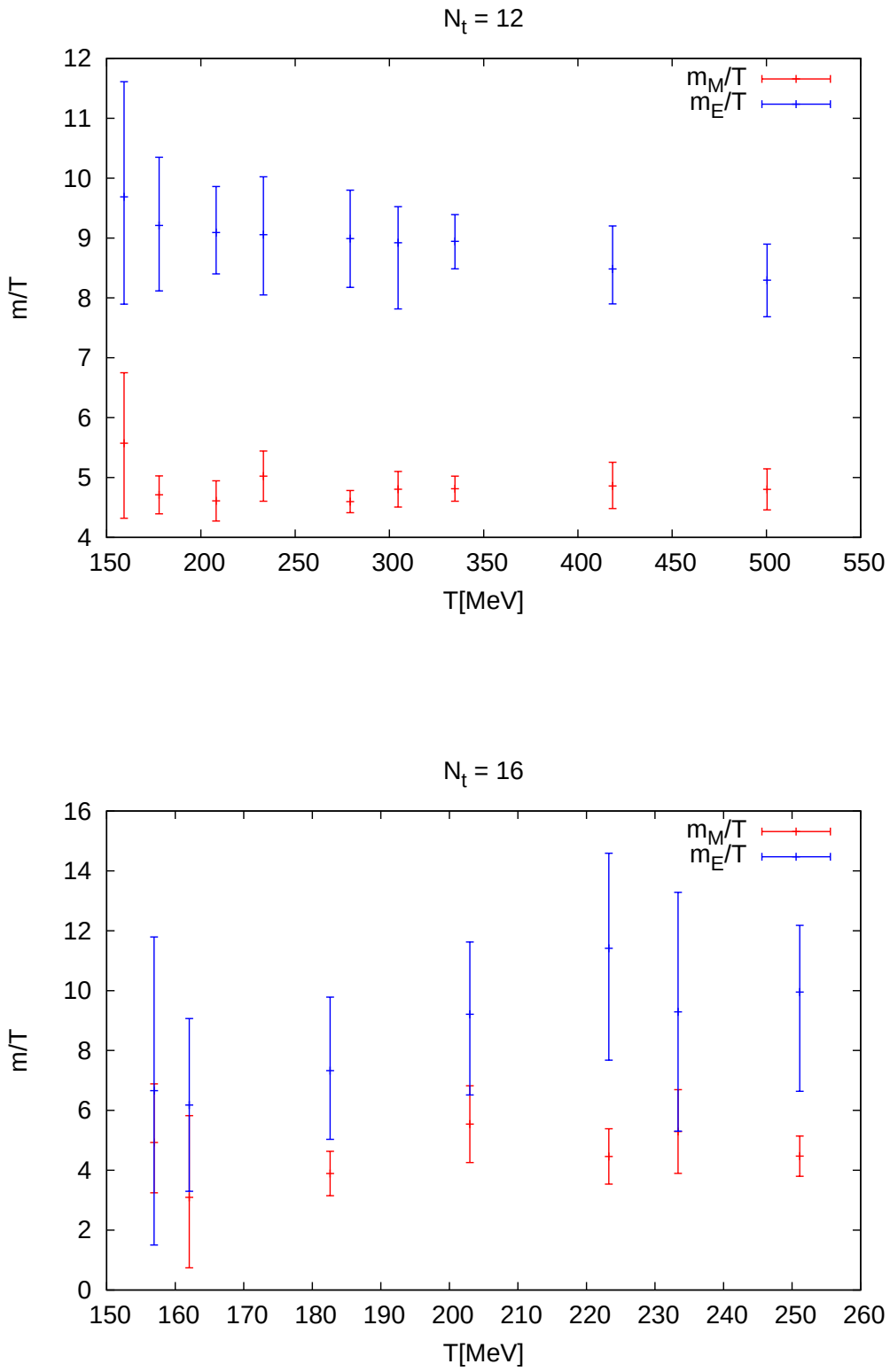

Figure 3.13: The fitted values of electric and magnetic screening masses at the different values of $N_t = 12, 16$.

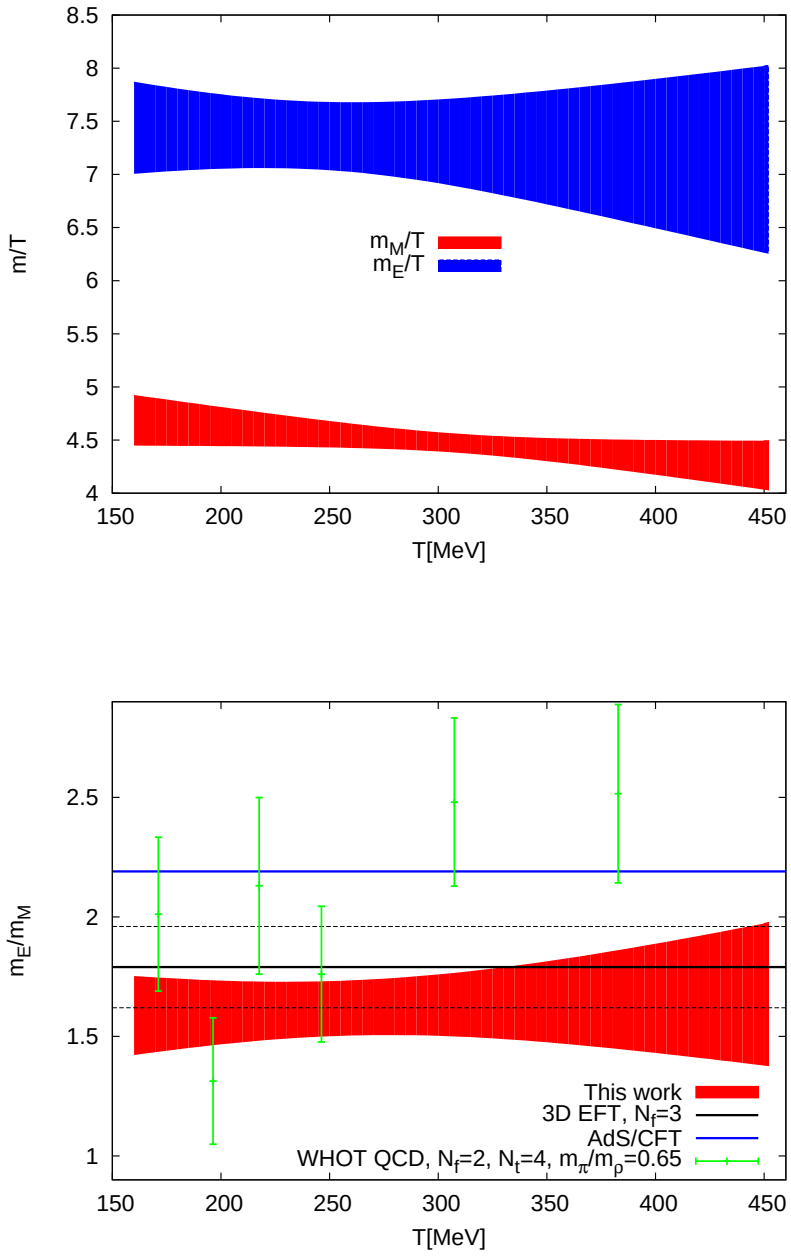

Figure 3.14: The continuum extrapolations of the screening masses and the ratio of the screening masses. For the ratio m_E/m_M we also included different estimates from the literature: Lattice results are from Ref. [104]. Dimensionally reduced 3D effective field theory results at $T = 2T_c$ are from Ref. [106]. In this model the ratio has a temperature dependence from the running coupling $m_E/m_M \sim 1/g(T)$. This is ignored in the plot and instead the $2T_c$ results is plotted in the whole range. If this temperature dependence was included, the ratio at $T = \Lambda_{QCD}$ would already be zero. Results from $\mathcal{N} = 4$ SYM plasma with AdS/CFT are from Ref. [108].

3.3.4 Comparisons with other approximations

We finish this section by comparing our results to those from earlier approximations in the literature. For comparison let us use our results at $T = 300\text{MeV} \approx 2\text{T}_\text{c}$. Here we have:

- This work: 2+1 flavour lattice QCD at the physical point after continuum extrapolation:

$$m_E/T = 7.31(25) \quad m_M/T = 4.48(9)$$
$$m_E/m_M = 1.63(8)$$

- Ref. [104]: 2 flavour lattice QCD with Wilson quarks, a somewhat heavy pion $m_\pi/m_\rho = 0.65$, no continuum extrapolation

$$m_E/T = 13.0(11) \quad m_M/T = 5.8(2)$$
$$m_E/m_M = 2.3(3)$$

- From Table 1 of Ref. [108]: $\mathcal{N} = 4$ SYM, large N_c limit, AdS/CFT

$$m_E/T = 16.05 \quad m_M/T = 7.34$$
$$m_E/m_M = 2.19$$

- From Figure 3 of Ref. [106]: dimensionally reduced 3D effective theory, $N_f = 2$ massless quarks

$$m_E/T = 7.0(3) \quad m_M/T = 3.9(2)$$
$$m_E/m_M = 1.79(17)$$

- From Figure 3 of Ref. [106]: dimensionally reduced 3D effective theory, $N_f = 3$ massless quarks

$$m_E/T = 7.9(4) \quad m_M/T = 4.5(2)$$
$$m_E/m_M = 1.76(17)$$

We note, that our results are closest to the results from dimensionally reduced effective field theory. This can also be seen in Figure 3.14 (bottom).

Chapter 4

Summary

In my thesis two approaches were discussed on studying deconfinement properties of QCD matter: a determination attempt of the charmonium spectral functions, and a study of Polyakov loop correlators. A lattice field theory approach was used for both cases. The main results of the work presented here are:

- The first Maximum Entropy lattice determination of charmonium spectral functions with 2+1 dynamical Wilson-fermions, with a somewhat heavy pion mass of $m_\pi = 545\text{MeV}$ and a small lattice spacing of $a = 0.057\text{fm}$.

- Showing that the temperature dependence of the charmonium correlators, up to a temperature of $1.4T_c$, is consistent with a constant spectral function, in the case of the pseudoscalar channel (η_c), and a constant $\omega > 0$ part plus a temperature dependent transport peak at low frequency, in the case of the vector (J/Ψ) channel.

- Introducing a new renormalization procedure for the Polyakov loop (or equivalently, the static quark free energy). The renormalization prescription was of the same kind as Ref. [15], but the implementation there was only suited for Wilson quarks. A procedure suited for staggered quarks was also needed.

- The first continuum extrapolated lattice determination of the static $Q\bar{Q}$ free energy at the QCD physical point, in a temperature range of 150MeV...350MeV.

- The first continuum extrapolated lattice determination of the electric and magnetic screening masses, corresponding to the symmetries $\mathcal{R}(\mathcal{C}) = +(-)$ and $\mathcal{R}(\mathcal{C}) = -(+)$, with $\mathcal{R}$ being Euclidean time reflection, and $\mathcal{C}$ being charge conjugation, at the QCD physical point. The results agree well with results from dimensionally reduced effective field theory.

Chapter 5

Appendix

5.1 Some properties of covariance matrices of data

In this work, we deal quite a lot with covariance matrices. Namely, the covariance matrix between correlators at different separations (in imaginary time, in the case of MEM, and in space, in the case of the screening masses). Therefore, it is useful to go through some important properties of these. Let us call the ith measured quantity in the kth configuration y_i^k. On the one hand, in case one estimates the covariance matrix from the configurations themselves one has:

$$C_{ij} = \frac{1}{N_{\rm conf}(N_{\rm conf}-1)} \sum_{k=1}^{N_{\rm conf}} (y_i^k - \bar{y}_i)(y_j^k - \bar{y}_j), \tag{5.1}$$

where the average is:

$$\bar{y}_i = \frac{1}{N_{\rm conf}} \sum_{k=1}^{N_{\rm conf}} y_i^k. \tag{5.2}$$

On the other hand, if we use jackknife samples to estimate the covariance matrix we have:

$$C_{ij} = \frac{N_{\rm jck}-1}{N_{\rm jck}} \sum_{k=1}^{N_{\rm jck}} (y_{(J)i}^k - \bar{y}_{(J)i})(y_{(J)j}^k - \bar{y}_{(J)j}), \tag{5.3}$$

where the average is:

$$\bar{y}_{(J)i} = \frac{1}{N_{\rm jck}} \sum_{k=1}^{N_{\rm jck}} y_i^k. \tag{5.4}$$

Here $y_{(J)i}^k$ is the average of y_i in the kth jackknife sample, that we get by leaving out some configurations from the full sample. For the single elimination jackknife method we leave out the kth configuration.

Because of the finite sample sizes, we might not be able to get a very good approximation of the true covariance matrix. In this part of the Appendix we will talk about this problem in some detail. Let us start with a simple exact theorem.

Theorem: If we measure the values of y_i with $i = 1, 2, ..., N$ and $N_{\text{conf}} < N$ (or $N_{\text{jck}} < N$) the estimated covariance matrix will have exact zero eigenvalues.

Proof: From equation (5.3) we have:

$$C_{ij} \propto \sum_{k=1}^{N_{\text{conf}}} (y_i^k - \bar{y}_i)(y_j^k - \bar{y}_j) = \sum_{k=1}^{N_{\text{conf}}} d_i^k d_j^k = \sum_{k=1}^{N_{\text{conf}}} C_{ij}^k. \tag{5.5}$$

The overall constant $1/N_{\text{conf}}/(N_{\text{conf}} - 1)$ does not effect the values of the zero eigenvalues, so we leave it out. In this equation $d_i^k = y_i^k - \bar{y}_i$ and $C_{ij}^k = d_i^k d_j^k$. Now, clearly $\text{Rank}\left(C_{ij}^k\right) = 1$, since all columns of the matrix C_{ij}^k are proportional to the same vector d_i^k. This means that:

$$\text{Rank}\left(C_{ij}\right) \leq \sum_{k=1}^{N_{\text{conf}}} \text{Rank}\left(C_{ij}^k\right) = N_{\text{conf}}. \tag{5.6}$$

The number of zero eigenvalues therefore satisfies:

$$N_{0\text{ev}} = N - \text{Rank}\left(C_{ij}\right) \geq N - N_{\text{conf}}. \tag{5.7}$$

In the case where $N_{\text{conf}} > N$ the right hand side is negative and therefore this statement does not really say anything, but if $N_{\text{conf}} < N$ it proves that there are exact 0 eigenvalues. We mention that the exact same proof can be repeated in the case where we estimate the covariance matrix with jackknife samples.

The true covariance matrix is positive definite. The unbiased estimators are however only positive semidefinite by construction, and we have seen in the previous case that in the case of extreme small sample sizes they must have exact 0 eigenvalues. Of course, the bigger the sample, the better we know the covariance matrix. If we start with a very small sample size, we will have non physical exact 0 eigenvalues, that in numerical calculations can manifest as small negative eigenvalues. If we start to increase the sample size, these small eigenvalues will become bigger and bigger, eventually reaching the true values.

It is important to note, that even in the case when we know the covariance matrix to very high precision, the condition number of the covariance matrix (i.e. the ratio of the highest to lowest eigenvalue) is high. An example of the eigenvalues of an actual covariance matrix, for the correlator of Polyakov loops can be seen in Figure 5.1. High condition

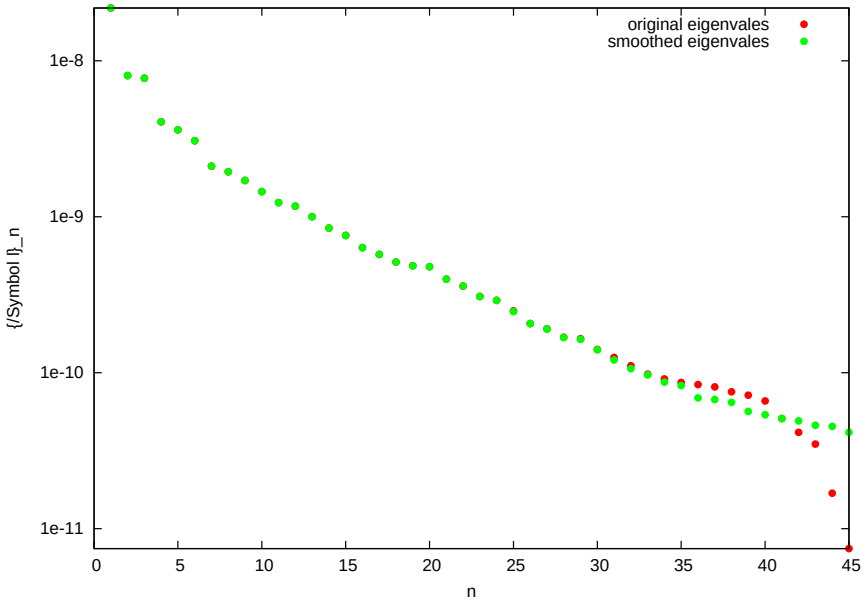

Figure 5.1: An example of the eigenvalues of the covariance matrix of the correlator of Polyakov loops. The eigenvalues of the covariance matrix of meson correlators looks very similar.

numbers ($10^{10} - 10^{20}$) have been encountered in this work, both for MEM and for the correlated fitting of screening masses. This is especially prominent for MEM, where we keep the whole correlator in the fit, not an interval, like in the case of the screening masses. Every algorithm of linear algebra is highly sensitive to this ratio, and works less reliably for large condition numbers. A high condition number sometimes makes double precision arithmetic unsatisfactory. For this reason, I have used arbitrary precision arithmetic for a lot of calculations in this work.

5.1.1 Eigenvalue smoothing

Here, we will briefly discuss the method of eigenvalue smoothing, introduced in Ref. [109]. This was originally introduced as a way to make correlated χ^2 fits more reliable, in the presence of poor statistics, and therefore not sufficiently accurate correlation matrices. With our level of statistics this turned out to be no longer the case. Nevertheless I implemented the procedure and used it to test stability.

Let us first introduce:

$$\tilde{C}_{ij} \equiv \frac{C_{ij}}{\sqrt{C_{ii}C_{jj}}}. \tag{5.8}$$

If $\tilde{C}$ has small (maybe) non-physical eigenvalues, they can influence unreasonably the inverse matrix. An obvious way to proceed is to modify these unreasonable eigenvalues by hand. The most brutal idea one might have is to remove the smallest eigenvalues. This is in the spirit of the SVD inverse of a singular matrix: only the contributions from the non-zero eigenvalues are retained in the inverse. This eigenvalue truncation clearly leads to a rather crude approximation of the inverse, as it removes its largest eigenvalues. A physical argument, for why this could be acceptable can be based on the observation that the smallest eigenvalues of $\tilde{C}$ usually correspond to eigenvectors which alternate in sign and so are not very relevant to smooth fit functions [110]. As we have argued, with a small sample size, the eigenvalues of the covariance matrix will be different from their true values. The largest relative effect will come when there are several true eigenvalues of similar size - since those eigen directions mix strongly. Therefore Ref. [109] suggested to change the smallest eigenvalues to their "average", by introducing the following "averaging" procedure:

- Go from C to $\tilde{C}$.
- Order the eigenvalues: $\lambda_1 < \lambda_2 < ... < \lambda_N$.
- Replace the eigenvalues of $\tilde{C}$, called λ_i by

$$\lambda'_i = \frac{1}{N_s}\sum_{j=1}^{N_s}\lambda_j \quad (i \leq N_s) \tag{5.9}$$

$$\lambda'_i = \lambda_i \quad (i > N_s) \tag{5.10}$$

  This procedure removes the very small eigenvalues of $\tilde{C}$ and replaces them with the average of the N_s smallest eigenvalues while retaining the property that $\mathrm{Tr}\,\tilde{C} = N$. The procedure also ensures a smooth eigenvalue distribution by allowing eigenvalues larger than this average to be retained.

- The eigenvectors of $\tilde{C}$ are retained, with the changed eigenvalues we get $\tilde{C}'$
- We get the modified covariance matrix $C'_{ij} = \tilde{C}'_{ij}\sqrt{C_{ii}C_{jj}}$

Ref. [109] also proposed the rule of thumb to keep $N - N_s = \sqrt{N_{\mathrm{conf}}}$ eigenvalues. For our data, this rule almost always leads to the conclusion that we can keep all of the eigenvalues

in our covariance matrices. When it does not, I kept $N - N_s = \sqrt{N_{\text{conf}}}$ as the rule of thumb says. I cases where this would lead to $N_s = 0$, I tried smoothing $5 - 10$ eigenvalues anyway. I performed the analysis with both the smoothed and the original covariance matrices. In every case, I got results consistent with each other. For this reason, the final results of this work do not include eigenvalue smoothing at all, and this was just a stability check.

Bibliography

[1] T. Muta. *Foundations of Quantum Chromodynamics*. World Scientific Publishing, 1987.

[2] I. Montvay and G. Münster. *Quantum fields on a lattice*. Cambridge University Press, 1994.

[3] Zoltán Fodor and Christian Hoelbling. Light Hadron Masses from Lattice QCD. *Rev.Mod.Phys.*, 84:449, 2012, hep-lat/1203.4789.

[4] M. Le Bellac. *Thermal Field Theory*. Cambridge University Press, 1996.

[5] J.I. Kapusta and C. Gale. *Finite Temperature Field Theory*. Cambridge University Press, 2006.

[6] Y. Aoki, G. Endrődi, Z. Fodor, S.D. Katz, and K.K. Szabó. The Order of the quantum chromodynamics transition predicted by the standard model of particle physics. *Nature*, 443:675–678, 2006, hep-lat/0611014.

[7] Szabolcs Borsányi et al. Is there still any T_c mystery in lattice QCD? Results with physical masses in the continuum limit III. *JHEP*, 1009:073, 2010, hep-lat/1005.3508.

[8] A. Bazavov, T. Bhattacharya, M. Cheng, N.H. Christ, C. DeTar, et al. Equation of state and QCD transition at finite temperature. *Phys.Rev.*, D80:014504, 2009, hep-lat/0903.4379.

[9] Szabolcs Borsányi, Gergely Endrődi, Zoltán Fodor, Antal Jakovác, Sándor D. Katz, et al. The QCD equation of state with dynamical quarks. *JHEP*, 1011:077, 2010, hep-lat/1007.2580.

[10] Owe Philipsen. The QCD equation of state from the lattice. *Prog.Part.Nucl.Phys.*, 70:55–107, 2013, hep-lat/1207.5999.

[11] Dominik J. Schwarz. The first second of the universe. *Annalen Phys.*, 12:220–270, 2003, astro-ph/0303574.

[12] S.P. Klevansky. The Nambu-Jona-Lasinio model of quantum chromodynamics. *Rev.Mod.Phys.*, 64:649–708, 1992.

[13] T. Matsui and H. Satz. J/ψ Suppression by Quark-Gluon Plasma Formation. *Phys.Lett.*, B178:416, 1986.

[14] M.C. Abreu et al. Evidence for deconfinement of quarks and gluons from the J / psi suppression pattern measured in Pb + Pb collisions at the CERN SPS. *Phys.Lett.*, B477:28–36, 2000.

[15] Szabolcs Borsányi, Stephan Dürr, Zoltán Fodor, Christian Hoelbling, Sándor D. Katz, et al. QCD thermodynamics with continuum extrapolated Wilson fermions I. *JHEP*, 1208:126, 2012, hep-lat/1205.0440.

[16] Sz. Borsányi, S. Dürr, Z. Fodor, C. Hoelbling, S.D. Katz, et al. Ab initio calculation of the neutron-proton mass difference. 2014, 1406.4088.

[17] M. Lüscher and P. Weisz. On-Shell Improved Lattice Gauge Theories. *Commun.Math.Phys.*, 97:59, 1985.

[18] B. Sheikholeslami and R. Wohlert. Improved Continuum Limit Lattice Action for QCD with Wilson Fermions. *Nucl.Phys.*, B259:572, 1985.

[19] S. Aoki et al. Light hadron spectrum and quark masses from quenched lattice QCD. *Phys.Rev.*, D67:034503, 2003, hep-lat/0206009.

[20] M. Lüscher. Computational Strategies in Lattice QCD. 2010, hep-lat/1002.4232.

[21] S. Duane, A.D. Kennedy, B.J. Pendleton, and D. Roweth. Hybrid Monte Carlo. *Phys.Lett.*, B195:216–222, 1987.

[22] M.A. Clark and A.D. Kennedy. Accelerating dynamical fermion computations using the rational hybrid Monte Carlo (RHMC) algorithm with multiple pseudofermion fields. *Phys.Rev.Lett.*, 98:051601, 2007, hep-lat/0608015.

[23] Roberto Frezzotti and Karl Jansen. A Polynomial hybrid Monte Carlo algorithm. *Phys.Lett.*, B402:328–334, 1997, hep-lat/9702016.

[24] Anna Hasenfratz and Francesco Knechtli. Flavor symmetry and the static potential with hypercubic blocking. *Phys.Rev.*, D64:034504, 2001, hep-lat/0103029.

[25] M. Albanese et al. Glueball Masses and String Tension in Lattice QCD. *Phys.Lett.*, B192:163–169, 1987.

[26] Colin Morningstar and Mike J. Peardon. Analytic smearing of SU(3) link variables in lattice QCD. *Phys.Rev.*, D69:054501, 2004, hep-lat/0311018.

[27] W. Greiner and Berndt Müller. *Theoretical physics. Vol. 2: Quantum mechanics. Symmetries*. Addison-Wesley, 1989.

[28] Nora Brambilla. Effective Field Theories for Heavy Quarkonium. *Few Body Syst.*, 43:25–30, 2008, hep-lat/0712.1227.

[29] Xiang-Qian Luo, Yong-Yao Li, and Helmut Kroger. Bound states and critical behavior of the Yukawa potential. *Sci.China*, G35:631–642, 2005, hep-ph/0407258.

[30] Harvey B. Meyer. Transport Properties of the Quark-Gluon Plasma: A Lattice QCD Perspective. *Eur.Phys.J.*, A47:86, 2011, hep-lat/1104.3708.

[31] A. Jakovác. Representation of spectral functions and thermodynamics. *Phys.Rev.*, D86:085007, 2012, hep-lat/1206.0865.

[32] A. Jakovác. Hadron melting and QCD thermodynamics. *Phys.Rev.*, D88:065012, 2013, hep-ph/1306.2657.

[33] T.S. Bíró and A. Jakovác. QCD above T_c: Hadrons, partons, and the continuum. *Phys.Rev.*, D90(9):094029, 2014, hep-lat/1405.5471.

[34] Larry D. McLerran and T. Toimela. Photon and Dilepton Emission from the Quark - Gluon Plasma: Some General Considerations. *Phys.Rev.*, D31:545, 1985.

[35] H.A. Weldon. Reformulation of finite temperature dilepton production. *Phys.Rev.*, D42:2384–2387, 1990.

[36] R. Rapp and J. Wambach. Chiral symmetry restoration and dileptons in relativistic heavy ion collisions. *Adv.Nucl.Phys.*, 25:1, 2000, hep-ph/9909229.

[37] Pavel Kovtun. Lectures on hydrodynamic fluctuations in relativistic theories. *J.Phys.*, A45:473001, 2012, hep-th/1205.5040.

[38] Gert Aarts and Jose Maria Martinez Resco. Transport coefficients, spectral functions and the lattice. *JHEP*, 0204:053, 2002, hep-ph/0203177.

[39] M. Asakawa, T. Hatsuda, and Y. Nakahara. Maximum entropy analysis of the spectral functions in lattice QCD. *Prog.Part.Nucl.Phys.*, 46:459–508, 2001, hep-lat/0011040.

[40] William H. Press, Saul A. Teukolsky, William T. Vetterling, and Brian P. Flannery. Numerical Recipes: The Art of Scientific Computing, 3rd edition. 2007.

[41] R. Narayan and R. Nityananda. Maximum entropy image restoration in astronomy. *Ann.Rev.Astron.Astrophys.*, 24:127–170, 1986.

[42] Yannis Burnier and Alexander Rothkopf. Bayesian Approach to Spectral Function Reconstruction for Euclidean Quantum Field Theories. *Phys.Rev.Lett.*, 111:182003, 2013, hep-lat/1307.6106.

[43] J. Skilling and S.F. Gull. Bayesian maximum entropy image reconstruction. *Spatial statistics and imaging*, page 341, 1991.

[44] R. K. Bryan. Maximum entropy analysis of oversampled data problems. *Eur. Biophys J.*, 18:165, 1990.

[45] A. Jakovác, P. Petreczky, K. Petrov, and A. Velytsky. Quarkonium correlators and spectral functions at zero and finite temperature. *Phys.Rev.*, D75:014506, 2007, hep-lat/0611017.

[46] Gert Aarts, Chris Allton, Justin Foley, Simon Hands, and Seyong Kim. Spectral functions at small energies and the electrical conductivity in hot, quenched lattice QCD. *Phys.Rev.Lett.*, 99:022002, 2007, hep-lat/0703008.

[47] J. Engels and O. Vogt. Longitudinal and transverse spectral functions in the three-dimensional O(4) model. *Nucl.Phys.*, B832:538–566, 2010, hep-lat/0911.1939.

[48] Takashi Umeda, Kouji Nomura, and Hideo Matsufuru. Charmonium at finite temperature in quenched lattice QCD. *Eur.Phys.J.*, C39S1:9–26, 2005, hep-lat/0211003.

[49] H. Ohno et al. Charmonium spectral functions with the variational method in zero and finite temperature lattice QCD. *Phys.Rev.*, D84:094504, 2011, hep-lat/1104.3384.

[50] Szabolcs Borsányi, Stephan Dürr, Zoltán Fodor, Sándor D. Katz, Stefan Krieg, et al. Anisotropy tuning with the Wilson flow. 2012, hep-lat/1205.0781.

[51] F. Karsch, E. Laermann, P. Petreczky, and S. Stickan. Infinite temperature limit of meson spectral functions calculated on the lattice. *Phys.Rev.*, D68:014504, 2003, hep-lat/0303017.

[52] Gert Aarts and Jose M. Martinez Resco. Continuum and lattice meson spectral functions at nonzero momentum and high temperature. *Nucl.Phys.*, B726:93–108, 2005, hep-lat/0507004.

[53] H.T. Ding, A. Francis, O. Kaczmarek, F. Karsch, H. Satz, et al. Charmonium properties in hot quenched lattice QCD. *Phys.Rev.*, D86:014509, 2012, hep-lat/1204.4945.

[54] K. Symanzik. Continuum Limit and Improved Action in Lattice Theories. 1. Principles and phi**4 Theory. *Nucl.Phys.*, B226:187, 1983.

[55] Roland Hoffmann, Anna Hasenfratz, and Stefan Schaefer. Non-perturbative improvement of nHYP smeared Wilson fermions. *PoS*, LAT2007:104, 2007, hep-lat/0710.0471.

[56] Stefano Capitani, Stephan Dürr, and Christian Hoelbling. Rationale for UV-filtered clover fermions. *JHEP*, 0611:028, 2006, hep-lat/0607006.

[57] S. Dürr, Z. Fodor, C. Hoelbling, R. Hoffmann, S.D. Katz, et al. Scaling study of dynamical smeared-link clover fermions. *Phys.Rev.*, D79:014501, 2009, hep-lat/0802.2706.

[58] S. Dürr, Z. Fodor, J. Frison, C. Hoelbling, R. Hoffmann, et al. Ab-Initio Determination of Light Hadron Masses. *Science*, 322:1224–1227, 2008, hep-lat/0906.3599.

[59] J.C. Sexton and D.H. Weingarten. Hamiltonian evolution for the hybrid Monte Carlo algorithm. *Nucl.Phys.*, B380:665–678, 1992.

[60] Tetsuya Takaishi and Philippe de Forcrand. Testing and tuning new symplectic integrators for hybrid Monte Carlo algorithm in lattice QCD. *Phys.Rev.*, E73:036706, 2006, hep-lat/0505020.

[61] Thomas A. DeGrand. A Conditioning Technique for Matrix Inversion for Wilson Fermions. *Comput.Phys.Commun.*, 52:161–164, 1988.

[62] C.T.H. Davies, C. McNeile, K.Y. Wong, E. Follana, R. Horgan, et al. Precise Charm to Strange Mass Ratio and Light Quark Masses from Full Lattice QCD. *Phys.Rev.Lett.*, 104:132003, 2010, hep-ph/0910.3102.

[63] S. Dürr, Z. Fodor, C. Hoelbling, S.D. Katz, S. Krieg, et al. Lattice QCD at the physical point: light quark masses. *Phys.Lett.*, B701:265–268, 2011, hep-lat/1011.2403.

[64] S. Dürr, Z. Fodor, C. Hoelbling, S.D. Katz, S. Krieg, et al. Lattice QCD at the physical point: Simulation and analysis details. *JHEP*, 1108:148, 2011, hep-lat/1011.2711.

[65] M. Asakawa and T. Hatsuda. J / psi and eta(c) in the deconfined plasma from lattice QCD. *Phys.Rev.Lett.*, 92:012001, 2004, hep-lat/0308034.

[66] Gert Aarts, Chris Allton, Mehmet Bugrahan Oktay, Mike Peardon, and Jon-Ivar Skullerud. Charmonium at high temperature in two-flavor QCD. *Phys.Rev.*, D76:094513, 2007, hep-lat/0705.2198.

[67] H. Iida, T. Doi, N. Ishii, H. Suganuma, and K. Tsumura. Charmonium properties in deconfinement phase in anisotropic lattice QCD. *Phys.Rev.*, D74:074502, 2006, hep-lat/0602008.

[68] G. Aarts, C.R. Allton, R. Morrin, A.O. Cais, M.B. Oktay, et al. Charmonium spectral functions in two-flavour QCD. *Nucl.Phys.*, A785:198–201, 2007, hep-lat/0608009.

[69] Aoife Kelly, Jon-Ivar Skullerud, Chris Allton, Dhagash Mehta, and Mehmet B. Oktay. Spectral functions of charmonium from 2 flavour anisotropic lattice data. *PoS*, LATTICE2013:170, 2014, hep-lat/1312.0791.

[70] Alessandro Amato, Gert Aarts, Chris Allton, Pietro Giudice, Simon Hands, et al. Electrical conductivity of the quark-gluon plasma across the deconfinement transition. *Phys.Rev.Lett.*, 111:172001, 2013, 1307.6763.

[71] G. Aarts, C. Allton, S. Kim, M.P. Lombardo, S.M. Ryan, et al. Melting of P wave bottomonium states in the quark-gluon plasma from lattice NRQCD. *JHEP*, 1312:064, 2013, hep-lat/1310.5467.

[72] Szabolcs Borsányi, Stephan Dürr, Zoltán Fodor, Christian Hoelbling, Sándor D. Katz, et al. Charmonium spectral functions from 2+1 flavour lattice QCD. *JHEP*, 1404:132, 2014, hep-lat/1401.5940.

[73] Szabolcs Borsányi, Stephan Dürr, Zoltán Fodor, Christian Hoelbling, Sándor D. Katz, et al. Spectral functions of charmonium with 2+1 flavours of dynamical quarks. 2014, hep-lat/1410.7443.

[74] Saumen Datta, Frithjof Karsch, Peter Petreczky, and Ines Wetzorke. Behavior of charmonium systems after deconfinement. *Phys.Rev.*, D69:094507, 2004, hep-lat/0312037.

[75] Takashi Umeda. A Constant contribution in meson correlators at finite temperature. *Phys.Rev.*, D75:094502, 2007, hep-lat/0701005.

[76] Szabolcs Borsányi, Zoltán Fodor, Sándor D. Katz, Attila Pásztor, Kálmán K. Szabó, et al. Static $\bar{Q}Q$ pair free energy and screening masses from correlators of Polyakov loops: continuum extrapolated lattice results at the QCD physical point. 2015, hep-lat/1501.02173.

[77] M. Laine, O. Philipsen, P. Romatschke, and M. Tassler. Real-time static potential in hot QCD. *JHEP*, 0703:054, 2007, hep-ph/0611300.

[78] Alexander Rothkopf, Tetsuo Hatsuda, and Shoichi Sasaki. Complex Heavy-Quark Potential at Finite Temperature from Lattice QCD. *Phys.Rev.Lett.*, 108:162001, 2012, hep-lat/1108.1579.

[79] Larry D. McLerran and Benjamin Svetitsky. Quark Liberation at High Temperature: A Monte Carlo Study of SU(2) Gauge Theory. *Phys.Rev.*, D24:450, 1981.

[80] Sudhir Nadkarni. Nonabelian Debye Screening. 2. The Singlet Potential. *Phys.Rev.*, D34:3904, 1986.

[81] O. Kaczmarek, F. Karsch, P. Petreczky, and F. Zantow. Heavy quark anti-quark free energy and the renormalized Polyakov loop. *Phys.Lett.*, B543:41–47, 2002, hep-lat/0207002.

[82] O. Kaczmarek, F. Karsch, F. Zantow, and P. Petreczky. Static quark anti-quark free energy and the running coupling at finite temperature. *Phys.Rev.*, D70:074505, 2004, hep-lat/0406036.

[83] Olaf Kaczmarek and Felix Zantow. Static quark anti-quark interactions in zero and finite temperature QCD. I. Heavy quark free energies, running coupling and quarkonium binding. *Phys.Rev.*, D71:114510, 2005, hep-lat/0503017.

[84] Ágnes Mócsy and Péter Petreczky. Can quarkonia survive deconfinement? *Phys.Rev.*, D77:014501, 2008, hep-ph/0705.2559.

[85] Owe Philipsen. Static potentials for quarkonia at finite temperatures. *Nucl.Phys.*, A820:33C–40C, 2009, hep-ph/0810.4685.

[86] S. Digal, P. Petreczky, and H. Satz. Quarkonium feed down and sequential suppression. *Phys.Rev.*, D64:094015, 2001, hep-ph/0106017.

[87] Cheuk-Yin Wong. Dissociation of a heavy quarkonium at high temperatures. *Phys.Rev.*, C65:034902, 2002, nucl-th/0110004.

[88] Edward V. Shuryak and Ismail Zahed. Towards a theory of binary bound states in the quark gluon plasma. *Phys.Rev.*, D70:054507, 2004, hep-ph/0403127.

[89] W.M. Alberico, A. Beraudo, A. De Pace, and A. Molinari. Heavy quark bound states above T(c). *Phys.Rev.*, D72:114011, 2005, hep-ph/0507084.

[90] Cheuk-Yin Wong. Quarkonia and quark drip lines in quark-gluon plasma. *Phys.Rev.*, C76:014902, 2007, hep-ph/0606200.

[91] W.M. Alberico, A. Beraudo, A. De Pace, and A. Molinari. Quarkonia in the deconfined phase: Effective potentials and lattice correlators. *Phys.Rev.*, D75:074009, 2007, hep-ph/0612062.

[92] Péter Petreczky, Chuan Miao, and Agnes Mócsy. Quarkonium spectral functions with complex potential. *Nucl.Phys.*, A855:125–132, 2011, hep-ph/1012.4433.

[93] Nora Brambilla, Jacopo Ghiglieri, Péter Petreczky, and Antonio Vairo. The Polyakov loop and correlator of Polyakov loops at next-to-next-to-leading order. *Phys.Rev.*, D82:074019, 2010, hep-ph/1007.5172.

[94] Nora Brambilla, Jacopo Ghiglieri, Antonio Vairo, and Péter Petreczky. Static quark-antiquark pairs at finite temperature. *Phys.Rev.*, D78:014017, 2008, hep-ph/0804.0993.

[95] Y. Aoki, Z. Fodor, S.D. Katz, and K.K. Szabó. The Equation of state in lattice QCD: With physical quark masses towards the continuum limit. *JHEP*, 0601:089, 2006, hep-lat/0510084.

[96] Z. Fodor, A. Jakovác, S.D. Katz, and K.K. Szabó. Static quark free energies at finite temperature. *PoS*, LAT2007:196, 2007, hep-lat/0710.4119.

[97] Szabolcs Borsányi, Zoltán Fodor, Christian Hoelbling, Sándor D. Katz, Stefan Krieg, et al. Full result for the QCD equation of state with 2+1 flavors. *Phys.Lett.*, B730:99–104, 2014, hep-lat/1309.5258.

[98] Y. Aoki, Z. Fodor, S.D. Katz, and K.K. Szabó. The QCD transition temperature: Results with physical masses in the continuum limit. *Phys.Lett.*, B643:46–54, 2006, hep-lat/0609068.

[99] Sourendu Gupta, Kay Huebner, and Olaf Kaczmarek. Renormalized Polyakov loops in many representations. *Phys.Rev.*, D77:034503, 2008, hep-lat/0711.2251.

[100] S. Dürr, Z. Fodor, J. Frison, C. Hoelbling, R. Hoffmann, et al. Ab-Initio Determination of Light Hadron Masses. *Science*, 322:1224–1227, 2008, hep-lat/0906.3599.

[101] A. Bazavov and P. Petreczky. Polyakov loop in 2+1 flavor QCD. *Phys.Rev.*, D87(9):094505, 2013, hep-lat/1301.3943.

[102] Sudhir Nadkarni. Nonabelian Debye Screening. 1. The Color Averaged Potential. *Phys.Rev.*, D33:3738, 1986.

[103] Eric Braaten and Agustin Nieto. Asymptotic behavior of the correlator for Polyakov loops. *Phys.Rev.Lett.*, 74:3530–3533, 1995, hep-ph/9410218.

[104] Y. Maezawa et al. Electric and Magnetic Screening Masses at Finite Temperature from Generalized Polyakov-Line Correlations in Two-flavor Lattice QCD. *Phys.Rev.*, D81:091501, 2010, hep-lat/1003.1361.

[105] Peter Brockway Arnold and Laurence G. Yaffe. The NonAbelian Debye screening length beyond leading order. *Phys.Rev.*, D52:7208–7219, 1995, hep-ph/9508280.

[106] A. Hart, M. Laine, and O. Philipsen. Static correlation lengths in QCD at high temperatures and finite densities. *Nucl.Phys.*, B586:443–474, 2000, hep-ph/0004060.

[107] H. Akaike. *IEEE Transactions on Automatic Control*, 19:716, 1974.

[108] Dongsu Bak, Andreas Karch, and Laurence G. Yaffe. Debye screening in strongly coupled N=4 supersymmetric Yang-Mills plasma. *JHEP*, 0708:049, 2007, hep-th/0705.0994.

[109] Christopher Michael and A. McKerrell. Fitting correlated hadron mass spectrum data. *Phys.Rev.*, D51:3745–3750, 1995, hep-lat/9412087.

[110] I.T. Drummond and R.R. Horgan. Improved Langevin methods for spin systems. *Phys.Lett.*, B302:271–278, 1993, hep-lat/9211037.

Heavy quark systems at finite temperature from lattice QCD

Attila Pásztor

- Summary -

My PhD thesis concerns heavy quarkonia at finite temperatures. We study the heavy quarkonia systems using lattice gauge theory. This is an important topic for heavy ion physics, since J/Ψ suppression is regarded as an important signature of quark gluon plasma formation. The document has two distinct parts. The first part deals with a Maximum Entropy determination of the charmonium spectral functions in the vector and pseudoscalar channels, corresponding to the J/Ψ and η_c mesons respectively. The second part deals with the infinite mass (or static) limit of such systems, and calculates the static $\bar{Q}Q$ pair free energy using the correlator of Polyakov loops. We also calculate two distinct correlation lengths in the Polyakov loop correlator. The main results are the following:

- The Maximum Entropy determination of charmonium spectral functions from lattice QCD data with $2+1$ flavours of dynamical (Wilson) quarks. The simulations were done with a heavy pion mass of $m_\pi = 545$MeV. I see no clear indication of J/Ψ or η_c melting up to a temperature of $1.3T_c$.

- Using the ratio G/G_{rec} I show that up to a temperature of $1.4T_c$ the Euclidean correlator of η_c is consistent with a temperature independent spectral function, and the Euclidean correlator of J/Ψ is consistent with a temperature dependent narrow transport peak close to $\omega = 0$ and a temperature independent part at $\omega > 0$. We see no indication of J/Ψ melting up to $1.4T_c$.

- The introduction of a non-perturbative renormalization procedure for the static quark-antiquark pair free energy, using only $T > 0$ data, that is applicable to staggered quarks. The method is not only more efficient computationally (as no $T = 0$ determinations of the Wilson loop are needed), but also allows for the extension of the temperature range for the continuum extrapolation.

- I performed a continuum extrapolated lattice determination of the static quark-antiquark pair free energy. The simulations used $2+1$ flavours of staggered quarks, with physical quarks masses. We use lattices with temporal extents of $N_t = 6, 8, 10, 12, 16$. We present results in the temperature range $150 - 350$MeV.

- A continuum extrapolated lattice determination of the electric and magnetic screening masses in the correlator of Polyakov loops. Both screening masses are proportional to the temperature to a very good approximation. For the screening masses at $T = 2T_c$ we get

$$m_E/T = 7.31(25) \quad m_M/T = 4.48(9)$$
$$m_E/m_M = 1.63(8)$$

  Comparing with results from the literature we see that our results are closest to the calculations in the dimensionally reduced effective field theory. We present results in the temperature range $160 - 450$MeV.

Nehézkvark-rendszerek vizsgálata véges hőmérsékleten rács QCD szimulációkkal

Pásztor Attila

- Összefoglaló -

A doktori értekezésem a nehéz kvarkok kötött állapotainak véges hőmérsékletű viselkedésével foglalkozik. A vizsgálatokhoz rácstéleméleti módszereket használtam. A téma különösen fontos a nehézion-fizikában, hiszen a J/Ψ elnyomást a kvark-gluon plazma keletkezés fontos kísérleti szignatúrájának tartják. Az értekezés két részre tagolható. Az elsőben charmonium spektrálfüggvényeket viszgálok a vektor és pszeudoskalár csatornában, a Maximum entrópia módszerét (MEM) használva. A másodikban a végtelen kvark tömeg, vagy statikus limeszben definiált $\bar{Q}Q$ pár szabadenergiával foglalkozom. Ez utóbbi a Polyakov-hurok korrelátorból számolható ki. Vizsgálom továbbá két plazmaárnyékolási hossz (elektromos és mágneses) hőmérsékletfüggését. Az eredményeim:

- A charmonium spektrálfüggvények vizsgálata MEM segítségével. A rács QCD szimulációkat 2+1 flavour dinamikus Wilson-fermionnal és $m_\pi = 545$MeV piontömegnél végeztük. Nincs jele se a J/Ψ, se az η_c mezonok elolvadásának az analízisben. A MEM rekonstrukciót $1,3T_c$ hőmérsékletig végeztem el.

- A $G/G_{\rm rec}$ hányados segítségével megmutattam, hogy $1,4T_c$ hőmérsékletig az η_c euklideszi korrelátora konzisztens egy konstans spektrálfügvénnyel, a J/Ψ-hez tartozó euklideszi korrelátor pedig konzisztens egy hőmérsékletfüggő $\omega \approx 0$ körüli transzport csúcs, és egy hőmérsékletfüggetlen $\omega > 0$ rész összegével. Ez azt jelenti, hogy $1,4T_c$-ig se a J/Ψ se az η_c olvadását nem látjuk.

- Bevezettem egy csak véges hőmérsékletű rácsokat alkalmazó, nem-perturbatív renormálási eljárást a statikus quark szabad energiára, amely staggered fermionokkal is alkalmazható. Az eljárás nemcsak a számolásigényen javít (hiszen nincs szükség $T = 0$ szimulációkra), hanem a kontinuum limesz hőmérséklettartományát is szélesítenil lehet vele.

- Elvégeztem egy statikus kvark-antikvark pár szabad energiájának kontinuum extrapolációját 150MeV és 350MeV hőmérséklet között. A szimulációkhoz 2+1 flavour staggered kvarkokat használtunk, fizikai tömegekkel. A kontinuum extrapolációhoz és a renormáláshoz $N_t = 6, 8, 10, 12, 16$-os rácsokat használtunk.

- A Polyakov-hurok korrelátorban megjelenő elektromos és mágneses árnyékolási hosszak kontinuum extrapolációja. Mindkét árnyékolási tömeg jó közelítéssel a hőmérséklettel arányos. $T = 2T_c$ hőmérsékleten az értékük:

$$m_E/T = 7.31(25) \quad m_M/T = 4.48(9)$$
$$m_E/m_M = 1.63(8)$$

  Ha a kapott kontinuum eredményeket összehasonlítjuk az irodalomban található, más közelítésekben számolt árnyékolási hosszakkal, akkor azt látjuk, hogy legjobban a dimenziós redukcióval kapott 3 dimenziós effektív térelmélettel egyezik az eredmény.

[38]**ADATLAP**

a doktori értekezés nyilvánosságra hozatalához

I. A doktori értekezés adatai

A szerző neve: Pásztor Attila

MTMT-azonosító: 10044937

A doktori értekezés címe és alcíme:

Heavy quark systems at finite temperature from lattice QCD

DOI-azonosító[39]: 10.15476/ELTE.2015.054

A doktori iskola neve: Fizika Doktori Iskola

A doktori iskolán belüli doktori program neve: Részecskefizika és csillagászat program

A témavezető neve és tudományos fokozata: Katz Sándor

A témavezető munkahelye: ELTE, Elméleti Fizika Tanszék

II. Nyilatkozatok

A doktori értekezés szerzőjeként[40]

a) hozzájárulok, hogy a doktori fokozat megszerzését követően a doktori értekezésem és a tézisek nyilvánosságra kerüljenek az ELTE Digitális Intézményi Tudástárban. Felhatalmazom a Természettudományi Kar Tudományszervezési és Egyetemközi Kapcsolatok Osztályának ügyintézőjét ,.....Bíró Évát....., hogy az értekezést és a téziseket feltöltse az ELTE Digitális Intézményi Tudástárba, és ennek során kitöltse a feltöltéshez szükséges nyilatkozatokat.

b) kérem, hogy a mellékelt kérelemben részletezett szabadalmi, illetőleg oltalmi bejelentés közzétételéig a doktori értekezést ne bocsássák nyilvánosságra az Egyetemi Könyvtárban és az ELTE Digitális Intézményi Tudástárban;[41]

c) kérem, hogy a nemzetbiztonsági okból minősített adatot tartalmazó doktori értekezést a minősítés *(dátum)*-ig tartó időtartama alatt ne bocsássák nyilvánosságra az Egyetemi Könyvtárban és az ELTE Digitális Intézményi Tudástárban;[42]

d) kérem, hogy a mű kiadására vonatkozó mellékelt kiadó szerződésre tekintettel a doktori értekezést a könyv megjelenéséig ne bocsássák nyilvánosságra az Egyetemi Könyvtárban, és az ELTE Digitális Intézményi Tudástárban csak a könyv bibliográfiai adatait tegyék közzé. Ha a könyv a fokozatszerzést követőn egy évig nem jelenik meg, hozzájárulok, hogy a doktori értekezésem és a tézisek nyilvánosságra kerüljenek az Egyetemi Könyvtárban és az ELTE Digitális Intézményi Tudástárban.[43]

2. A doktori értekezés szerzőjeként kijelentem, hogy

a) az ELTE Digitális Intézményi Tudástárba feltöltendő doktori értekezés és a tézisek saját eredeti , önálló szellemi munkám és legjobb tudomásom szerint nem sértem vele senki szerzői jogait;

b) a doktori értekezés és a tézisek nyomtatott változatai és az elektronikus adathordozón benyújtott tartalmak (szöveg és ábrák) mindenben megegyeznek.

3. A doktori értekezés szerzőjeként hozzájárulok a doktori értekezés és a tézisek szövegének plágiumkereső adatbázisba helyezéséhez és plágiumellenőrző vizsgálatok lefuttatásához.

Kelt: 2015. március 20.

Pásztor Attila

.....

a doktori értekezés szerzőjének aláírása

[38] Beiktatta az Egyetemi Doktori Szabályzat módosításáról szóló CXXXIX/2014. (VI. 30.) Szen. sz. határozat. Hatályos: 2014. VII.1. napjától.

[39] A kari hivatal ügyintézője tölti ki.

[40] A megfelelő szöveg aláhúzandó.

[41] A doktori értekezés benyújtásával egyidejűleg be kell adni a tudományági doktori tanácshoz a szabadalmi, illetőleg oltalmi bejelentést tanúsító okiratot és a nyilvánosságra hozatal elhalasztása iránti kérelmet.

[42] A doktori értekezés benyújtásával egyidejűleg be kell nyújtani a minősített adatra vonatkozó közokiratot.

[43] A doktori értekezés benyújtásával egyidejűleg be kell nyújtani a mű kiadásáról szóló kiadói szerződést.